MutSγ FUNCTION DURING MOUSE MEIOSIS

A Dissertation

Presented to the Faculty of the Graduate School

of Cornell University

In Partial Fulfillment of the Requirements for the Degree of

Doctor of Philosophy

by

Carolyn Rose Milano

May 2019

MutSγ FUNCTION DURING MOUSE MEIOSIS

Carolyn Rose Milano, Ph. D.

Cornell University 2019

MutSγ is a highly conserved heterodimer comprised of MSH4 (MutS homolog 4) and MSH5 (MutS homolog 5). MutSγ complex is widely conserved across many linages of eukaryotes with few exceptions. Unlike other MutS complexes, MSH4-MSH5 function is specific to, and essential for meiosis. Prophase I of meiosis harbors two events critical for proper segregation of homologs at the end of meiosis I: pairing/synapsis and homologous recombination. Loss of MutSγ function results in severe defects in one or both of these events in budding yeast (*S. cerevisiae)*, in the nematode (*C. elegans)*, among some plants including *A. thaliana*, and in mammals such as *M. musculus*. Specifically, in *M. musculus* loss of either MSH4 or MSH5 results in loss of meiocytes prior to pachynema. This suggests a function for MutSγ preceding pachynema has a critical role for cell vitality in mammals. The loss of meiocytes prior to pachynema in $Msh5^{-/-}$ or $Msh4^{-/-}$ makes it impossible to understand the function of MutSγ in crossover regulation.

To further establish a function for mammalian MSH5, this work looks at two mouse lines, each with a different mutation in the Msh5 coding sequence. The first mouse ($Msh5^{GA/GA}$) harbors a point mutation in the ATP binding domain of MSH5, predicted to disrupt binding. The second line ($Msh5^{\Delta C/\Delta C}$) contains a deletion of the MSH5 c-terminus. Both of these mouse lines show a less severe phenotype in spermatogenesis than does $Msh5^{-/-}$, allowing for phenotypic analysis of homologous recombination events throughout prophase I.

A proportion of *Msh5*$^{GA/GA}$ spermatocytes can progress to diakinesis of MI, thus alleviating the early loss of spermatocytes in *Msh5*$^{-/-}$ animals. Chromosome spread analysis of *Msh5*$^{GA/GA}$ spermatocytes reveals abnormal pairing/synapsis between non-homologous chromosomes. Across eukaryotes MutSγ is associated with class I CO repair events. Surprisingly in *Msh5*$^{GA/GA}$ spermatocytes, all chiasmata are lost or fail to form in these mutant spermatocytes. These findings identify MutSγ as essential to all CO regulation in mouse.

The *Msh5*$^{\Delta C/\Delta C}$ mice confer infertility phenotypes, a result which identifies this domain as essential for proper MutSγ function. A proportion of *Msh5*$^{\Delta C/\Delta C}$ spermatocytes achieve full autosomal synapsis during pachynema, suggesting the c-terminal domain is less important for homolog synapsis. In the *Msh5*$^{\Delta C/\Delta C}$ pachynema spermatocytes there is a reduction of class I CO establishment in, identifying this domain as necessary for normal CO establishment. These findings provide the first direct evidence that MutSγ is necessary for the normal recruitment of class I CO machinery during prophase I.

Taken together the results suggest that MutSγ function is integral to not only homolog pairing and synapsis, but also to the establishment of all crossovers in mouse.

BIOGRAPHICAL SKETCH

NAME: Carolyn Rose Milano

EDUCATION/TRAINING

INSTITUTION AND LOCATION	DEGREE	START DATE MM/YYYY	END DATE MM/YYYY	FIELD OF STUDY
Stony Brook University	BS	08/2009	05/2013	Developmental Biology
Cornell University	PHD	08/2013	05/2019	Genetics

Personal Statement

I began my work in science an undergraduate researcher in Dr. Howard Sirokin's lab investigating early neurogenesis in zebrafish. This training taught me invaluable gene targeting techniques and led to a research publication prior to graduation. My doctoral training and thesis research under Dr. Paula Cohen has prepared me for a career in the field of meiosis. The Cohen lab has fostered a collaborative and encouraging environment, which was proficient in providing me the skills needed to complete this thesis. The graduate field of Genetics Genomics & Development provided me with ample support in career development, writing, and additional support essential to my success. my entire thesis committee, as well as many of the people in their labs, have provided crucial training and support needed to execute the experiments laid out in this thesis. I have completed one first author paper and have contributed to a second authorship. As I embark on my post-doctor position in Dr. Andreas Hochwagen's lab at NYU, I am excited to continue my research journey, focusing on meiosis in *S.*

cerevisiae. Ultimately, I would like to be a primary investigator at a research-intensive university focusing on DNA repair research and undergraduate/graduate student training.

1. Taibi A, Mandavawala KP, Noel J, Okoye EV, Milano CR, Martin BL, Sirotkin HI. Zebrafish churchill regulates developmental gene expression and cell migration. Dev Dyn. 2013 Jun;242(6):614-21. PubMed PMID: 23443939; PubMed Central PMCID: PMC3690002.

2. Milano CR, Holloway JK, Zhang Y, Jin B, Smith C, Bergman A, Edelmann W, Cohen PE. Mutation of the ATPase domain of MutS homolog-5 (MSH5) reveals a requirement for a functional MutSγ complex for all crossovers in mammalian meiosis. G3 2019 Aprl [Epub ahead of print]. PubMed PMID: 30944090 doi: 10.1534/g3.119.400074

3. Toledo M, Sun X, Brieño-Enríquez MA, Raghava V, Gray S, Pea J, Milano CR, Venkatesh A, Patel L, Borst PL, Alani E, Cohen PE. A mutation in the endonuclease domain of mouse MLH3 reveals novel roles for MutLy during crossover formation in meiotic prophase I. Accepted to PLoSGenetics May 2019, in print.

Positions and Honors

Positions and Employment

2011 - 2013	Research Assistant, Stony Brook University
2013 - 2013	Teaching Assistant, Marine Biological Laboratory
2013 - 2015	Graduate Student, Cornell University
2015 – 2019	Doctoral Candidate, Cornell University

2019 - Postdoctoral Associate, New York University

Other Experience and Professional Memberships

2013 - 2014 Member, Society for Developmental Biology

2014 - 2015 Field Representative, Graduate & Professional Student Association

2014 - 2015 Board Member, Graduate & Professional Women's Network

2016 - Member, The American Association for the Advancement of Science

2017 - Member, New York Academy of Sciences

I dedicate this thesis to the people who raised me: Veronica, Alfred, Freddie Milano and Mariette Cullity. These people are responsible for giving me the best resources, encouragement and love I could have ever needed to be successful in this life. If you had asked me ten years ago what I would be doing at 28 years old, I would never have guessed correctly. Mom, Dad, and my beautiful god mother would have though.

I was in my first conference, just after I gave my first research presentation, when I found out my god mother passed away. This left me and the family heart broken. I am happy to know that the completion of this work will make her proud. I am I am so grateful. Cornell has taught me many lessons that I will never forget. I am so grateful to have spent time in beautiful Ithaca. It is here that I fell in love with Christopher Bambach Grady who moved all the way from the NYC to live near me while I completed this journey. I cannot thank Christopher enough for all that he has done, especially for the many discussions on how to use a comma. And lastly, I have to thank the puppy who has licked away many happy, and sad tears, Rachel Carson. She is the top dog.

ACKNOWLEDGMENTS

This work would not have been accomplished without the help, especially help from Dr. Paula Cohen and lab members. I would also like to acknowledge the members of Dr. Alani's lab, as well as the members of Dr. Joshua Chappie's lab for allowing me to attend meetings and have valuable discussions.

TABLE OF CONTENTS

List of Figures

Abbreviations

CO: crossover

dHJ: double Holliday junction

DSB: double strand break

HR: homologous recombination

LE: lateral element

NCO: non-crossover

SC: synaptonemal complex

SEI: single end invasion

SDSA: synthesis dependent strand annealing

TF: transverse filament

WT: wild-type

CHAPTER 1

INTRODUCTION

Meiosis: the generation of haploid gametes and the crossover events that mediate accurate chromosome inheritance

Meiosis is a specialized cell division that is fundamental to the propagation of all sexually reproducing organisms. Meiosis differs from mitosis in that it is preceded by one round of DNA replication and consists of two rounds of chromosome segregation, meiosis I and meiosis II. This results in haploid gametes necessary to propagate the next generation. During meiosis I, homologous chromosomes segregate, a feature unique to meiosis (Ohkura 2015). In meiosis II, chromosome segregation occurs between sister chromatids in a process more similar to mitosis (Ohkura 2015). The segregation of homolog pairs depends on physical contact between homologous chromosomes as the spindle assembles, giving tension between homologous chromosomes needed to align homologs at the metaphase plate. In many eukaryotic lineages, including humans, mice, and the budding yeast species *S. cerevisiae*, crossover (CO) events, or the exchange of genetic material between homologous chromosomes, together with cohesions, create this physical contact between homolog pairs. Failure to establish CO events to tether homolog pairs during meiosis I can cause homologs to prematurely and randomly segregate, resulting in aneuploid meiotic products (Lamb et al. 2005; Gray and Cohen 2016). In humans and mice, loss of COs is associated with infertility and higher rates of aneuploid gametes (Herbert et al. 2015).

CO establishment is best understood in the single cell eukaryote *S. cerevisiae.* The number and placement of COs between homologs is strictly regulated to ensure every homolog pair receives at least one CO, known as the obligate CO (Broman et al.

2002; Jones 1984; Jones and Franklin 2006). *S. cerevisiae* contains 16 chromosomes and at each meiosis, about 100 COs are generated. In addition to the obligate CO, CO positioning also correlates with chromosome size, such that longer homologs are more likely to have more than one CO (Chakraborty et al. 2017).

There are at least two Classes of COs, those that exhibit interference, such that one CO inhibits the manifestation of a proximal CO, and those that do not (Broman et al. 2002). Interfering COs and non-interfering COs are often referred to as Class I and Class II. Class I COs are driven by the mismatch repair (MMR) proteins, Mlh1-Mlh3, also called MutLγ (Lipkin et al. 2002; Zakharyevich et al. 2012). Class II COs are driven in part by structure specific endonuclease Mus81-Mms4 (Matos and West 2014; Cromie et al. 2006; Jessop and Lichten 2008; Oh et al. 2008). In *S. cerevisiae,* the Class I COs make up about half of all COs that occur during meiosis (Hunter and Borts 1997; Manhart and Alani 2016; Argueso et al. 2004). The obligate CO, as well as CO interference, is largely dependent on Class I CO machinery and the Class II COs alone are insufficient to generate COs on every homolog (Chakraborty et al. 2017; Krishnaprasad et al. 2015).

The interfering Class I COs are widely conserved across eukaryotes. Notably, Class I COs are not always utilized and some lineages lack Class I COs altogether, such as in fission yeast (Smith et al. 2003). The absence of Class I COs appears to be rare and most eukaryotic lineages studied to-date utilize Class I CO pathway, including the plant family *A. thaliana*, invertebrates such as the nematode *C. elegans*, the female flies *D. melanogaster*, and in vertebrates such as mouse and humans (Broman et al. 2002; Copenhaver et al. 2002; Meneely et al. 2002; Rasmussen and Holm 1984; Page and Hawley 2001; de Boer et al. 2009).

Of the organisms that utilize the Class I pathway, the degree to which this pathway is utilized to establish the total CO number varies. For example, in *C.*

elegans, all COs are driven by the Class I CO pathway (Zalevsky et al. 1999). *A. thaliana*, like yeast, has both Class I and Class II COs, unlike yeast, the majority of its COs are driven by the Class I pathway (Copenhaver et al. 2002; Lu et al. 2008). Class I COs are also responsible for the majority of COs among vertebrate lineages, most notably in mammalian species such as humans and mice (Lipkin et al. 2002; Pashaiefar et al. 2013; Plug et al. 1998).

The properties of CO repair observed in yeast are conserved in mice, including the obligate CO and CO interference (Broman et al. 2002). Mice have both Class I and Class II COs that generate 20-30 COs consistently at every meiosis in mouse (Lipkin et al. 2002; Holloway et al. 2008). Dissimilar to yeast, in mouse COs are driven predominately via the Class I pathway, attributing to about 90% of all COs. The remaining 10% of COs in mice are attributed to the Class II CO pathway, driven in part by MUS81-EME1 (Holloway et al. 2008). This observation demonstrates the different regulation of CO repair between mice and budding yeast.

Despite ongoing research efforts to investigate human CO repair, ethical and temporal constraints innate to human gametogenesis make the undertaking of these studies difficult (Hassold & Hunt, 2001; Jamsai & O'Bryan, 2011). Instead, species that are more amenable to study are utilized to further investigate CO repair (Hassold, Sherman, & Hunt, 2000; Jamsai & O'Bryan, 2011).

Mammalian meiosis is a sexually dimorphic process

Gamete development is sexually dimorphic in mammals and occurs during distinct developmental times in each sex. Female meiosis begins *in utero* at 11 weeks in humans, and 13.5 days in mouse (Le Bouffant et al. 2010; Childs et al. 2011). Meiosis then arrests at diakinesis of prophase I and does not resume in humans until a

female reaches puberty around a decade later. Male meiosis does not begin until puberty, when the stem cell niche is formed in the seminiferous tubules becomes active and initiates the first wave of meiosis. The stem cell population allows for meiosis to occur continuously throughout their life.

Human fertility is largely inefficient, evidenced by the fact that 7-10% of human pregnancies recognized by a doctor have an abnormal number of chromosomes (Hassold and Hunt 2001). A proportion of aneuploidies in humans are attributed to defects in meiosis I events, specifically due to the loss of homolog interactions. These events are a source of genetic birth defects, miscarriage, and infertility in the human population (Handyside et al. 2012). Consequently, understanding CO formation during meiosis will facilitate our understanding of some human infertility defects (Hunt and Hassold 2008).

CO regulation is also sexually dimorphic in mammals (Reeves et al. 1990; Hunt 2006). In humans and mouse strains, recombination rates are higher in females than males (Doniskeller 1987; Neff et al. 1999; Mikawa et al. 1999). Variation in the number of COs observed in female meiosis may contribute to the higher rate of aneuploidy compared to males. This is not without consequence, as female meiosis is also associated with a higher rate of aneuploidy compared to males (Hassold and Hunt 2001). In young mothers, aneuploidies have also been attributed to an increase in COs (Saiyed et al. 2018). In humans, with increasing female age, the rate of aneuploid due to a loss of CO structures increases (Herbert et al. 2015). This is of particularly practical importance given that according to the CDC, the age at which women are having their first baby is increasing over time (Mathews and Hamilton 2002). It has been postulated that the variation in COs observed in females may be beneficial to the organism, as the reduction in progeny allows for more care to be given to the successful progeny (Wang, Hassold, et al. 2017; Wang, Kleckner, et al. 2017) .

The machinery that drives COs in males and females is largely the same. Mutations in genes associated with CO establishment results in apoptosis in spermatogenesis, while oocyte meiosis will tolerate these disruptions (Hunt and Hassold 2002; Nagaoka et al. 2011). The different responses of male and female meiocytes to CO defects are not caused by genetic differences in the sex chromosomes (XY), but instead is thought to be driven by differences between spermatocyte and oocyte cell environments (Koehler et al. 2002; Lynn et al. 2005). In order to understand differences between CO establishment in the sexes, it is important that the molecular mechanism for CO control is understood.

Crucial to CO establishment across eukaryotes is the MutSγ complex, a heterodimer of MSH4 and MSH5. Mutation of either *Msh4* or *Msh5* in humans results in infertility in both males and females (Carlosama et al. 2017; Mandon-Pépin et al. 2008; Guo et al. 2017; Ni et al. 2015). Similarly, in mouse disruptive mutations affecting the coding sequences in either of these genes also results in infertility in both sexes. In spermatogenesis, cell death occurs early in meiosis I, prior to CO formation (Edelmann et al. 1999; Kneitz et al. 2000; de Vries et al. 1999). Because of the severity of these phenotypes, little is known about the function of MutSγ during mammalian meiosis. The human infertility associated with MutSγ highlights the importance of understanding these proteins in mammals.

This thesis will focus on understanding MutSγ in mammalian meiosis utilizing the mouse model system. The mouse model provides a fixed genetic background (a known contributor to CO variations) as well as control over environmental and temporal variables that could influence results (Hunt 2006; Reeves et al. 1990; Koehler et al. 2002). Meiosis occurs continuously within the seminiferous tubules of a mature testis (Nakata 2019). Spermatogenesis is therefore more amenable for analysis than oogenesis, where meiosis occurs only once in an animal, at a specific stage of

embryogenesis. The focus of this thesis is on a more explicit understanding of MutSγ activity during CO repair in mouse spermatogenesis.

Mismatch Repair Proteins

MutLγ and MutSγ are members of a broader family of MMR proteins. Canonical MMR maintains genome integrity, correcting mis-matches or slippage events incorporated during DNA synthesis (Su and Modrich 1986). DNA Polymerase III has proof-reading capabilities that are not entirely efficient, such that it mis-incorporates every 1:10,000 – 1:100,000 base pair during replication, resulting in mis- paired bases (Arana and Kunkel 2010). Loss of MMR results in a high mutation rate and is therefore detrimental to the organism. MMR has a critical role in maintaining genome integrity across eukaryotes and some bacteria (Jiricny 2000).

The core bacterial MMR proteins are MutS, MutH, MutL, and uvrE (Su and Modrich 1986). The uvrD helicase protein is

Figure 1

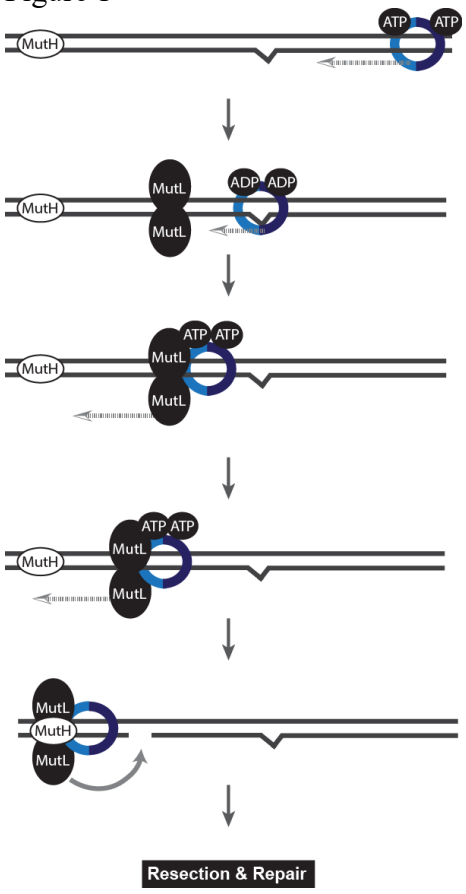

MutS activity in bacterial MMR.
DNA molecule is shown (black lines) in association with MMR proteins (light blue and dark blue lines forming MutS complex, MutH in white and MutL in black ovals). Dashed lines represents protein movement. A DNA lesion, is depicted by the triangle in DNA. MutS sliding activity is dependent on ATP binding. Upon encountering a lesion, the ATP hydrolysis activity of MutS complex is stimulated. This results in an ADP bound clamp, allowing for association with the MutL complex. MutS and MutL heterodimerize triggering another round of ATP binding. The tetra-complex of MutS and MutL slide along DNA in another ATP dependent manor. The MutS-MutL complex slides along DNA until encountering MutH, which will initiate a nick of the phosphate backbone containing the lesion, stimulating downstream excision and repair.

also considered part of the core MMR machinery, however this protein is not specific to MMR and plays roles in other repair pathways (Epshtein 2015). In this system, the MutS complex is a homodimer of two MutS subunits which function as an ATP-dependent sliding clamp (Carraway and Marinus 1993; Dohet et al. 1986; Learn and Grafstrom 1989; Parker et al. 1992; Lebbink et al. 2010; Acharya et al. 2003; Jeong et al. 2011) . In a contemporary model, MutS complex forms a sliding clamp around the DNA, moving along DNA in an ATP hydrolysis independent mechanism (Figure 1). Once MutS encounters a lesion, a conformational change in the dimer is triggered by the exchange of ADP to ATP, and the MutS subunit slides away from the mis-pair, towards the next MutL complex. The MutL complex (a homodimer of two MutL subunits) is directed to the lesion via interaction with MutS. This interaction is also dependent on ATP (Mendillo et al. 2009).

Together, MutS and MutL slide along DNA away from the lesion until interaction with MutH (Figure 1). Upon interaction with MutL-MutS, the endonuclease activity of MutH is triggered, creating a nick in the newly synthesized strand of the DNA, either 5' or 3' of the lesion (Au et al. 1992; Welsh et al. 1987; Lahue et al. 1987). The UvrD helicase then unwinds DNA to make it accessible to downstream repair enzymes. Excision of the mis-incorporated base is executed by ssDNA exonucleases. DNA polymerase III acts to resynthesize the gapped DNA and repair is completed by ligation of the phosphate backbone, facilitated by DNA ligase (Kunkel and Erie 2005). In this bacterial system, endonuclease MutH protein carries out the function of strand discrimination by nicking the unmethylated strand at hemi-methylated GATC sites (Welsh et al. 1987; Au et al. 1992). Eukaryotes, however, lack a MutH homolog. Instead, eukaryotic MutL complexes display an endonuclease activity that is thought to be directed to newly replicated DNA strand by interaction

with PCNA (Pluciennik et al. 2010; Genschel et al. 2017; Kadyrova and Kadyrov 2016).

Eukaryotes have a broader family of MMR proteins: three heterodimers of MutS homologs MutSα (MSH2-MSH6), MutSβ (MSH2-MSH3), MutSγ (MSH4-MSH5), and three MutL homologs, MutLα (MLH1-PMS2), MutLβ (MLH1-PMS1), and MutLγ (MLH1-MLH3) (Kunkel and Erie 2005). Similar to MutS and MutL interaction in bacteria, eukaryotic MutSα, MutSβ, MutLα, and MutLβ function in somatic MMR. MutSγ and MutLγ, however, have no function in somatic MMR (Hollingsworth et al. 1995; Wang et al. 1999). Instead these proteins have a conserved role in meiosis. The conservation of MutSγ between MMR paralogs suggests a similar signaling system for MutSγ and MutLγ in CO control, however a direct relationship between these two proteins remains to be seen *in vivo* (Mendillo et al. 2009).

Meiotic prophase I: Early Double Strand Break (DSB) processes mediate homolog interactions and synaptonemal complex formation

Successful chromosome segregation during meiosis I depends on the carefully orchestrated homolog interactions (and ultimately CO establishment) during prophase I. The Class I CO machinery is usually accompanied by the existence of the synaptonemal complex (SC), a multiprotein complex that acts as a scaffold to stabilize homologous chromosomes during prophase I (Romanienko and Camerini-Otero 2000). The SC is necessary for the proper CO patterning associated with Class I CO machinery in prophase I (Tsubouchi et al. 2006; de Vries et al. 2005). This structure is conserved in organisms that utilize the Class I CO pathway, as observed in *S. cerevisiae*, *C. elegans*, *A. thaliana*, female *D. melanogaster*, mice, and humans (Loidl

2016; Osman et al. 2006; Page and Hawley 2001; Moses et al. 1984; Plug et al. 1998; Sym et al. 1993).

In yeast, as well as in mouse, DSBs promote the construction of the SC between homologs (Henderson and Keeney 2004; Romanienko and Camerini-Otero 2000; Hong et al. 2019). The mature SC is a tripartite protein structure that forms between homologous chromosomes during prophase I, such that each homolog pair has two lateral elements (LE) structures, localized along the length of each homologous chromosome and one central element (CE) structure that synapses the LE structures together (Moses et al. 1984).

In mouse, prophase I is the longest substage of meiosis I and is further divided into five substages based on the progression of the SC assembly: leptonema, zygonema, pachynema, diplonema, and diakinesis (Moses et al. 1984) (Figure 2). During leptonema, the formation of the SC begins with the localization of axial element proteins (including SYCP3 in mouse) along sister chromatids (Figure 2) (Moses et al. 1984). During zygonema, axial element proteins are localized along the entire length of homologs, with these structures now considered mature LEs. Transverse filaments (including SYCP1 in mouse) begin to synapse the LEs of homologous chromosomes together (Figure 2). Synapsis between homologs forms the CE, a multi-protein complex, which provides further stabilization while also playing a role in signaling during DSB repair (Fukuda et al. 2012). Complete synapsis occurs forms for each autosome, while the XY homologs only pair at the pseudo-autosomal region (PAR) (Alavattam et al. 2018). At pachynema, the full SC is formed, and each independently synapsed homolog pair can be counted: 20 in mouse (Figure 2) or 23 in human. In diplonema, the SC begins to desynapsis, disassociating the LEs (Moses et al. 1984). By the time of diakinesis in mouse, the SC is completely disassembled. At

Figure 2

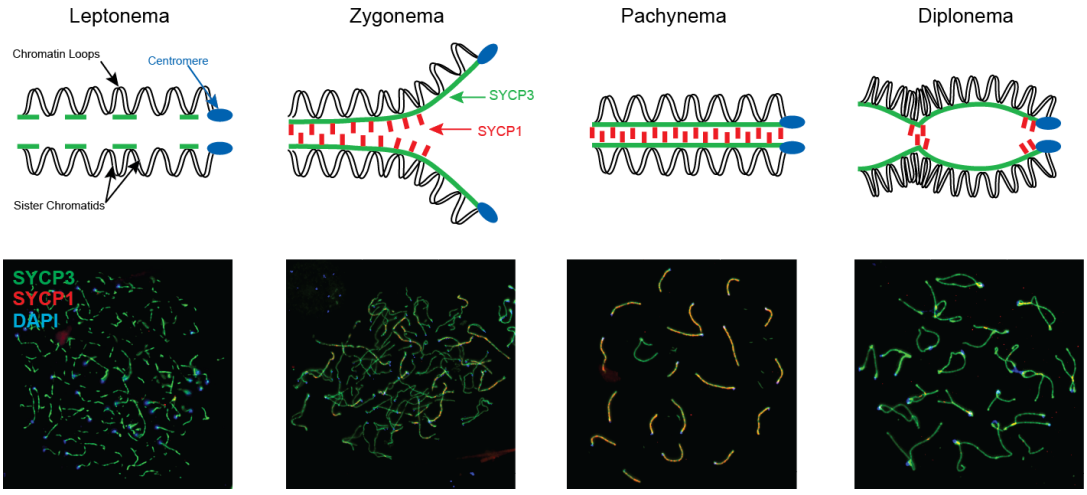

Prophase I substages in mouse spermatocytes.

Prophase I Substages in mouse spermatocytes are shown for the first four substages, leptonema, zygonema, pachynema, and diplonema spermatocytes. Cartoons are shown for SC dynamics for each substage. Below each cartoon is immunofluorescence with antibodies recognizing components of the SC in addition to the centromere

this time chiasmata, the visible manifestation of CO structures, are visualized (Jones 1984).

Mammalian meiosis occurs in a heterogenous cell population within the seminiferous tubules. Despite recent advances, to-date it is impossible to progress spermatogonia through spermatogenesis in culture, and there remains to be a suitable substitute for spermatogenesis *in vivo*. Few cell isolation techniques exist and those that do are laborious. For those reasons, the SC has been a pivotal tool for mouse cytologists by providing a visible structure through which to identify prophase I sub stage identification from heterogenous cell populations (Plug et al. 1998).

DSB repair common to CO and NCO in yeast

Endogenous DSBs induced during meiosis are needed for CO repair. The highly conserved topoisomerase protein Spo11 induces meiotic DSBs in both yeast

and mouse (Keeney 2008; Keeney and Kleckner 1995). In both yeast and mouse, the number of DSBs that are initiated, outweigh the final number of COs that repair. The abundance of DSBs in these organisms is believed to contribute to early DNA interactions that lead to homolog pairing, prior to the establishment of COs (Tsubouchi and Roeder 2005; Humphryes and Hochwagen 2014). DSB repair is not an exclusive homolog pairing mechanism across eukaryotes. In *C. elegans* for example, centromere pairing centers are utilized to mediate homolog interactions in a DSB independent mechanism (Rog and Dernburg 2013)**.** Unlike in organisms with DSB dependent pairing, in *C. elegans* DSBs are initiated after SC assembly, and the number of DSBs induced is more consistent with the final number of COs generated (Garcia-Muse and Boulton 2007).

The dynamics of DSB repair are better understood in organisms more amenable to biochemical analysis, such as in the budding yeast species, *S. cerevisiae*. In budding yeast, DSB repair results in about 90 CO events across the cell's 16 homolog pairs (Mancera et al. 2008; Pan et al. 2011; Chakraborty et al. 2017; Keeney 2001). After DSB induction, Spo11 remains covalently attached to the 5' end of the break (Keeney and Kleckner 1995). Spo11 is removed by cleavage of a short oligonucleotide segment covalently attached to Spo11, leaving 3' single-strand overhangs (Figure 3) (Neale et al. 2005). Mre11 and/or Sae2 release SPO11 oligos, by cleaving DNA on either side of SPO11, producing single-strand DNA (Garcia et al. 2011). Single-strand DNA is further resected, mediated by 5'-3' exonuclease Mre11 and Exo1, resulting in 3' single-strand DNA ends (Mimitou and Symington 2008; Trujillo et al. 1998). Like budding yeast, the mechanisms and proteins that mediate DSBs are conserved in mouse, including SPO11 (Neale et al. 2005).

Single-stranded DNA ends that result from end resection provide a good substrate for homologous recombination (HR) repair proteins (Humphryes and

Figure 3

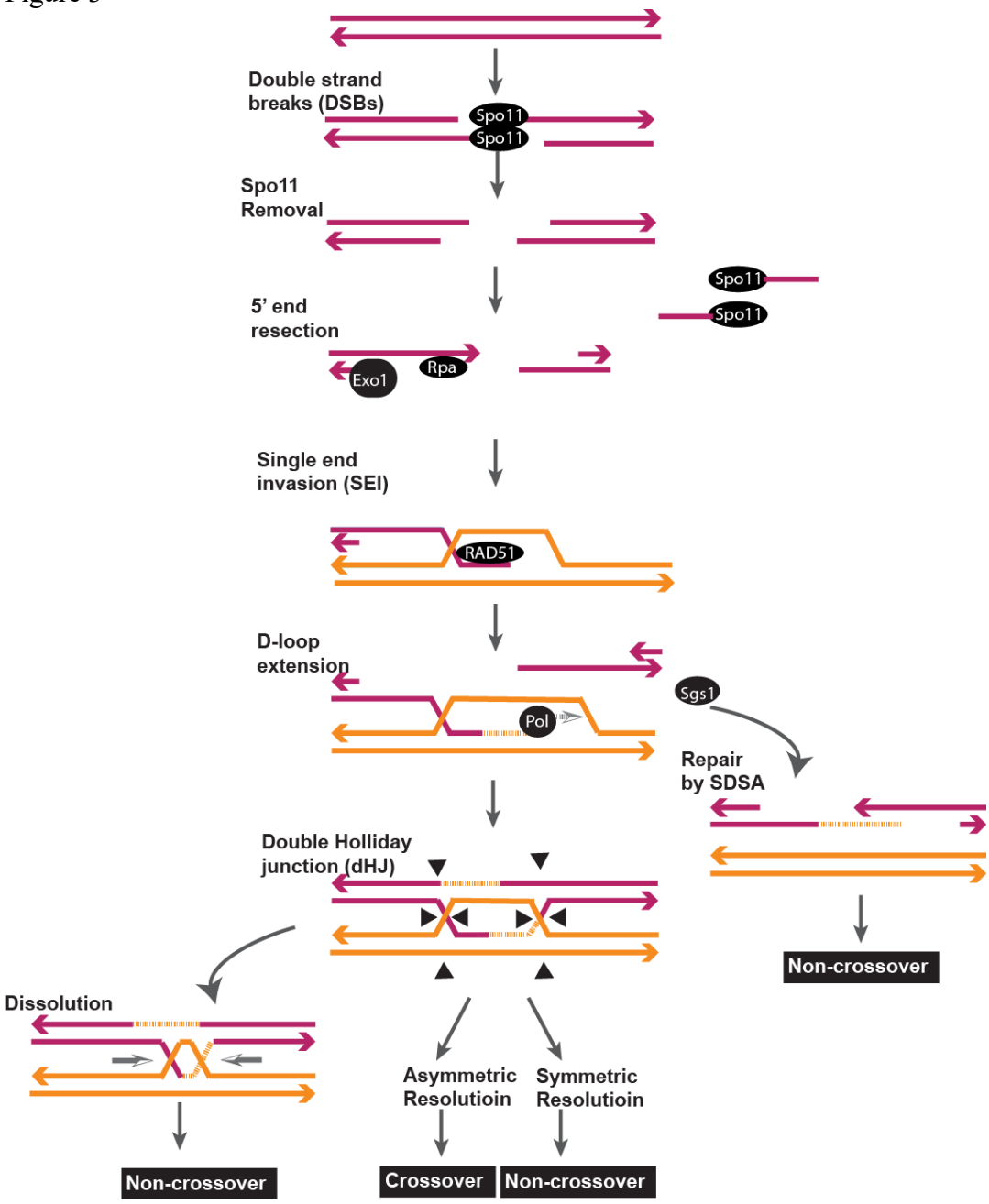

Model of meiotic DSB repair.
Meiotic double strand break repair model adapted from Szostak and contemporary studies. Maroon and orange lines represent homologous chromatids; arrowhead points toward 5' end of DNA depicts polarity. Each DSB repair intermediate step is named on the top left of each cartoon structure. Black ovals represent a protein that facilitates that repair intermediate. Each protein shown here is conserved in mouse meiosis, and these proteins have the same name (with the exception of Sgs1, which is named BLM in mouse and humans). Dashed DNA tract represents new synthesis. Gray arrows associated with a protein depicts the direction of that protein movement. Black arrow heads on dHJ molecule represents possible resolvase cut sites. Gray arrow between Holliday junctions in Dissolution step represent branch migration.

Hochwagen 2014). HR proteins drive the repair of these 3' single stranded ends,

maintaining genome integrity. Mediated by RecA homologs, RAD51 and DMC1 in mouse and budding yeast, single-strand DNA invades neighboring DNA in search of homology (Symington 2002; Trujillo et al. 1998; Bishop et al. 1992; Shinohara et al. 1992) (Figure 3). The invasion of a 3' end into a neighboring DNA molecule forms a D-loop DNA repair intermediate molecule (Gupta et al. 1997; Sehorn et al. 2004). After invasion of a homologous partner, the D-loop can be extended by the action of polymerase, utilizing the homologous chromatid as the donor DNA (Li et al. 2009) (Figure 3).

Unlike a mitotic cell, in which the sister chromatid is the preferred repair template, the meiotic cell prefers invasion of a homologous chromosome in search of a repair template (Lao et al. 2013). This shutdown of inter-sister repair is driven, in part, by SC associated proteins in yeast, and by the resulting close proximity of the homolog (Humphryes and Hochwagen 2014). Similarly in mouse the homologous chromosome is the preferred repair template in meiosis and inter-sister repair is shut down. This is instituted in part by, a group of proteins that associate with the LE of the SC called HORMADS (Wojtasz et al. 2009). The genome-wide search for homology is thought to be essential for homolog pairing, and ultimately the overall organization of homolog pairs early in prophase I. The D-loop is a key structure in the search for homology, allowing for the identification of the homologous partner by mediating downstream repair via the homologous template.

The first distinction between NCO and CO repair fate hinges on the stabilization, or destabilization of initial D-loop structures, and later extended D-loop structures. In yeast, the majority of D-loop intermediate structures are dismantled by the SgsI helicase protein and are subsequently repaired as non-COs via the synthesis-dependent strand annealing (SDSA) repair pathway (McMahill et al. 2007). Similarly

in mouse, BLM helicase is responsible for driving NCO repair in mouse (De Muyt et al. 2012).

DSB repair is exquisitely regulated to ensure that the proper number of COs occur (Anderson, Oke, Yam, Zhuge, & Fung, 2015; Baudat & de Massy, 2007). The major Class I and Class II CO repair pathways are largely conserved among budding yeast and mice, however the regulation of these pathways is distinct between budding yeast and mice (Argueso, Wanat, Gemici, & Alani, 2004; Holloway, Booth, Edelmann, McGowan, & Cohen, 2008; Lipkin et al., 2002). In yeast, about 150 DSBs initiate and only about half of these will repair as COs. In mouse, the ratio of DSBs induced to the number of COs that form is even more dramatic, where around 300 DSBs are initiated and only 20-30 will repair as COs (Lange et al. 2016).

In yeast, Class II COs arise prior to pachytene, from the resolution of single HJ structures by structure specific endonuclease Mus81-Mms4 (Figure 3) (Matos and West 2014; de los Santos et al. 2003; Jessop and Lichten 2008). These Class II COs in yeast are thought to be necessary for preventing excess heteroduplex DNA between homologs, which prevents their later segregation (Schwartz & Heyer, 2011; West et al., 2015; Zakharyevich, Tang, Ma, & Hunter, 2012). In mouse, MUS81-EME1 are responsible for Class II COs, however it remains unclear at what time these COs repair (Holloway et al. 2008).

A subset of extended D-loop structures undergo second-end capture, to mature into a double Holliday Junction (dHJ) (Figure 3). The repair of a dHJ can result in both CO and NCO depending on the pattern of cleavage, such that only the asymmetric resolution of a dHJ will result in a CO (Szostak et al. 1983). In yeast, Class I COs occur resolve from dHJ after entry into pachynema (Hunter & Kleckner, 2001). The asymmetric resolution of dHJs in yeast and mouse is driven by the Class I CO pathway during pachytene (Zakharyevich et al. 2012; Manhart and Alani 2016;

Hunter and Kleckner 2001). The timing of Class I CO resolution is less clear in mouse, but this repair is likely to also occur after entry into pachynema. In yeast and in mouse Class I COs are drive by MutLγ (Lipkin et al. 2002; Nishant et al. 2008; Wang et al. 1999; Hunter and Borts 1997). To understand the different utilization of the Class I CO pathway between budding yeast and mouse, it is important to understand the mechanisms driving MutLγ activity.

Class I COs are established by Zip-Msh4-Msh5 (ZMM) proteins in S. cerevisiae

In yeast, the Zip-Msh4-Msh5 (ZMM) interacting proteins coordinate CO repair in the context of SC assembly (Lynn et al. 2007). The ZMM proteins include Zip1, Zip2, Zip3, Zip4 (also known as Spo22), Spo16, Msh4, Msh5, and Mer3 (Lynn et al. 2007; Nakagawa and Ogawa 1999; Edelmann et al. 1999; Voelkel-Meiman et al. 2015; Sym et al. 1993; Chua and Roeder 1998). Each member plays a role in either SC assembly or DSB repair, and together they coordinate the interference observed in the Class I COs (Lynn et al. 2007).

Zip1, the transverse filament of the SC in yeast, is not only the building block necessary for synapsis, but is necessary for the CO repair (Sym et al. 1993). Zip1 is necessary to progress yeast through meiosis and loss of Zip1 is considered nonviable. Upon perturbation of the cell cycle, Zip1Δ cells can be forced through meiosis, and in this case CO structures are rarely observed (Sym et al. 1993). Loss of Zip2, Zip3, or Zip4 results in homologs that pair, but fail to synapse, and COs are lost (Tsubouchi et al. 2006; Agarwal and Roeder 2000; Chua and Roeder 1998). Zip3 is a SUMO E3 ligase associated with synapsis initiation sites and is essential for the recruitment of Zip2 and Zip4 (Agarwal and Roeder 2000). In association to the SC, Zip2, Zip3 and

Zip4 direct the remaining ZMM proteins, which function directly on DNA to mediate CO repair.

CO locations are established by Msh4-Msh5 and Mer3 (Nishant et al. 2010). Mer3 is a helicase that can unwind DNA and catalyzes the unwinding of Holliday junctions to promote CO formation (Nakagawa and Ogawa 1999; Börner et al. 2004). Msh4 and Msh5 are meiosis specific MMR homologs that form the MutSγ complex required to stabilize DNA intermediates. *In vitro*, the MutSγ heterodimer forms a clamp around two DNA molecules (Snowden et al. 2004). Disruption of either of these genes (*Msh4* or *Msh5*) results in disruption of early homolog pairing and alignment events essential for proper synapsis, resulting in a 2-3 fold reduction of CO structures in yeast (Hollingsworth et al. 1995; Novak et al. 2001). MutSγ *in vivo* functions to stabilize SEI intermediates, the first critical distinction between CO and NCO fate in DSB repair (Börner et al. 2004).

Zip2 and Zip4 are associated with synapsis initiation between homologs (Tsubouchi et al. 2006; Chua and Roeder 1998). Zip2, Zip3, and (later) Zip4 localize to the SC as foci that demonstrate interference similar to the interference observed in Class I COs (Tsubouchi et al. 2006; Agarwal and Roeder 2000; Chua and Roeder 1998). This suggests that ZMM proteins establish interference early in DSB repair. Msh4 and Msh5 also localize to the SC as foci, demonstrating interference properties (Fung et al. 2004). This suggests that MutSγ is a major player in driving the interference properties of CO repair associated with ZMM proteins. The remaining COs generated in the absence of Msh4 or Msh5 are not subject to interference and are largely attributed to structure specific endonucleases such as Mus81 (de los Santos et al. 2003). Msh4 and Msh5 function in coordination with ZMM proteins to stabilize CO locations, preserving a pool of joint molecule intermediates with the potential for later repair as COs.

The last ZMM protein, Spo16, binds with Zip2 and Zip4 to form a complex able to bind to structure specific DNA intermediates (Arora and Corbett 2018). In the absence of Spo16, COs are reduced, and those that do form display interference (Shinohara et al. 2008). The action of Spo16 is therefore attributed to CO assurance, the mechanism by which the obligate CO constructed (Shinohara et al. 2008).

Together, ZMM proteins and SC formation provide the proper environment to generate the interfering Class of COs between homologs. In mouse there is also a tight relationship between the SC formation and CO repair. SYCP1 is the Zip1 equivalent in mouse, functioning as the transverse filament that allows for synapsis in mouse SC (Moses et al. 1984). Similarly, in mice most *Sycp1*$^{-/-}$ spermatocyte populations fail to progress to diakinesis, but those that do appear to only have univalent chromosomes (de Vries et al. 2005). These results identify synapsis as necessary for chiasmata formation during diakinesis in spermatocytes. Of the yeast ZMM proteins, only MSH4, MSH5, MER3, and SPO16 have direct orthologs in mouse (Guiraldelli et al. 2013; Zhang et al. 2019; de Vries et al. 1999; Kneitz et al. 2000; Edelmann et al. 1999). Instead of Zip1, Zip2, Zip3, and Zip4 mouse have adopted proteins which serve as functional equivalents. CO regulation in mouse is discussed in detail below.

Establishment and regulation COs in mouse

In mouse spermatocytes, MutLγ foci appear on the SC during mid-pachytene, in frequencies consistent with the final generated COs (Lipkin et al. 2002). Like yeast, mouse MutLγ COs exhibit interference and are tightly regulated (Gray and Cohen 2016). The remaining 10% of COs that remain when MutLγ activity is lost are attributed to the Class II structure specific endonucleases, including MUS81-EME,1 and do not exhibit interference (Holloway et al. 2008). CO control is well conserved

and MutLγ also predominates the formation of COs in humans (Hassold and Hunt 2001; Xu et al. 2010; Pashaiefar et al. 2013).

Many ZMM proteins identified in yeast are conserved in mouse meiosis, including MSH4-MSH5 MutSγ. MSH4 and MSH5 in mouse has not function in canonical mismatch repair, and is instead needed during meiosis (Kneitz et al. 2000; Edelmann et al. 1999; de Vries et al. 1999). Loss of MSH4 or MSH5 in mouse results in early cell death prior to CO formation and direct evidence for MutSγ function in establishing CO locations remains unclear (Kneitz et al. 2000; Edelmann et al. 1999). In mouse spermatocytes, MutSγ associates with the SC in leptotene and zygotene, remaining associated until pachytene. Initially, MutSγ foci are abundant, with about 150 foci on the SC in zygonema. As prophase I progresses, the observed MutSγ foci on the SC decline and by pachynema, the number of MutSγ foci on the SC is about double the frequency of MutLγ foci (Santucci-Darmanin et al. 2000).

The extensive regulation of Class I COs ensures the proper CO amount. This regulation includes crosstalk between Class I and Class II crossover pathways. This is evident in mice carrying mutations in MUS81, such that loss of MUS81 results in an elevated MutLγ association to the SC in pachynema spermatocytes, as well as a WT number of crossovers at diakinesis. Furthermore, loss of both MLH3 and MUS81 results in fewer remaining COs at diakinesis, suggesting that a third CO pathway may exist in mammals (Holloway et al. 2008).

Multiple proteins exist that are known to affect CO amounts, including orthologs of the yeast ZMM proteins. RNF212, similar to Zip3 in yeast, is a SUMO E3 ligase that functions in conjunction with the SC to regulate COs (Reynolds et al. 2013). In mouse spermatocytes, loss of RNF212 results in the loss of COs (Reynolds et al. 2013). RNF212 foci that appear on the SC display interference and a subset of RNF212 foci colocalize with MutSγ foci (Reynolds et al. 2013). Only the MutSγ foci

that colocalize with RNF212 persist into pachytene, suggesting RNF212 functions with MutSγ to establish CO locations (Qiao et al. 2014). HEI10, a ubiquitin ligase, also functions to regulate COs in mouse (Qiao et al. 2014). Normally, HEI10 localizes to a subset of RNF212-MutSγ associated locations and when HEI10 is absent, RNF212-MutSγ persist, and COs are reduced, suggesting that HEI10 is essential to establish CO locations (Qiao et al. 2014).

These observations suggest CO regulators such as HEI10 and RNF212 function to modify the number of MutSγ positions, and likely for later MutLγ driven CO events. However due to the early spermatocyte cell death in mice, direct evidence for MutSy function during CO repair remains to be seen.

Our understanding of MutS in vitro and our understanding of in vivo conservation-regulation

MSH4 and MSH5 share structural homology with canonical MutS homologs (Figure 4A-B) (Rakshambikai, Srinivasan, & Nishant, 2013). The MutS homologs come together as heterodimers to form a complete circular clamp around DNA (Figure 4A) (Jiricny, 2000; Obmolova, Ban, Hsieh, & Yang, 2000). Five domains are highly conserved among MutS homologs (Figure 4B) (Kunkel & Erie, 2005; Tachiki et al., 1998). Domains I and IV are important for DNA mismatch recognition. Domain V contains residues necessary for ATP binding and hydrolysis. Domain III connects nucleotide binding sites in domain V to DNA binding domain IV through domain II. Domain II has structural similarities to RNase H and likely contribute to substrate binding. The eukaryotic MutSγ subunits maintain all of these domains except for domain I, which is important for mismatch DNA recognition (Rakshambikai, Srinivasan, & Nishant, 2013). The loss of this domain, as in MSH4-MSH5, is

Figure 4

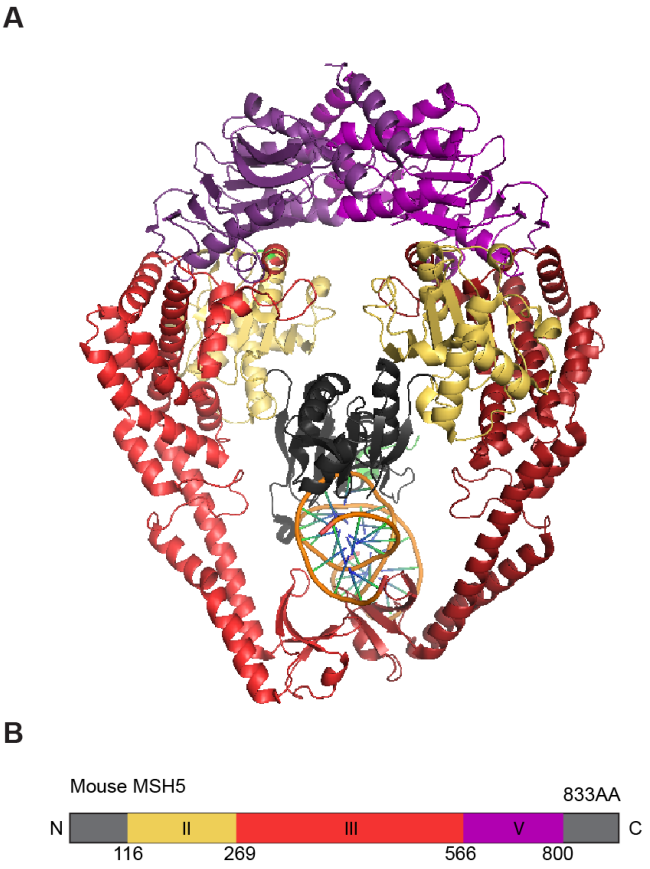

The major MutS domains are largely conserved in mouse MSH5 protein.
(A) Crystal structure of MutS complex bound to mismatch DNA in *E. coli.* This complex is a homodimer of two MutS subunits. Each domain is labeled. Domain I in black, this is the only domain not present in MSH5. Domain II is in yellow, Domain III is in red, domain V containing ATP biding domain is in purple. (B) Map of mouse MSH5 peptide chain with domains positioned relative to each other. Blue depicts the last 38 amino acids of the C – terminus.

predicted to form a clamp protein with a central cavity large enough to encircle two double-strand DNA molecules instead of just one (Kunkel & Erie, 2005; Rakshambikai et al., 2013; Snowden, Acharya, Butz, Berardini, & Fishel, 2004).

In humans, MSH4 and MSH5 form a novel heterodimer (Bocker et al. 1999). Both MSH4 and MSH5 lack domain I, which is important for mismatch DNA binding. Moreover, both contain domain II-V and there is a mammalian specific C-terminus that is highly conserved among mammals and partially conserved in yeast (Chapter 3) (Rakshambikai et al. 2013).

MutSγ has been shown to bind to SEI and dHJ substrates *in vitro* (Lahiri et al. 2018). Purified human MutSγ *in vitro* bind to Holliday junction structures and, upon ATP binding, forms a sliding clamp moving away from the HJ, in an ATP independent manner (Snowden et al. 2004; Snowden et al. 2008). The substrate for MutSγ *in vivo* remains to be identified.

The objective of this thesis is an investigation of MutSγ

Currently, it is thought that MutSγ stabilizes an excess of potential CO repair sites upstream of MutLγ. Through the analysis of two mutant mouse models, each with a unique mutation in MSH5, this work seeks to present a novel understanding of MutSγ function in mammalian meiosis. The hypothesis is that MutSγ is a critical component of mammalian CO formation.

The first mouse line under consideration is an ATP binding mutant of the MutSγ subunit MSH5 ($Msh5^{GA}$), which harbors a point mutation in the P-loop of the ATPase domain of MSH5. This point mutation appears to disrupt meiotic recombination but allows cells to progress further in meiotic prophase I, thus alleviating the earlier loss of spermatocytes in the n $Msh5^{-/-}$ animals. Analysis of prophase I progression in $Msh5^{GA/GA}$ spermatocytes by chromosome spread analysis revealed abnormal pairing/synapsis between non-homologous chromosomes in $Msh5^{GA/GA}$ spermatocytes and is presented in Chapter 2 of this thesis.

Furthermore, we observe persistent DNA damage late into prophase I compared to $Msh5^{+/+}$ spermatocytes, as well as an abnormal retention of homologous recombination repair intermediates on chromosomes of $Msh5^{GA/GA}$ spermatocytes. Normally, MutSγ is tightly associated with Class I repair events and, through localization studies, has been suggested to account for 90% of observable chiasmata. Surprisingly, in $Msh5^{GA/GA}$ spermatocytes, all chiasmata are lost or fail to form in these

mutant spermatocytes. This suggests that MSH5 ATP binding is necessary for all CO events.

A second mouse has a truncation of the last 38 amino acids of a conserved C-terminal of MSH5, is discussed in Chapter 3 of this thesis. This mouse line has infertility phenotypes, a result that identifies this domain as essential for MutSγ function. Meiosis in mice homozygous for the C-terminal mutation thus far has shown that loss of MSH5 C-terminus does not impede meiotic progression (as it does in the full *Msh5*$^{-/-}$ animals), suggesting that the C-terminal domain is not important for early meiotic functions of MutSγ. Currently, analysis of crossover progression in these mutants is underway to see how loss of MSH5 C-terminal domain affects crossover progression.

REFERENCES

Acharya, S., Foster, P.L., Brooks, P., & Fishel, R. 2003. The coordinated functions of the E. coli MutS and MutL proteins in mismatch repair. *Molecular Cell 12*(1), pp. 233–246.

Agarwal, S., & Roeder, G.S. 2000. Zip3 provides a link between recombination enzymes and synaptonemal complex proteins. *Cell 102*(2), pp. 245–255.

Arana, M.E., & Kunkel, T.A. 2010. Mutator phenotypes due to DNA replication infidelity. *Seminars in Cancer Biology 20*(5), pp. 304–311.

Au, K.G., Welsh, K., & Modrich, P. 1992. Initiation of methyl-directed mismatch repair. *The Journal of Biological Chemistry 267*(17), pp. 12142–12148.

Bocker, T., Barusevicius, A., Snowden, T., Rasio, D., Guerrette, S., Robbins, D., ... Fishel, R. 1999. hMSH5: a human MutS homologue that forms a novel heterodimer with hMSH4 and is expressed during spermatogenesis. *Cancer Research 59*(4), pp. 816–822.

Carraway, M. and Marinus, M.G. 1993. Repair of heteroduplex DNA molecules with multibase loops in Escherichia coli. *Journal of Bacteriology 175*(13), pp. 3972–3980.

Chua, P.R., & Roeder, G.S. 1998. Zip2, a meiosis-specific protein required for the initiation of chromosome synapsis. *Cell 93*(3), pp. 349–359.

De Vries, F.A.T., de Boer, E., van den Bosch, M., Baarends, W.M., Ooms, M., Yuan, L., ... Pastink, A. 2005. Mouse Sycp1 functions in synaptonemal complex assembly, meiotic recombination, and XY body formation. *Genes & Development 19*(11), pp. 1376–1389

Dohet, C., Wagner, R. & Radman, M. 1986. Methyl-directed repair of frameshift mutations in heteroduplex DNA. *Proceedings of the National Academy of Sciences of the United States of America 83*(10), pp. 3395–3397.

Gray, S. & Cohen, P.E. 2016. Control of Meiotic Crossovers: From Double-Strand Break Formation to Designation. *Annual Review of Genetics*.

Gupta, R.C., Bazemore, L.R., Golub, E.I. & Radding, C.M. 1997. Activities of human recombination protein Rad51. *Proceedings of the National Academy of Sciences of the United States of America 94*(2), pp. 463–468.

Handyside, A.H., Montag, M., Magli, M.C., Repping, S., Harper, J., Schmutzler, ... Geraedts, J. 2012. Multiple meiotic errors caused by predivision of chromatids in women of advanced maternal age undergoing in vitro fertilisation. *European Journal of Human Genetics 20*(7), pp. 742–747.

Hassold, T. & Hunt, P. 2001. To err (meiotically) is human: the genesis of human aneuploidy. Nature Reviews. *Genetics 2*(4), pp. 280–291.

Henderson, K.A. Keeney, S. 2004. Tying synaptonemal complex initiation to the formation and programmed repair of DNA double-strand breaks. *Proceedings of the National Academy of Sciences of the United States of America 101*(13), pp. 4519–4524.

Hollingsworth, N.M., Ponte, L. & Halsey, C. 1995. MSH5, a novel MutS homolog, facilitates meiotic reciprocal recombination between homologs in Saccharomyces cerevisiae but not mismatch repair. *Genes & Development 9*(14), pp. 1728–1739.

Holloway, J.K., Booth, J., Edelmann, W., McGowan, C.H. & Cohen, P.E. 2008. MUS81 generates a subset of MLH1-MLH3-independent crossovers in mammalian meiosis. *PLoS Genetics 4*(9), p. e1000186.

Holloway, J.K., Sun, X., Yokoo, R., Villeneuve, A.M. & Cohen, P.E. 2014. Mammalian CNTD1 is critical for meiotic crossover maturation and deselection of excess precrossover sites. *The Journal of Cell Biology 205*(5), pp. 633-641.

Hunt, P.A., & Hassold, T.J. 2008. Human female meiosis: what makes a good egg go bad? *Trends in Genetics 24*(2), pp. 86–93.

Jeong, C., Cho, W.-K., Song, K.-M., Cook, C., Yoon, T.-Y., Ban, C., ... Lee, J.-B. 2011. MutS switches between two fundamentally distinct clamps during mismatch repair. *Nature Structural & Molecular Biology 18*(3), pp. 379–385.

Ji, G., Long, Y., Zhou, Y., Huang, C., Gu, A., &Wang, X. 2012. Common variants in mismatch repair genes associated with increased risk of sperm DNA damage and male infertility. *BMC Medicine 10*, p. 49.

Kauppi, L., Barchi, M., Lange, J., Baudat, F., Jasin, M., & Keeney, S. 2013. Numerical constraints and feedback control of double-strand breaks in mouse meiosis. *Genes & Development 27*(8), pp. 873–886.

Keeney, S. 2001. Mechanism and control of meiotic recombination initiation. *Current Topics in Developmental Biology 52*, pp. 1–53.

Lahiri, S., Li, Y., Hingorani, M.M., & Mukerji, I. 2018. MutSγ-Induced DNA Conformational Changes Provide Insights into Its Role in Meiotic Recombination. *Biophysical Journal 115*(11), pp. 2087–2101.

Lahue, R.S., Su, S.S., & Modrich, P. 1987. Requirement for d(GATC) sequences in Escherichia coli mutHLS mismatch correction. *Proceedings of the National Academy of Sciences of the United States of America 84*(6), pp. 1482–1486.

Lao, J.P., Cloud, V., Huang, C.-C., Grubb, J., Thacker, D., Lee, C.-Y., ... Bishop, D.K. 2013. Meiotic crossover control by concerted action of Rad51-Dmc1 in homolog template bias and robust homeostatic regulation. *PLoS Genetics 9*(12), p. e1003978.

Learn, B.A., & Grafstrom, R.H. 1989. Methyl-directed repair of frameshift heteroduplexes in cell extracts from Escherichia coli. *Journal of Bacteriology 171*(12), pp. 6473–6481.

Lebbink, J.H.G., Fish, A., Reumer, A., Natrajan, G., Winterwerp, H.H.K., & Sixma, T.K. 2010. Magnesium coordination controls the molecular switch function of DNA mismatch repair protein MutS. *The Journal of Biological Chemistry 285(*17), pp. 13131–13141.

Lipkin, S.M., Moens, P.B., Wang, V., Lenzi, M., Shanmugarajah, D., Gilgeous, A., ... Cohen, P.E. 2002. Meiotic arrest and aneuploidy in MLH3-deficient mice. *Nature Genetics 31*(4), pp. 385–390.

Lynn, A., Soucek, R., & Börner, G.V. 2007. ZMM proteins during meiosis: crossover artists at work. *Chromosome Research 15*(5), pp. 591–605.

Mandon-Pépin, B., Touraine, P., Kuttenn, F., Derbois, C., Rouxel, A., Matsuda, F., … Fellous, M. 2008. Genetic investigation of four meiotic genes in women with premature ovarian failure. *European Journal of Endocrinology 158*(1), pp. 107–115.

McMahill, M.S., Sham, C.W., & Bishop, D.K. 2007. Synthesis-dependent strand annealing in meiosis. *PLoS Biology 5*(11), p. e299.

Mendillo, M.L., Hargreaves, V.V., Jamison, J.W., Mo, A.O., Li, S., Putnam, C.D., ... Kolodner, R.D. 2009. A conserved MutS homolog connector domain interface interacts with MutL homologs. *Proceedings of the National Academy of Sciences of the United States of America 106*(52), pp. 22223–22228.

Mimitou, E.P., & Symington, L.S. 2008. Sae2, Exo1 and Sgs1 collaborate in DNA double-strand break processing. *Nature 455*(7214), pp. 770–774.

Nakagawa, T., & Ogawa, H. 1999. The Saccharomyces cerevisiae MER3 gene, encoding a novel helicase-like protein, is required for crossover control in meiosis. *The EMBO Journal 18*(20), pp. 5714–5723

Novak, J.E., Ross-Macdonald, P.B., & Roeder, G.S. 2001. The budding yeast Msh4 protein functions in chromosome synapsis and the regulation of crossover distribution. *Genetics 158(3)*, pp. 1013–1025.

Parker, J., Precup, J., & Fu, C. 1992. Misreading of the argI message in Escherichia coli. *FEMS Microbiology Letters 100*(1-3), pp. 141–145.

Qiao, H., Prasada Rao, H.B.D., Yang, Y., Fong, J.H., Cloutier, J.M., Deacon, D.C., ... Hunter, N. 2014. Antagonistic roles of ubiquitin ligase HEI10 and SUMO ligase RNF212 regulate meiotic recombination. *Nature Genetics 46*(2), pp. 194–199.

Reynolds, A., Qiao, H., Yang, Y., Chen, J.K., Jackson, N., Biswas, ... Hunter, N. 2013. RNF212 is a dosage-sensitive regulator of crossing-over during mammalian meiosis. *Nature Genetics 45*(3), pp. 269–278.

Sehorn, M.G., Sigurdsson, S., Bussen, W., Unger, V.M., & Sung, P. 2004. Human meiotic recombinase Dmc1 promotes ATP-dependent homologous DNA strand exchange. *Nature 429*(6990), pp. 433–437.

Snowden, T., Acharya, S., Butz, C., Berardini, M., & Fishel, R. 2004. hMSH4-hMSH5 recognizes Holliday Junctions and forms a meiosis-specific sliding clamp that embraces homologous chromosomes. *Molecular Cell 15*(3), pp. 437–451.

Snowden, T., Shim, K.-S., Schmutte, C., Acharya, S., & Fishel, R. 2008. hMSH4-hMSH5 adenosine nucleotide processing and interactions with homologous

recombination machinery. *The Journal of Biological Chemistry 283*(1), pp. 145–154.

Su, S.S., & Modrich, P. 1986. Escherichia coli mutS-encoded protein binds to mismatched DNA base pairs. *Proceedings of the National Academy of Sciences of the United States of America 83*(14), pp. 5057–5061.

Sym, M., Engebrecht, J.A., & Roeder, G.S. 1993. ZIP1 is a synaptonemal complex protein required for meiotic chromosome synapsis. *Cell 72*(3), pp. 365–378.

Trujillo, K.M., Yuan, S.S., Lee, E.Y., & Sung, P. 1998. Nuclease activities in a complex of human recombination and DNA repair factors Rad50, Mre11, and p95. *The Journal of Biological Chemistry 273*(34), pp. 21447–21450.

Tsubouchi, T., Zhao, H., & Roeder, G.S. 2006. The meiosis-specific zip4 protein regulates crossover distribution by promoting synaptonemal complex formation together with zip2. *Developmental Cell 10*(6), pp. 809–819.

Welsh, K.M., Lu, A.L., Clark, S., & Modrich, P. 1987. Isolation and characterization of the Escherichia coli mutH gene product. *The Journal of Biological Chemistry 262*(32), pp. 15624–15629.

Wojtasz, L., Daniel, K., Roig, I., Bolcun-Filas, E., Xu, H., Boonsanay, ...Toth, A. 2009. Mouse HORMAD1 and HORMAD2, two conserved meiotic chromosomal proteins, are depleted from synapsed chromosome axes with the help of TRIP13 AAA-ATPase. *PLoS Genetics 5*(10), p. e1000702

CHAPTER 2

MUTATION OF THE ATPase DOMAIN OF THE MutS HOMOLOG-5 (MSH5) REVEALS A REQUIREMENT OF A FUNCTIONAL MutSγ COMPLEX FOR ALL CROSSOVERS IN MAMMALIAN MEIOSIS

Abstract

During meiosis, induction of DNA double strand breaks (DSB) leads to recombination between homologous chromosomes, resulting in crossovers (CO) and non-crossovers (NCO). In the mouse, only 10% of DSBs resolve as COs, mostly through a class I pathway dependent on MutSγ (MSH4-MSH5) and MutLγ (MLH1/MLH3), the latter representing the ultimate marker of these CO events. A second Class II CO pathway accounts for only a few COs, but is not thought to involve MutSγ/ MutLγ, and is instead dependent on MUS81-EME1. For class I events, loading of MutLγ is thought to be dependent on MutSγ, however MutSγ loads very early in prophase I at a frequency that far exceeds the final number of class I COs. Moreover, loss of MutSγ in mouse results in apoptosis before CO formation, preventing analysis of its CO function. We generated a mutation in the ATP binding domain of *Msh5* (*Msh5*^{GA}). While this mutation was not expected to affect MutSγ complex formation, MutSγ foci do not accumulate during prophase I. However, most spermatocytes from *Msh5*$^{GA/GA}$ mice progress to late pachynema and beyond, considerably further than meiosis in *Msh5*$^{-/-}$ animals. At pachynema, *Msh5*$^{GA/GA}$ spermatocytes show persistent DSBs, incomplete homolog pairing, and fail to accumulate MutLγ. Unexpectedly, *Msh5*$^{GA/GA}$ diakinesis-staged spermatocytes have no chiasmata at all from any CO pathway, indicating that a functional MutSγ complex is critical for all CO events regardless of their mechanism of generation.

Credits

The work in this Chapter is done a collaboration between Carolyn R. Milano[1], J. Kim Holloway[1], Yongwei Zhang[2], Bo Jin[2], Cameron Smith[3], Aviv Bergman[3], Winfried Edelmann[2], and Paula E. Cohen[1]. The mouse line was created an maintained by Winfried Edelmann, Aviv Bergaman, Cameron Smith, Bo Jin, and Yongwei Zhang. The mouse analysis, including weights, spermcoutns and testis histology were conducted by Carolyn Milano. Immunofluorescence and analysis were done by Carolyn Milano. Diakinesis preparations and analysis was done by Kim Holloway.

[1]Department of Biomedical Sciences and Center for Reproductive Genomics, Cornell University, Ithaca, NY 14853; Departments of [2]Cell Biology, [3]Systems and Computational Biology, Albert Einstein College of Medicine, Bronx, NY 10461

Introduction

MSH5 (MutS homolog 5) belongs to the DNA mismatch repair (MMR) family of proteins that perform multiple DNA repair activities, most prominently the correction of mispaired bases that result from erroneous DNA replication (Modrich & Lahue, 1996). Like other family members, MSH5 acts with a MutS homolog partner, specifically with MSH4, to form the MutSγ heterodimer (Bocker et al., 1999). Unlike other MutS heterodimers, MutSγ does not participate in mismatch correction in somatic cells, but instead acts exclusively during meiotic prophase I in budding yeast, mice, humans, plants, and worms (Bocker et al., 1999; de Vries et al., 1999; Edelmann et al., 1999; Higgins et al., 2008; Kneitz et al., 2000; Pochart, Woltering, & Hollingsworth, 1997; Santucci-Darmanin & Paquis-Flucklinger, 2003; Zalevsky, MacQueen, Duffy, Kemphues, & Villeneuve, 1999),. Indeed, the heterodimer was named MutSγ, with the "γ" referring to "germ cell" (Kolas et al., 2005). Importantly, mutation of either MutSγ subunit results in infertility in humans and mice (Carlosama et al., 2017; de Vries et al., 1999; Edelmann et al., 1999; Kneitz et al., 2000). Prophase I is the defining stage of meiosis, encompassing the unique events that give rise to pairing and equal segregation of homologous chromosomes at the first meiotic division. In early prophase I, homologous chromosomes undergo a physical tethering process known as synapsis. Synapsis is mediated by the proteinaceous structure called the Synaptonemal Complex (SC) whose status defines the sub-stages of prophase I: leptonema, zygonema, pachynema, diplonema, and diakinesis. Synapsis is dependent on, and facilitated by, homologous recombination, which is triggered by the formation of DNA double strand breaks (DSBs) by the topoisomerase-like SPO11 protein and its co-factors (Baudat & de Massy, 2007; Keeney, 2008; Kim, Peterson, Jasin, & Keeney, 2016; Robert et al., 2016; Romanienko & Camerini-Otero, 2000). DSBs ends undergo resection to reveal 3' single-strand tails that become coated with the replication

protein A (RPA) which protects the potentially fragile ssDNA molecule and impairs secondary structure formation. RPA is gradually replaced by the RecA family members, RAD51 and DMC1, which promote strand invasion to search for homology in opposing chromosomes (Gray & Cohen, 2016; Neil Hunter, 2015). Strand invasion results in a nascent intermediate known as a displacement loop (D- loop), which may be resolved via multiple distinct, yet overlapping, pathways that result in either a crossover (CO) or a non-crossover (NCO) (Gray & Cohen, 2016; Neil Hunter, 2015). In mouse, the majority (approximately 90%) of the 250+ DSBs that form are processed to become NCOs, the remaining 10% being resolved as COs (Cole et al., 2014). In yeast, NCOs arise at temporally earlier time points than do the CO repair products (Allers & Lichten, 2001; Baudat & de Massy, 2007; Jessop & Lichten, 2008; Kaur, De Muyt, & Lichten, 2015).

COs can arise from several pathways down stream of DSB formation, and result in reciprocal exchange of DNA between maternal and paternal homologs, giving rise to the chiasmata that ensure equal segregation of chromosomes at the first meiotic division. Following D-loop formation, a metastable structure known as a single end invasion (SEI) arises, followed by second end capture of the other side of the DSB, to produce a double Holliday Junction (dHJ). These events are promoted through stabilization of the SEI structure by the ZMM group of proteins, of which the MutSγ constituents are members, along with Zip1-4, Mer3, and Spo16 (Lynn, Soucek, & Börner, 2007). Once formed, the dHJ must then be resolved via the action of resolvases which cleave the dHJs to release the recombined homologous chromosomes. In mouse, this is the major Class I crossover pathway, accounting for 90% of all COs, and involves resolution of the dHJ by the MutLγ heterodimer, consisting of the MMR proteins MLH1 and MLH3 (Edelmann et al., 1996; N Hunter & Borts, 1997; Lipkin et al., 2002; Nishant, Plys, & Alani, 2008; Svetlanov, Baudat,

Cohen, & de Massy, 2008; Wang, Kleckner, & Hunter, 1999). In mouse, at least one other CO pathway has been described, known as the class II pathway. Class II events account for fewer than 10% of COs in the mouse and these are dependent on the MUS81-EME1 endonuclease (Holloway, Booth, Edelmann, McGowan, & Cohen, 2008; Oh, Lao, Taylor, Smith, & Hunter, 2008). This pathway does not involve canonical dHJ formation but instead may resolve a diverse set of repair intermediates that would not ordinarily be strong substrates for the class I machinery. MutLγ and MutSγ are present on the SC during late pachynema, at a frequency and distribution that resemble class I CO numbers (Santucci-Darmanin & Paquis-Flucklinger, 2003). This suggests that, similar to other MMR complexes, MutSγ functions to recruit MutLγ to the SC during pachynema. However, MutSγ foci first appear on meiotic chromosome cores in zygonema, prior to MutLγ localization, and at frequencies that far exceed the final CO tally (approximately 150 foci, or 10-fold higher than the final MutLγ count). These cytogenetic differences in MutSγ/MutLγ appearance suggest additional early functions for MutSγ that are distinct from its interactions with MutLγ. Indeed, the meiotic phenotype of mice lacking components of either complex underscore the temporally distinct roles for each heterodimer. Prophase I spermatocytes from *Mlh1*$^{-/-}$ and *Mlh3*$^{-/-}$ male mice show normal early progression of meiosis, with cells progressing all the way through prophase I. However, by diplonema, mostly univalent chromosomes are observed in these mutants, with a 90% reduction in chiasmata frequency and loss of spermatocytes prior to the first meiotic division (Edelmann et al., 1996; Lipkin et al., 2002). By contrast, loss of Msh4 or Msh5 results in an earlier loss of prophase I progression, with almost complete failure of homologous synapsis, and cell death prior to pachynema (de Vries et al., 1999; Edelmann et al., 1999; Kneitz et al., 2000). Thus, MutSγ plays an essential role in early events of DSB repair prior to, and distinct from, its proposed role in recruiting

MutLγ. *In vitro* studies have demonstrated that the human and yeast MutSγ heterodimer can bind to D loops, HJs, single-stranded overhangs and other DNA substrates (Lahiri, Li, Hingorani, & Mukerji, 2018; Snowden, Acharya, Butz, Berardini, & Fishel, 2004). Binding to junctions enhances stability of these structures, while binding to single-stranded DNA promotes displacement of the overhang that could potentially allow for nucleoprotein filament formation involving, for example, RPA (Lahiri et al., 2018). Like all MutS heterodimers, MSH4 and MSH5 each possess an ATPase domain that, upon substrate binding, promotes ADP to ATP exchange and subsequent formation of a sliding clamp that can encircle DNA and translocate away from the binding site, potentially allowing further rounds of MutSγ binding and translocation (Snowden et al., 2004; Snowden, Shim, Schmutte, Acharya, & Fishel, 2008). To explore MSH5 ATPase function *in vivo*, we mutated a highly conserved residue within the P-loop domain of mouse *Msh5* (G to A mutation at residue 596, termed $Msh5^{GA}$), which has been shown previously to affect ATP binding by MutS homologs. A similar mutation in S. cerevisiae has no effect on the dimerization with its wild-type (WT) MSH4 partner, but reduces crossing over and spore viability (Nishant, Chen, Shinohara, Shinohara, & Alani, 2010). Based on this study, we anticipated that the G-to-A mutation within the MSH5 ATP binding domain would not affect MutSγ complex formation. Interestingly, although spermatocytes in $Msh5^{-/-}$ mice fail to progress beyond zygonema, a subset of $Msh5^{GA/GA}$ spermatocytes escape this fate, progressing through prophase I and entering metaphase I. Thus, this mutant allele allowed for the first time an investigation of the role of MSH5 in crossing over during the prophase I. Interestingly, diakinesis-staged chromosomes from spermatocytes of $Msh5^{GA/GA}$ mice show exclusively univalent chromosomes and a complete absence of chiasmata, including those residual chiasmata that would presumably arise from the class II CO (MUS81-EME1) pathway. Such residual

chiasmata are always observed in mice lacking key class I CO mediators, such as *Mlh1*$^{-/-}$ and *Mlh3*$^{-/-}$ animals (Edelmann et al., 1999; Kolas et al., 2005; Lipkin et al., 2002). These observations indicate that the ATPase domain of MSH5 is essential for MutSγ activity early in DSB repair, and that mutation of this domain results in disrupted homolog interactions and aberrant DNA repair, leading to a failure to form any COs at the end of prophase I. Thus, loss of a functional MutSγ complex impacts CO formation regardless of the chosen pathway for CO generation.

Materials and Methods

Generation of Msh5^{GA} *mice*

The mouse *Msh5* genomic locus was cloned from a P1 mouse ES cell genomic library (Genome Systems) (Edelmann et al., 1999). A 3.6 kb genomic HindIII fragment of mouse *Msh5* spanning exons 17-25 was inserted into pBluescript SK vector. Positive clones were identified by PCR. The G596A mutation and an analytic BlpI restriction site, were generated by site-directed mutagenesis in exon 19. A loxP flanked PGK hygromycin/neomycin cassette was inserted into the MscI site in intron 19. The targeting vector was linearized at the single NotI site and electroporated into WW6 ES cells. After selection in hygromycin, resistant colonies were isolated and screened by PCR. Positive clones were identified and injected into C57BL/6J blastocysts to produce chimeric animals. The PGK hygromycin/neomycin cassette was deleted by Cre-loxP- mediated recombination after mating of chimeric mice to Zp3Cre recombinase transgenic females (C57BL/6J). F1 offspring were genotyped and heterozygote animals were intercrossed to generate F2 homozygous mutant *Msh5*$^{GA/GA}$ mice and appropriate controls. Previously generated *Msh4*$^{-/+}$ and *Msh5*$^{-/+}$ mice were used for cross breeding studies to provide *Msh5*$^{-/-}$ null mice for comparison (Edelmann

et al., 1999; Kneitz et al., 2000). All *Msh4*$^{+/+}$, *Msh4*$^{-/-}$, *Msh5*$^{+/+}$, *Msh5*$^{+/-}$, *Msh5*$^{-/-}$ and *Msh5*$^{GA/GA}$ mice used in these studies were backcrossed more than 10 times onto a C57BL/6J genetic background. Due to loss of the allele, *Msh5*$^{-/-}$ null mice were not available in the latter half of these studies.

Genotyping of Msh5^{GA} *mice*

Reverse transcription-PCR was performed on total RNA isolated from mouse tails with forward primer 5' – AGACCTGCACTGTGAGATCCG – 3' (5'-18d-3') located in exon 16 and reverse primer 5'- TTGGTGGCTACAAAGACGTG-3' located in exon 22 using the One Tube reverse transcription-PCR reaction kit (Roche) according to the manufacturer's instructions. The following cycling conditions were used: 30 min at 50°C (1 cycle); 2 min at 94°C, 45 s at 60°C, and 45 s at 68°C (37 cycles); and 7 min at 68°C (1 cycle). The resulting 480 bp PCR product was subsequently restricted with BlpI.

Care and use of experimental animals

Mice were maintained under strictly controlled conditions of light and temperature, with *ad libitum* access to food and water. All experiments were conducted with prior approval from the Albert Einstein College of Medicine and Cornell Institutional Animal Care and Use Committees. At least six mice per genotype were used for all studies.

Histological analysis and TUNEL staining of mouse testis

Testes from 12 week- old mice were fixed in Bouin's fixative for 6 hours at room temperature or 10% formalin overnight at 4°C, and then washed in 70% ethanol. Fixed and paraffin-embedded tissues were sectioned at 5 μm. Hematoxylin and eosin

(H&E) staining and TUNEL staining and were performed as described previously (Holloway et al., 2008; Holloway, Morelli, Borst, & Cohen, 2010), the latter using Apoptag-peroxidase kit (Millipore).

Chromosome preparation and spreads

The testes were decapsulated and incubated in hypotonic extraction buffer (HEB; 30 mM Tris, pH 8.2, 50 mM sucrose, 17 mM trisodium citrate dihydrate, 5 mM EDTA, 0.5 mM DTT, and 0.5 mM PMSF) for 1 hour on ice. About three to five millimeters length of seminiferous tubule was transferred into a drop of 20 µl hypotonic sucrose (100 mM, pH 8.2). After adding another drop of 20 µl of sucrose the tubule was macerated and the cell suspension was pipetted up and down for about 3-4 times. Remaining tubule fragments were removed from the cell suspension. Slides were coated with 1% paraformaldehyde containing 0.15% Triton X. 20 µl of the cell suspension were dispersed across the surface of one slide containing a layer of fixative. Slides were transferred to a humid chamber for 1-2 hours at room temperature and then allowed to air dry. Slides were washed three times for 3 min (0.4% Kodak Photo-Flo 200 in water) and air-dried and stored at -80°C until use, not longer than 2 weeks.

Immunofluorescence

The slides were washed in 0.4% Kodak Photo-Flo 200 in PBS and 0.1% Triton X-100 in PBS for 5 minutes each, blocked for 10 minutes in 10% antibody dilution buffer (ADB) in PBS (ADB: 3% bovine serum albumin, 0.05% Triton in 1 x PBS)

followed by an overnight incubation in primary antibodies (at varying concentrations in ADB; Supplementary Table 1) at room temperature in a humid chamber. Slides were washed as described earlier and incubated for 1 h at 37°C in secondary fluorochrome conjugated antibodies in the dark. Primary and secondary antibodies used are listed in Supplementary table 1. All secondary antibodies were raised specifically against Fc fraction, Fab-fraction purified and conjugated to Alexafluor 594, 488, or 647.

Spermatocyte diakinesis spread preparations to observe chiasmata

Diakinesis chromosome spreads were prepared as previously described (Holloway et al., 2008; Holloway, Sun, Yokoo, Villeneuve, & Cohen, 2014). Slides were stained with 20% Giemsa for 2.5 min, washed, air-dried and mounted with Permount.

Data Availability

All mice, plasmids, and reagents created as part of this study are available on request.

Results

Generation of Msh5^{G596A} mutant mice

We generated a mouse line bearing a mutation that disrupts the conserved Walker "type A" motif GXXXXGKS/T (G refers to the modified G596 amino acid residue) in the ATPase domain of MSH5, which is important for ATP binding (Figure

Figure 5

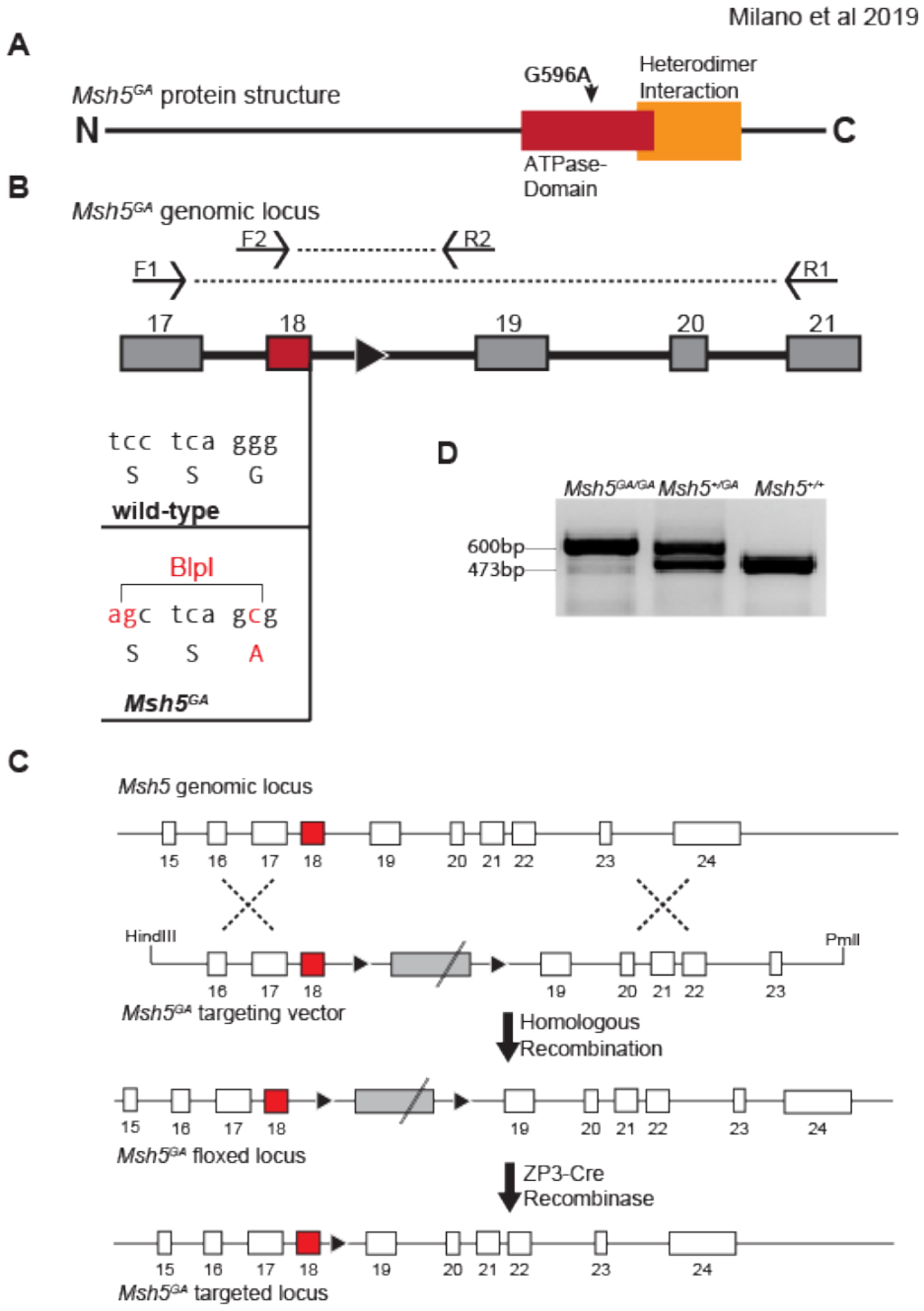

Description of the *Msh5*$^{GA/GA}$ mouse model.
(a) Cartoon of *Msh5*^{GA} predicted protein structure showing relative location of G569 point mutation in the ATPase domain. (b) Genotyping strategy for *Msh5*^{GA} mice. Primers F1 [5'-CGGGACTACGGCTATTCGAGA-3'] and R1 [5'-GGCTACAAAGACGTGGGG-3'] are used for sequencing of the allele and F2 [5'-CAGGGTCAAAGTCATCACTG-3']and R2 [5'-GGGCCATGAAAGTGATCAAG-3'] are used for genotyping. Novel RE site introduced in to exon 18 for additional genotyping conformation. (c) Gene targeting strategy used to introduce point mutation. (d) Example PCR results using primers F2 and R2 for *Msh5*$^{+/+}$, *Msh5*$^{+/GA}$, and *Msh5*$^{GA/GA}$ littermates.

5A). The targeting vector introduces a glycine to alanine change at amino acid residue

596 into exon 19 (Figure 5A,B). The mutant allele of this mouse line is designated *Msh5*^{G596A} (*Msh5*^{GA}) and was predicted to impair ATP binding in the MSH5 subunit. This mutation has previously been shown to preserve interaction with MSH4, allowing for the appropriate assembly of the MutSγ heterodimer (Nishant et al. 2010). An additional diagnostic BlpI restriction site that does not alter the amino acid sequence was generated in the *Msh5* coding regions that overlaps with the mutation (Figure 5B). Transmission of the mutant *Msh5*^{GA} allele was confirmed by PCR genotyping of genomic tail DNA and subsequent restriction of the associated BlpI site (Figure 5C,D). Likewise, RT-PCR and subsequent BlpI restriction digestion confirmed expression of the mutant transcript in *Msh5*$^{+/GA}$ and *Msh5*$^{GA/GA}$ mice (Figure 5D). In addition, while homozygous null mice lack all detectable MSH5 protein, the mutant MSH5^{GA} protein signal was found in testis extracts from both *Msh5*$^{GA/+}$ and *Msh5*$^{GA/GA}$ mice at levels similar to wildtype (WT) mice (Figure 5E). In all subsequent studies, *Msh5*$^{GA/GA}$ mutant animals were compared to *Msh5*$^{+/+}$ (WT) littermates, as well as *Msh4*$^{-/-}$ and/or *Msh5*$^{-/-}$ mice (Edelmann et al., 1999; Kneitz et al., 2000). All alleles of *Msh4* and *Msh5* were maintained on a C57Bl/6J background.

Msh5$^{GA/GA}$ *mice exhibit severely impaired meiotic progression, reduced testis size, and no spermatozoa*

Similar to *Msh5*$^{-/-}$ and *Msh4*$^{-/-}$ mice, *Msh5*$^{GA/GA}$ mice are infertile as a result of defects in meiotic prophase I. By contrast, *Msh5*$^{GA/+}$ females and males are fertile (not shown), with no change in testis weights in *Msh5*$^{GA/+}$ males compared to WT littermates (Figure 6A). Homozygous mutant *Msh5*$^{GA/GA}$ males display a 40% reduced testis size compared to their WT littermates (Figure 6A) associated with complete loss of epididymal spermatozoa (Figure 6B). Sperm production in *Msh5*$^{GA/+}$ males was similar to that of WT animals (Figure 6B). Hematoxylin and Eosin (H&E) staining of

Figure 6

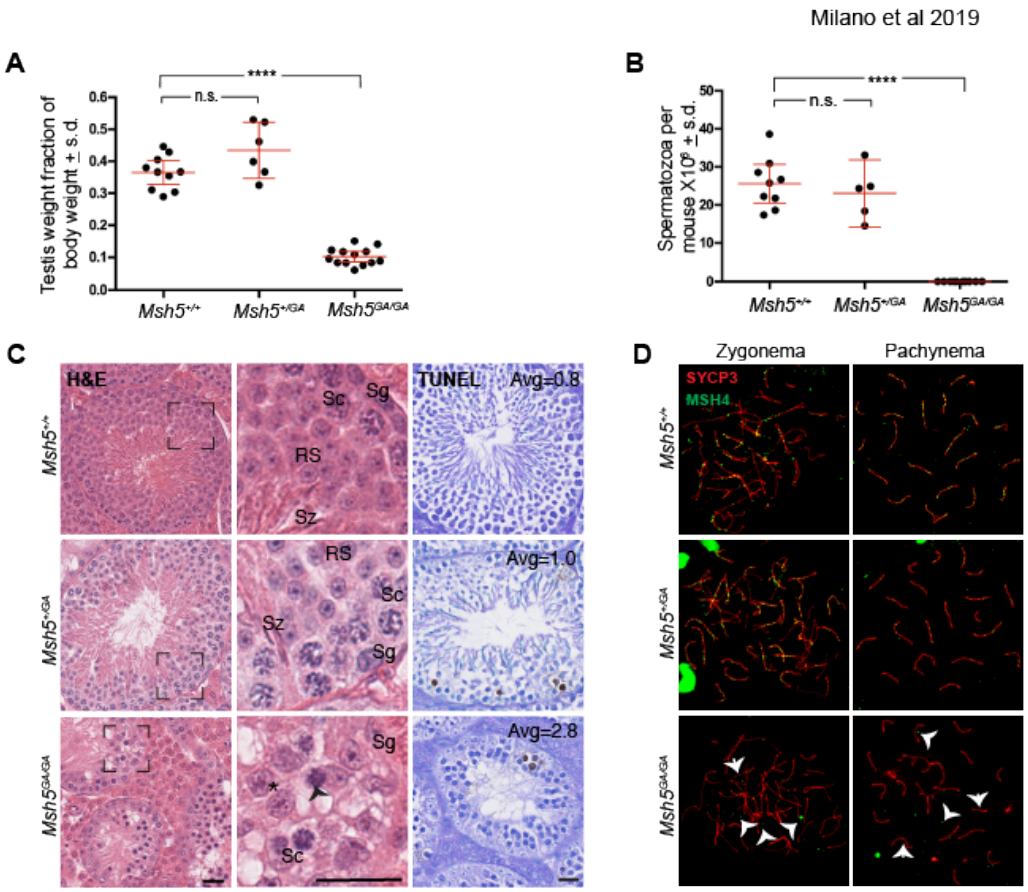

Msh5$^{GA/GA}$ mice confer an infertility phenotype that is not observed in *Msh5*$^{+/+}$ or *Msh5*$^{GA/+}$ littermates.

(a) Adult testis weights are significantly smaller in *Msh5*$^{GA/GA}$ compared to *Msh5*$^{+/+}$ littermates ($p < 0.0001$, unpaired t-test with Welch's correction) while *Msh5*$^{GA/+}$ was not found significantly smaller than wild type littermates (*Msh5*$^{GA/GA}$ –0.10% of total body weight ± 0.03, n = 13 testes; *Msh5*$^{+/+}$ - 0.37% ± 0.05, n = 10; *Msh5*$^{+/GA}$ – 0.43% ±0.08, n = 6) (n.s.-not significant, **** $p<0.0001$). *Msh5*$^{GA/GA}$ have zero epididymal sperm (b) (WT –17.4 X 106+ 6.6; $p < 0.0001$ t-test, n = 9, n = 10; error bars show standard deviation). (c) Hematoxylin and Eosin staining of paraffin-embedded testis sections from *Msh5*$^{+/+}$, *Msh5*$^{+/GA}$, and *Msh5*$^{GA/GA}$ littermates. WT and heterozygous testes show meiotic and post-meiotic cells whereas *Msh5*$^{GA/GA}$ testes are absent of spermatids and spermatozoa and apoptotic cells are observed (Sg –spermatogonial, Sc–spermatocytes, RS –Round spermatids, Sz –Spermatozoa, arrow head shows apoptotic cell; scale bar represents 25nM) Boxes in panel represent magnified image on the right. TUNEL assays reveal apoptotic cells within seminiferous tubules. *Msh5*$^{+/+}$ had less than one TUNEL positive cell/tubule (Avg=0.8) on average, *Msh5*$^{+/GA}$ were comparable and had one TUNEL positive cell per tubule (Avg=1.0), while *Msh5*$^{GA/GA}$ had 2.7 TUNEL positive cells per tubule on average. (d) MSH4 (green) staining on chromosome spreads for adult *Msh5*$^{+/+}$ and *Msh5*$^{+/GA}$ zygotene and pachytene spermatocytes show localization of MSH4 to SC (red) during zygotene and pachytene while this association between the SC and MSH4 is largely disrupted in *Msh5*$^{GA/GA}$ spermatocytes. Arrow heads in zygotene shows common localization of MSH4 with few foci associated with the SC and frequent foci of varying sizes localized away from the SC. Arrow heads in mutant pachytene spermatocytes point out faint MSH4 signal on or near the SC suggesting the association between MSH4 and SC is not entirely abolished in the mutants.

testis sections from WT adult male mice showed normal cell populations within the

seminiferous epithelium, while spermatogenesis was severely disrupted in *Msh5*$^{GA/GA}$ testis sections (Figure 6C). Testis sections from *Msh5*$^{GA/GA}$ male mice contained Leydig cells, Sertoli cells, and spermatogonia, and spermatocytes, along with a high proportion of TUNEL-positive apoptotic germ cells within the seminiferous tubules (Figure 6C). Most notably, testis sections from *Msh5*$^{GA/GA}$ males contained pachytene and post-pachytene spermatocytes (Figure 6C, bottom panels, arrow), including cells that were clearly at metaphase I (Figure 6C, bottom arrows, asterisks). This is in contrast to our previous observations in *Msh5*$^{-/-}$ and *Msh4*$^{-/-}$ males, in which the majority of the spermatocyte pool is lost at or prior to entry into pachynema (Figure 7A) (Edelmann et al., 1999; Kneitz et al., 2000). Seminiferous tubules from WT and *Msh5*$^{GA/+}$ males have an average of one or less than one TUNEL-positive cell per tubule section, while in *Msh5*$^{GA/GA}$ males, TUNEL-positive cell frequencies were higher, at 2.7 TUNEL-positive cells per tubule (Figure 7B). The important difference between the histological appearance of *Msh5*$^{GA/GA}$ tubules and that of *Msh5*$^{-/-}$ and *Msh4*$^{-/-}$ males is the increased progression into pachynema and the appearance of metaphase cells in the tubules of *Msh5*$^{GA/GA}$ males.

A functional ATP binding domain of MSH5 is important for early homolog interactions and complete homolog synapsis

To assess progression through prophase I, immunofluorescence (IF) staining was performed on chromosome spreads of spermatocytes from *Msh5*$^{+/+}$ and *Msh5*$^{GA/GA}$ adult male mice using antibodies against components of the SC, SYCP3 and SYCP1 (Figure 8A). In leptonema, the SC begins to form, with SYCP3 localization appearing in a punctate pattern along asynapsed chromosomes. Such a staining pattern was evident on leptotene chromosome preparations from mice of all genotypes (Figure 8A). Upon entry into zygonema, the transverse filaments and

central element of the SC begin to assemble, as shown by the localization of SYCP1 between the chromosome axes on chromosome spreads from both *Msh5*$^{+/+}$ and *Msh5*$^{GA/GA}$ adult male mice (Figure 8A). By pachynema, when autosomes in *Msh5*$^{+/+}$ adult males are now fully synapsed along their entire lengths, the first signs of synapsis failure become evident in *Msh5*$^{GA/GA}$ animals. While WT pachytene cells contain 20 discrete synapsed homologs, spermatocytes from *Msh5*$^{GA/GA}$ animals show variable degrees of synapsis, coupled with frequent occurrences of inappropriate synapsis between more than two chromosome partners (Figure 8A, arrowheads), indicating non-homologous synapsis events between multiple chromosomes, but also some occurrences of apparently normal homolog

Figure 7

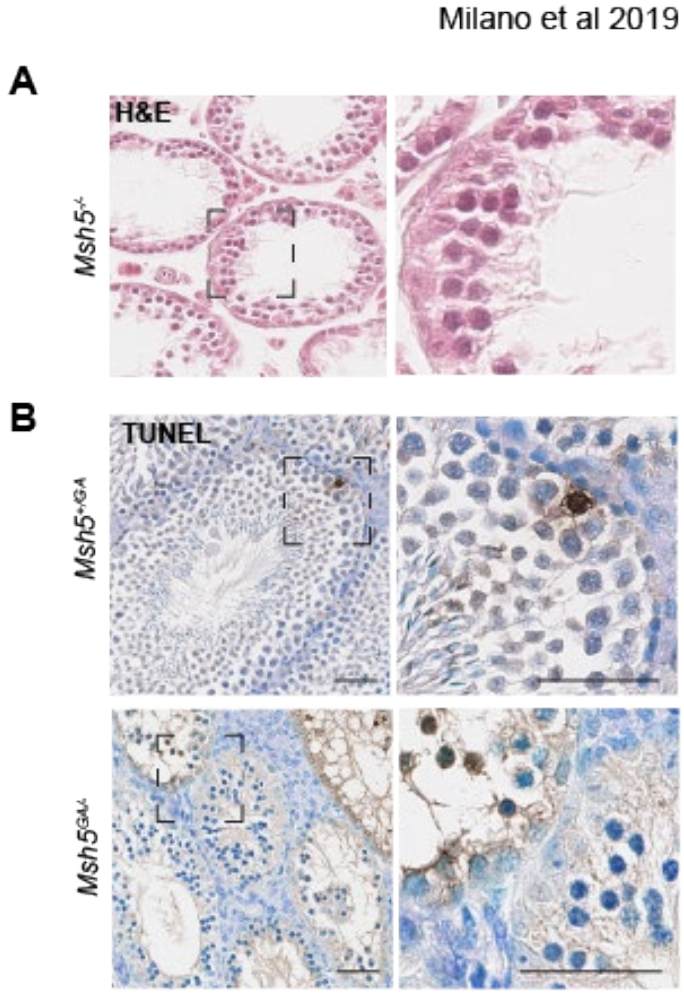

Post-spermatocyte cell populations are absent in *Msh5*$^{-/-}$ histology and apoptotic cells are observed in *Msh5*$^{GA/GA}$ suggesting increased cell death (a) H&E staining of adult paraffin embedded *Msh5*$^{-/-}$ testis sections lack cells beyond spermatocyte stage. (b) TUNEL of adult paraffin embedded *Msh5*$^{+/+}$, *Msh5*$^{+/GA}$, and *Msh5*$^{GA/GA}$ littermate testis sections fixed in 10% formaldehyde. Scale bars show 50uM. Insets in right panels are show with increased magnification on the left panel.

Figure 8

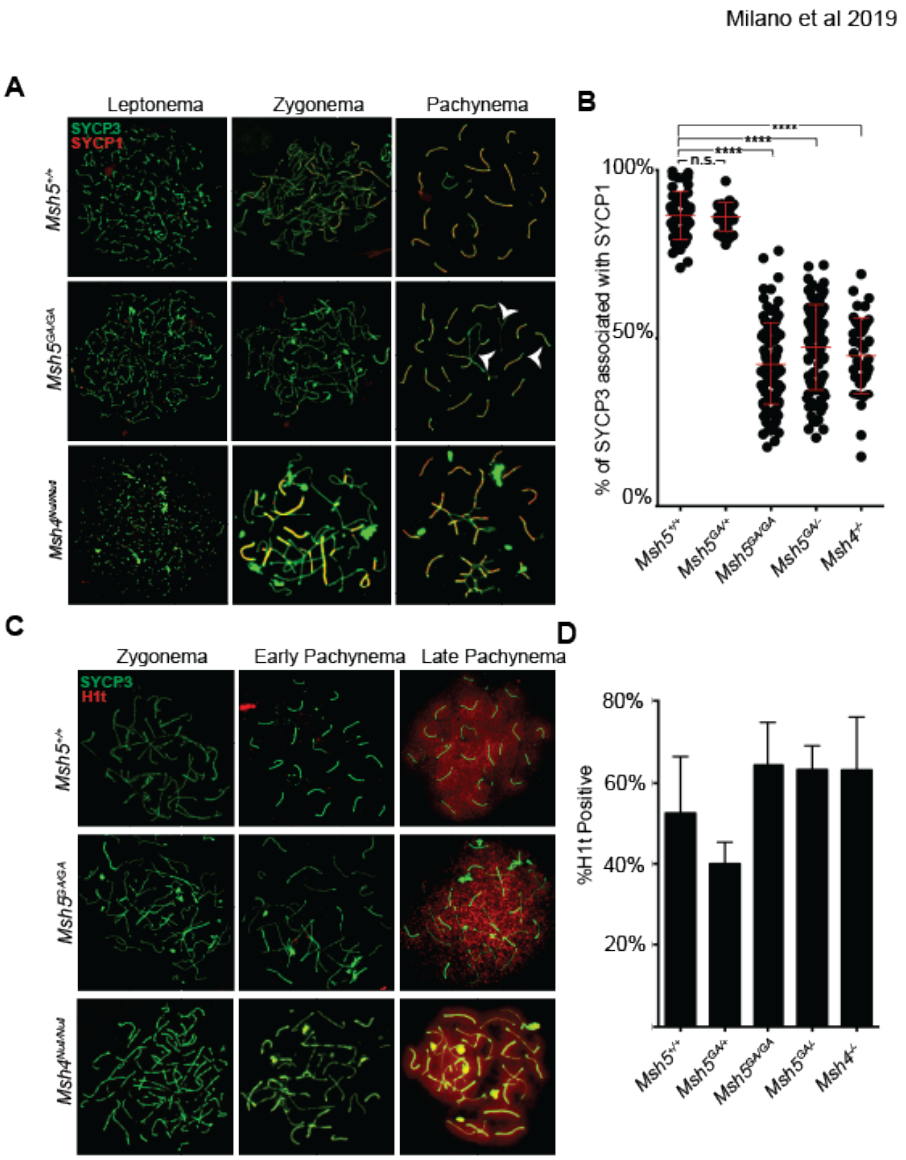

<u>*Msh5*$^{GA/GA}$ spermatocytes show inappropriate synapsis between non-homologous chromosomes and progress through mid-pachytene</u>. Localization of lateral element SYCP3 (green) (a,c) with the localization of central element protein SYCP1 (red) (a) in adult chromosome spreads show the normal progression of synaptonemal complex through prophase I in *Msh5*$^{+/+}$ spermatocytes. *Msh5*$^{GA/GA}$ spermatocytes show varying degrees of synapsis during mid-prophase I with notable inappropriate synapsis between multi-homologs associations (arrow heads). (b) Synapsis was measured by comparing lengths of total SYCP3 tracks to the total lengths of SYPC1 tracts in each pachytene-like cell using Image J. Percentage of synapsis is calculated per cell by dividing SYCP1 length with SYCP3 length and multiplying by 100. Each point represents a different pachytene-like cell, overlay lines display depicting the average $\pm$ SD. On average, *Msh5*$^{+/+}$ pachytene spermatocytes had 86.5% ($\pm$ 0.1%) synapsis. Compared to wild-type, *Msh5*$^{GA/+}$ animals were not found to be significantly different and had an average of 78% synapsis (unpaired t-test with Welch's correction, p=0.47). *Msh5*$^{GA/GA}$, *Msh5*$^{GA/-}$, *and Msh4*$^{null/null}$ animals were all found to be significantly different from wild-type (unpaired t-test with Welch's correction, $p < 0.0001$, $p < 0.0001$, and $p < 0.0001$ respectively). Average synapsis for *Msh5*$^{GA/GA}$, *Msh5*$^{GA/-}$, *and Msh4*$^{null/null}$ pachytene-like cells was 42%, 47%, and 45% respectively. (c) Localization of mid pachytene histone marker H1t (red) is observed on both *Msh5*$^{+/+}$ and *Msh5*$^{GA/GA}$ mid pachytene to diplotene spermatocytes. (d) Percentage of each prophase I sub stage of all the prophase I cells were tallied for each genotype. (e) % H1t positive prophase I stages are shown for each genotype (late pachytene and diplotene populations). When compared to wild-type, the *Msh5*$^{GA/GA}$, *Msh5*$^{GA/-}$, *and Msh4*$^{null/null}$ animals all had comparable H1t positive populations across prophase I (unpaired t-test with Welch's correction, $p = 0.1143$, $p = 0.1714$, and $p = 0.3243$ respectively).

synapsis. Thus, in order to stage these spermatocytes from *Msh5*$^{GA/GA}$ animals, we defined certain criteria for each prophase I substage. Zygotene and diplotene spermatocytes, which often look similar, were distinguished based on the length of the SC (longer in zygonema), differences in telomeric ends of the chromosomes (more bulbous in diplonema), and by H1t localization (see below). A "pachytene-like" stage was defined as having >4 discrete synapsed chromosome pairs, either wholly or partially, along with a more condensed SC appearance across all chromosomes. Using these criteria, we observed many cells in a pachytene-like stage, and beyond, in *Msh5*$^{GA/GA}$ animals. The aberrant synapsis phenotype observed in *Msh5*$^{GA/GA}$ spermatocytes range in severity, with some pachytene-like cells showing synapsis defects across the majority of homolog pairs, while other pachytene-like cells showed defects among a few homolog pairs.

Utilizing Image J software, we obtained quantitative measurements of synapsis across our mouse model. For each cell, we measured the total track length of SYCP3 signal and compared it to the total track length of SYPC1 to obtain the percent synapsis (SYCP1/SYCP3 X 100). For this analysis, we used *Msh4*$^{-/-}$ mice as a comparison with *Msh5*$^{GA/GA}$ males because the original reports suggested slightly higher levels of synapsis than observed in *Msh5*$^{-/-}$ mice, and because *Msh5*$^{-/-}$ mice are no longer available. Since MSH4 and MSH5 always act as a heterodimer, *Msh4*$^{-/-}$ mice reflect overall MutSγ function. Previous descriptions of *Msh4*$^{-/-}$ males indicated no pachytene entry, an observation that was based on the 20 independently synapsed homologs as defined by WT pachytene. In the current study however, we defined pachytene-like as >4 synapsed or partially synapsed chromosomes. Under these criteria, we observe pachytene-like cells in both *Msh4*$^{-/-}$ males and in *Msh5*$^{GA/GA}$ males. The average synapsis in WT spermatocytes during pachynema, remembering the XY chromosome pair in males is only synapsed at the autosomal region, is 86.5 $\pm$ 7.2%

(Figure 8B) with *Msh5*$^{GA/+}$ spermatocytes showing similar synapsis rates at 86.3 ± 4.2% (Figure 8B). Overall there is a remarkable degree of synapsis in *Msh5*$^{GA/GA}$ animals, with spermatocytes exhibiting an average of 43.2 ± 12.4%, and some cells achieving up to 76% of chromosome axes. By contrast, synapsis in *Msh5*$^{-/-}$ animals is less than 5% in two previous reports (de Vries et al., 1999; Edelmann et al., 1999). The level of synapsis in *Msh5*$^{GA/-}$ males is comparable to that of *Msh5*$^{GA/GA}$ males, at 47.4 ± 12.7% synapsis. Synapsis in *Msh4*$^{-/-}$ males was slightly lower than *Msh5*$^{GA/GA}$ males, at 44.9 ± 11.3% synapsis (Figure 8B). Importantly, synapsis in *Msh5*$^{GA/-}$ spermatocytes is similar to that seen in *Msh5*$^{GA/GA}$ homozygous mutant animals, while synapsis in *Msh5*$^{GA/+}$ spermatocytes is similar to WT, indicating that the *Msh5*^{GA}

Figure 9

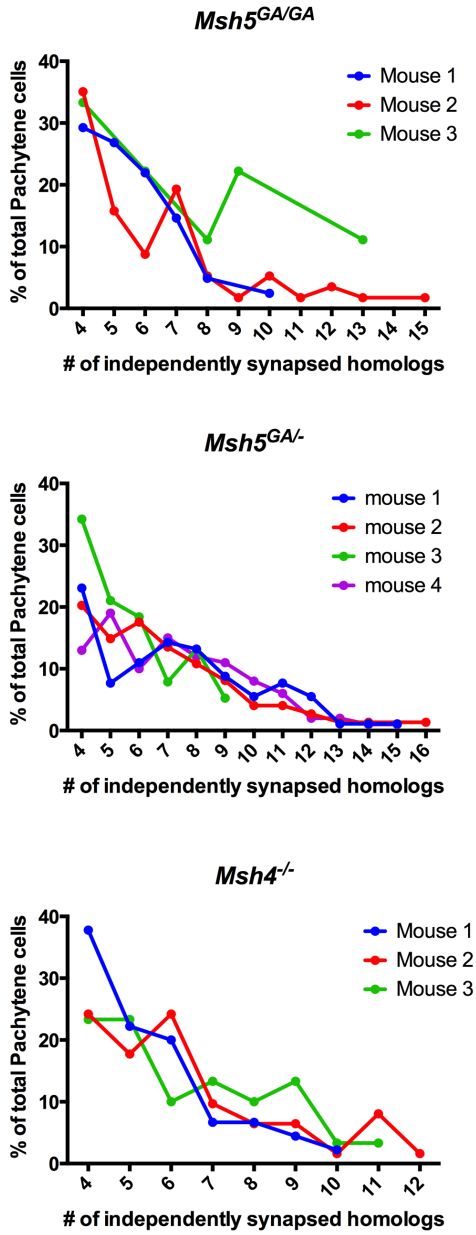

The frequency of independently synapsed homologs per pachytene-like cell are similar across synapsis mutants. (a) The frequency of the number of independently synapsed homologs per pachytene-like cell for *Msh5*$^{GA/GA}$, *Msh5*$^{-/GA}$, and *Msh4*$^{null/null}$ in each of the three graphs respectively.

allele is recessive and not causing a dominant negative effect.

To further assess the degree of synapsis in different mice, the number of independently synapsed homologs were counted in each pachytene-like cell from *Msh5*$^{GA/GA}$, *Msh5*$^{GA/-}$, and *Msh4*$^{-/-}$ males (Figure 9). In none of these cases are cells from mutant testes able to achieve a wild-type pachytene configuration of 20 independently synapsed homologs. While some *Msh4*$^{-/-}$ pachytene cells were only able to achieve as many as 12 independently synapsed homologs, only 4.8% of the pachytene-like population had more than 10 independently synapsed homologs. The degree of synapsis is significantly greater in *Msh5*$^{GA/GA}$ and *Msh5*$^{GA/-}$ spermatocytes with instances of cells achieving up to 15 independently synapsed homologs occurring in each genotype, and *Msh5*$^{GA/GA}$ having 5.6% homologs having more than 10 independently synapsed homologs and *Msh5*$^{GA/-}$ having 11.6% homologs having more than 10 independently synapsed homologs (Figure 9). Thus, we observe a greater degree of synapsis in spermatocytes from *Msh5*$^{GA/GA}$ or *Msh5*$^{GA/-}$ males compared to that of *Msh4*$^{-/-}$ cells suggesting that the presence of the mutant MSH5^{GA} protein allows for more proficient early homolog pairing and progression through later stages of prophase I. Thus, homolog pairing and/or synapsis initiation/progression does not rely on a fully functional MutSγ heterodimer. The histone marker, H1t, allows for differentiation of pachytene cells into “early” and “late”, since H1t only associates with the latter population (Wiltshire, Park, Caldwell, & Handel, 1995). Moreover, H1t positive staining allows for differentiating between zygotene and diplotene-like cells in *Msh5*$^{GA/GA}$ males. Despite the incomplete synapsis and inappropriate synapsis between multiple chromosomes in spermatocytes from *Msh5*$^{GA/GA}$ animals, these cells are competent to achieve a mid-pachytene-like stage of meiosis, at least as assessed by acquisition of H1t signal (Figure 8C). Synapsis mutants (*Msh5*$^{GA/GA}$, *Msh5*$^{GA/-}$, *Msh4*$^{-/-}$) do not achieve the normal 20 independently synapsed homologs as observed in WT.

However, the localization of H1t to these mutants suggests that they achieve a pachytene-like stage. To compare prophase I populations across genotypes, we looked at the total number of H1t-positive cells in prophase I (Figure 8D). Across all prophase I cells in WT males, we observe that 52.3 $\pm$ 14.1% of cells are H1t-positive. Surprisingly, our mutant animals gave values similar to WT: in *Msh5*$^{GA/GA}$ animals we observe a 64.4 $\pm$ 10.1% H1t positive prophase I population, in *Msh4*$^{-/-}$ 63.2 $\pm$ 12.9%; *Msh5*$^{-/GA}$ 63.3 $\pm$ 5.8%. The *Msh5*$^{+/GA}$ spermatocytes are the only population for which we observed a lower, albeit not statistically different H1t-positive prophase I pool of 40.0 $\pm$ 5.3%. Overall, we observed a comparable prophase I progression in *Msh5*$^{GA/GA}$ mutant spermatocytes and in *Msh4*$^{-/-}$ spermatocytes, although the degree of synapsis observed in these mutants is markedly different.

MutSγ association with the synaptonemal complex is drastically reduced in spermatocytes from Msh5$^{GA/GA}$ *males*

In WT mice, MSH4 and MSH5 localize on chromosome cores of the SC from zygonema through pachynema, with approximately 200 foci in zygonema, reducing progressively through until late pachynema (Kneitz et al., 2000). We investigated whether MutSγ localization on SCs was affected by loss of a functional ATP binding domain within MSH5. To this end, chromosome spreads from *Msh5*$^{+/+}$, *Msh5*$^{+/GA}$, and *Msh5*$^{GA/GA}$ male mice were subjected to IF staining using antibodies against MSH4 and SYCP3. MSH4 localization in early prophase I cells looks comparable between *Msh5*$^{+/+}$ and *Msh5*$^{+/GA}$ adult males, with abundant foci associated with early SC structures in zygonema (Figure 6D, Figure 10). Interestingly, in spermatocytes from *Msh5*$^{GA/GA}$ males, there appears to be a dramatically decreased association of MSH4 to the SC and an observable increase in MSH4 foci not associated with the SC in zygotene and pachytene nuclei (Figure 6D, Figure 10).

Figure 10

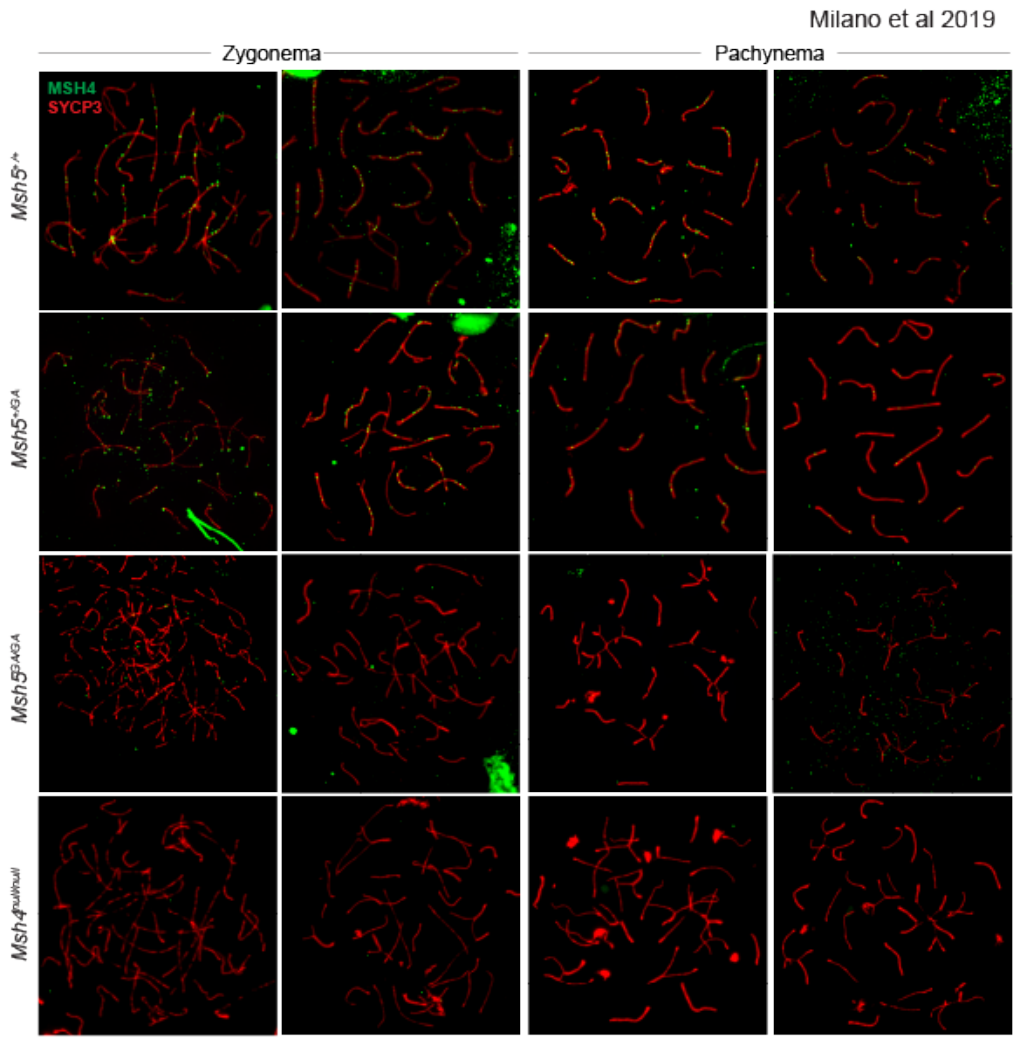

MSH4 localization is disrupted in *Msh5*$^{GA/GA}$ mutant spermatocytes.
Localization of MSH4 (green) to SC (red) in adult *Msh5*$^{+/+}$, *Msh5*$^{+/GA}$, and *Msh5*$^{GA/GA}$ littermate chromosome spreads during zygonema and pachynema. *Msh4*$^{null/null}$ is included for a negative control.

Overall the intensity of MSH4 staining in zygotene and pachytene spermatocytes from *Msh5*$^{GA/GA}$ males is lower than that of WT littermates, although some foci are clearly associated with the SC at both zygonema and pachynema (Figure 6D, arrows, Figure 10). Further examples of MSH4 staining at this stage are provided

in Figure 10 which provide additional evidence of a broader but fainter distribution of MSH4 signal in spermatocytes from *Msh5*$^{GA/GA}$ males.

The ATP binding domain of MSH5 is essential for timely progression of DSB repair events

To assess progression of DSB repair through prophase I, IF was performed on chromosome spreads from *Msh5*$^{+/+}$, *Msh5*$^{GA/GA}$, and *Msh5*$^{+/GA}$ adult littermates using antibodies against γH2AX, a phosphorylated histone variant that marks sites of DSB (Figure 11A). Spermatocytes from *Msh5*$^{+/+}$ animals show a strong γH2AX signal during leptonema and zygonema of prophase I indicating normal induction of DSBs, with loss of the γH2AX signal at pachynema signaling progression of DSB repair (Figure 11A). As expected, the γH2AX signal is intensified on the sex chromosomes at pachynema, a phenomenon that is not related to DSB formation (Turner et al., 2004); (Figure 11A, top row). Spermatocytes from *Msh5*$^{GA/GA}$ animals show a similarly strong γH2AX signal during leptonema and zygonema, indicating DSBs are induced at the expected time. Unlike in *Msh5*$^{+/+}$ cells, however, γH2AX signal is retained on autosomes throughout prophase I in *Msh5*$^{GA/GA}$ cells, indicating persistent DNA damage (Figure 11A, bottom row).

During DSB repair, one of the earliest common intermediate steps involves strand invasion and homology search, which is mediated by the RecA homologs, RAD51 and DMC1. MutSγ has been suggested to participate in stabilization of these strand invasion events *in vitro* (Snowden et al., 2004). During leptonema in WT spermatocytes, RAD51 foci are observed on axial elements of the SC in high numbers (Figure 11B,C), and similar numbers of RAD51 foci are observed on leptotene spreads from *Msh5*$^{GA/GA}$ spermatocytes. As WT cells progress from zygonema to pachynema, RAD51 foci numbers drop dramatically, reflecting the repair of DSBs. The RAD51

Figure 11

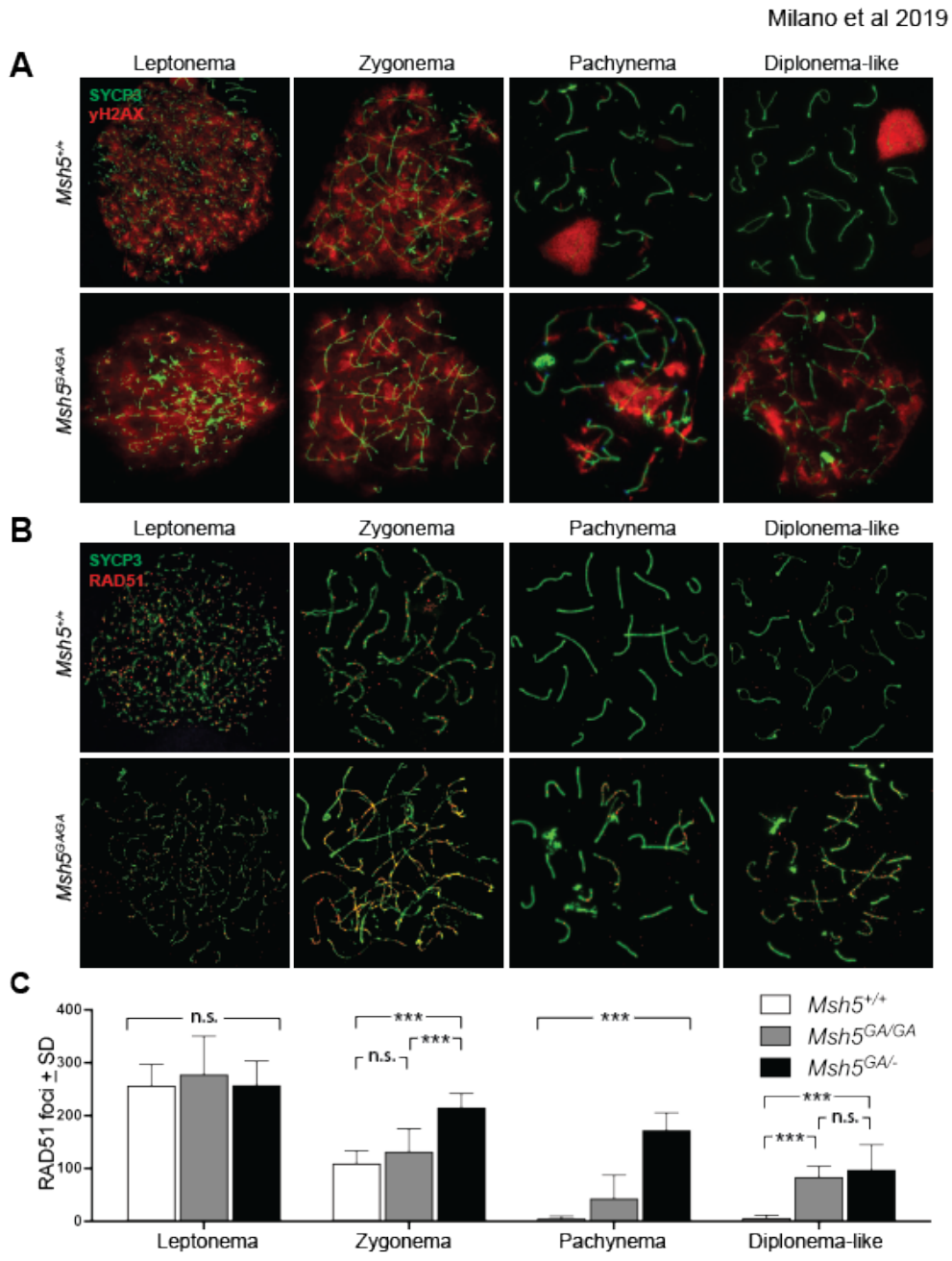

DNA damage persists in *Msh5*$^{GA/GA}$ spermatocytes throughout prophase I.(a) Immunofluorescent staining of yH2aX (red) on chromosome spreads of *Msh5*$^{+/+}$ and *Msh5*$^{GA/GA}$ littermates. (b) DNA repair marker RAD51 (red) on *Msh5*$^{+/+}$ and *Msh5*$^{GA/GA}$ chromosome spreads persists throughout prophase I. (c) Quantification of RAD51 foci associated with the SC of chromosome spreads during leptonema (*Msh5*$^{+/+}$ - 257.2 + 39.74, n = 13; *Msh5*$^{GA/GA}$ - 278.6 ± 71.92, n = 14; p=0.88, Mann-Whitney) zygonema (*Msh5*$^{+/+}$ -109.9 ±23.72, n=30; *Msh5*$^{GA/GA}$ - 132.4±43.04, n=29; p=0.14, Mann-Whitney), pachynema (*Msh5*$^{+/+}$ - 6.11 ± 4.12, n=26; *Msh5*$^{GA/GA}$ - 97.66 ± 43.84, n = 35; p<0.0001, Mann-Whitney) and diplonema (*Msh5*$^{+/+}$ - 6.91 ± 4.85, n=11; *Msh5*$^{GA/GA}$ - 88.18 ± 20.02, n=11; p <0.0001, Mann-Whitney).

focus numbers in *Msh5*$^{GA/GA}$ and *Msh5*$^{GA/-}$ spermatocytes remain significantly elevated above that of WT spermatocytes throughout prophase I ($p<0.0001$, Figure 11C). Interestingly, the RAD51 focus counts at zygonema and pachynema are significantly higher in *Msh5*$^{GA/-}$ spermatocytes than in homozygous mutant *Msh5*$^{GA/GA}$ spermatocytes ($p<0.0001$, Figure 11C), indicating more DSB repair activity during this stage in the presence of only one copy of ATPase defective Msh5. At diplonema, WT spermatocytes have lost

Figure 12

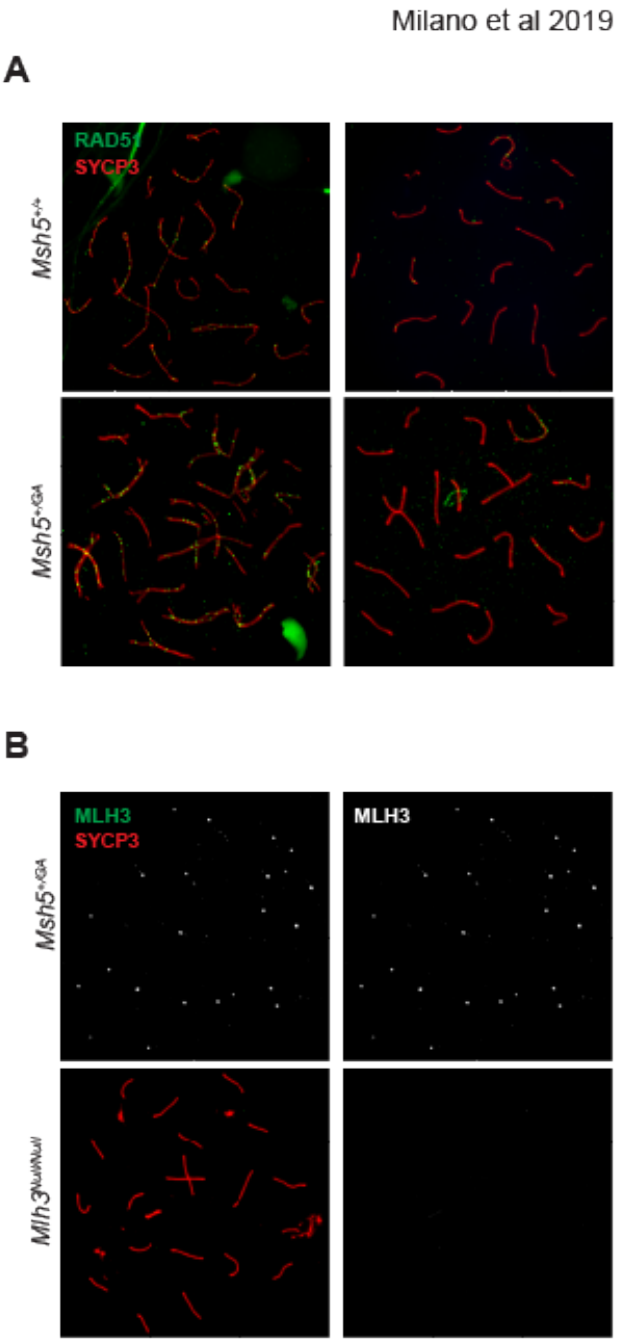

Heterozygous animals show normal RAD51 and MLH3 localization. (a) Immunofluorescent staining of DNA damage repair intermediate marker RAD51 (green) on synaptonemal complex proteins (red) in adult *Msh5*$^{+/+}$ and *Msh5*$^{+/GA}$ littermate chromosome spreads. (d) Immunofluorescent staining of MLH3 (green) in adult *Msh5*$^{+/GA}$ chromosome spreads show normal localization to SC (red) in pachytene, *Mlh3*$^{null/null}$ is included as a negative control.

all RAD51 foci, but these foci remain significantly higher in *Msh5*$^{GA/GA}$ and *Msh5*$^{GA/-}$ spermatocytes, albeit at lower frequency to that seen in pachynema ($p<0.0001$). At this stage, RAD51 counts in *Msh5*$^{GA/GA}$ and *Msh5*$^{GA/-}$ spermatocytes are not statistically different from each other. Importantly, spermatocytes from *Msh5*$^{GA/+}$ males are similar to WT with few abnormalities and normal dynamics of RAD51 loss (Figure 11C, B). Taken together, these data demonstrate the presence of the ATP binding- defective MSH5GA protein is critical for normal progression of DSB repair. Alternatively, it is possible that the high rate of RAD51 foci observed at pachynema in *Msh5*$^{GA/GA}$ males results from additional induction of DSBs through prophase I, but the current tools preclude our ability to differentiate between these two options. Importantly, the presence of only one *Msh5*^{GA} allele on a WT background (*Msh5*$^{GA/+}$ males) results in normal temporal dynamics of RAD51 loss, while the presence of one *Msh5*^{GA} allele on a null background (*Msh5*$^{GA/-}$ males) results in a significantly more delayed processing of DSBs, as characterized by RAD51 accumulation and loss. These observations argue strongly against a dominant negative effect of the GA point mutation.

An intact MSH5 ATP binding domain is essential for formation of all classes of crossover

MutSγ recruits the MutLγ complex during pachynema as part of a canonical class I CO machinery. IF staining using antibodies against MLH3 was compared across genotypes (Figure 13A). In WT and *Msh5*$^{GA/+}$ mice during pachynema, MLH3 appears on chromosome cores at a frequency that correlates with final class I CO numbers (Figure 13A, top row), but is absent in spermatocytes from *Mlh3*$^{-/-}$ males (Figure 12B). In pachytene-like spermatocytes from *Msh5*$^{GA/GA}$ males, MLH3 foci do not form on chromosome cores (Figure 13A). Occasional very faint signal was observed throughout the chromatin, as well on the SC cores, when the microscope

Figure 13

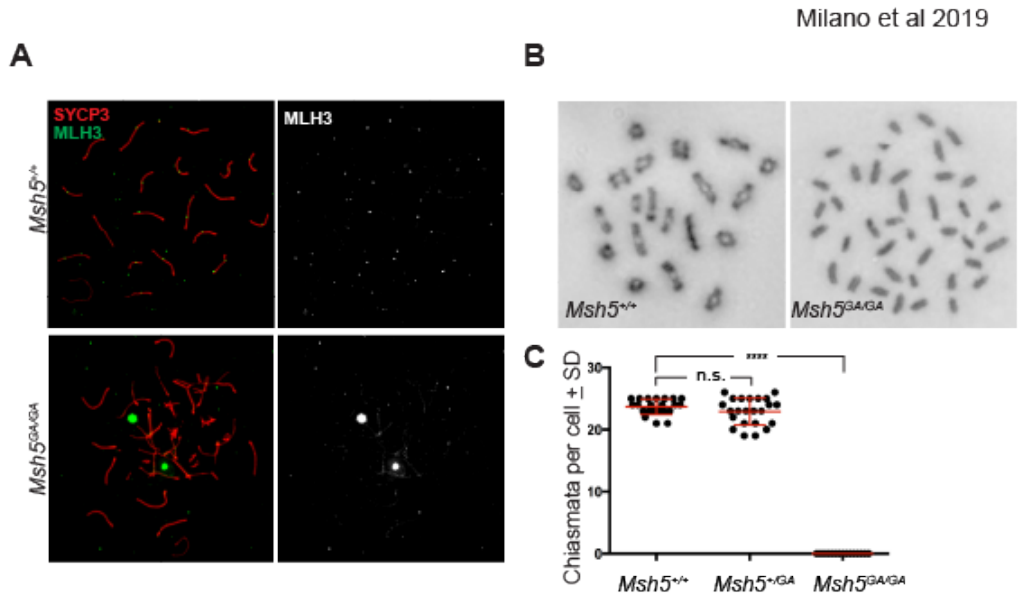

No crossovers form in *Msh5*$^{GA/GA}$ spermatocytes.
(a) Immunofluorescent staining of MLH3 (green) in adult pachytene *Msh5*$^{+/+}$ and *Msh5*$^{GA/GA}$ chromosome spreads show localization of MLH3 to SC (red) as expected in wild type and no MLH3 localization to the SC in mutant. (b) Giemsa staining of diakinesis preparations from *Msh5*$^{+/+}$ and *Msh5*$^{GA/GA}$ litter mates showing normal chiasmata in wild type and completely univalent chromosomes in mutants. (c) Chiasmata counts for *Msh5*$^{+/+}$ (23.68 $\pm$ 1.25, n=22) and *Msh5*$^{GA/GA}$ (0.0, n = 15) litter mates ($p<0.0001$, unpaired t-test).

intensity gain is increased, but it was not possible to obtain reliable images depicting this weak signal. Nonetheless, such staining was never observed in chromosome spread preparations from *Mlh3*$^{-/-}$ males, suggesting that this weak staining might be specific for MLH3 protein (Figure 12B). Given the diffuse and faint nature of this staining, it cannot be determined if this MLH3 signal is associated with sites of DSB repair. Thus, a fully functional MSH5 protein is required for appropriate association of the MutLγ with the synaptonemal complex and establishment of nascent class I CO sites. To assess crossing over across the genome, diakinesis spreads were prepared to assess chiasmata formation (Holloway et al., 2010). In WT males, each bivalent chromosome pair had at least one chiasmata (Figure 13B). Since a small number of spermatocytes from *Msh5*$^{GA/GA}$ males are capable of progressing into diakinesis, we

were able to count chiasmata in these homozygous mutant mice (Figure 13B,C). Unexpectedly, diakinesis-staged cells from *Msh5*$^{GA/GA}$ males displayed exclusively univalent chromosomes and did not form any chiasmata (Figure 13B,C). Thus, normal MSH5 ATP processing is essential for all crossover formation in mammals. Such analysis has not been possible in *Msh5*$^{-/-}$ males because spermatocytes from these mice fail to reach diakinesis, and die predominantly in zygonema.

Discussion

The data presented herein demonstrate that intact MutSγ function is required for normal prophase I progression in male meiosis. Importantly, this work is the first to show a definitive requirement for an intact MutSγ heterodimer in crossing over in the mouse and, unexpectedly, that MutSγ is critical for all crossovers regardless of their route of generation from DSB precursors. These observations were made possible by the fact that the mutation in the MSH5 ATP binding domain can allow for limited progression through to the end of prophase I, whereas most spermatocytes from *Msh5*$^{-/-}$ mice die prior to pachynema (de Vries et al., 1999; Edelmann et al., 1999). Mutation of the ATP binding domain within *Msh5* results in normal DSB induction but prolonged RAD51 installation on chromosome cores, either due to delayed DSB repair or due to extended DSB initiation through prophase I. As a result, we demonstrate a greater degree of synapsis observed in spermatocytes from *Msh5*$^{GA/GA}$ or *Msh5*$^{GA/-}$ males compared to that of *Msh4*$^{-/-}$ cells, suggesting that the presence of the MSH5^{GA} protein allows for more proficient early homolog pairing, or that the SC is established more robustly in the presence of defective MutSγ heterodimer than in the complete absence of any heterodimer. Data presented herein also demonstrate altered distribution of MutSγ throughout the nucleus of *Msh5*$^{GA/GA}$

prophase I spermatocytes, with significant localization off the SC, and a reduction in overall MSH4 signal on chromosome cores. These results indicate that the MSH5 ATP binding domain is essential for the recruitment and retention of MutSγ on SC cores from zygonema through until pachynema. Loss of ATP binding in *Msh5*$^{GA/GA}$ mutants is predicted to result in a clamp protein that is unable to slide along DNA, and thus is unable to allow successive rounds of MutSγ loading. In our *Msh5*$^{GA/GA}$ mutants we see a dramatic reduction in MSH4 signal along chromosome cores, suggesting either minimal loading of MutSγ complex onto the DNA and/or enhanced (but not complete) degradation of the complex. Thus, the low amount of MSH5^{GA}-MSH4 heterodimer that can associate with the SC may still provide some stabilization between homologs, allowing for small amounts of synapsis in *Msh5*$^{GA/GA}$ animals. However, without the MSH5 ATP domain, the normal function of MutSγ in SC establishment and/or DSB repair processing is abolished. Taken together, we conclude that early DSB repair events and synapsis are perturbed in our *Msh5*$^{GA/GA}$ mutants, but that some progression remains possible. Importantly, these observations suggest that the ATP binding domains of both MutSγ subunits must be intact in order to facilitate a complete repertoire of MutSγ functions, which is not surprising given the fact that MSH5 has been shown to bind ATP with a higher affinity than MSH4 (Snowden et al., 2008).

In the mouse, MutSγ accumulation on SCs in zygonema is in excess of the final number of MutLγ foci, but the two heterodimeric complexes are shown to localize at similar frequencies by late pachynema, albeit with number of MutSγ foci remaining slightly higher than MutLγ (Novak, Ross-Macdonald, & Roeder, 2001; Santucci-Darmanin & Paquis-Flucklinger, 2003). The earlier and more abundant localization of MutSγ in zygonema implies that MutLγ is recruited to only a subset of MutSγ sites upon entry into pachynema, with the remaining sites that fail to accumulate MutLγ presumably being processed to become NCO events via other

repair pathways. Thus, the higher numbers of MutSγ foci in zygotene and early pachytene mouse spermatocytes, together with the earlier loss of spermatocytes in *Msh5*$^{-/-}$ animals compared to *Mlh3*$^{-/-}$ or *Mlh1*$^{-/-}$ mice, implies a role for MSH4 and MSH5 in DSB processing at an early intermediate stage for multiple repair pathways. Such a possibility is supported by our data showing that diakinesis preps from *Msh5*$^{GA/GA}$ spermatocytes display no chiasmata (Figure 13), which indicates that a functional MutSγ complex is essential for all CO, acting at a stage that is upstream of both class I and class II CO designation, and thus may be a common intermediate for all CO pathways early in prophase I. Indeed, both Class I and Class II crossovers arise from a common DNA repair intermediate structure downstream of RAD51/DMC1 activity. While the class II CO pathway, which in mice involves MUS81-EME1, is not traditionally viewed to be dependent on the ZMM class of proteins, and persists in mice lacking either *Mlh1* or *Mlh3*, our data indicate that a functional MSH5 protein is required to promote both classes of CO (Holloway et al., 2008; Schwartz & Heyer, 2011). Conversely, while we briefly considered the possibility that the mutant MutSγ complex may bind irreversibly to DSB repair intermediates that might otherwise have been processed via the Class II pathway, thus blocking the recruitment of appropriate Class II repair factors, this does not appear to be the case since severely reduced MSH4 signal is observed on the SC, while no meiotic phenotype is observed in *Msh5*$^{GA/+}$ males, arguing against a dominant negative effect. Thus, loss of appropriate loading of MutSγ on the SC is sufficient to prevent any CO processing, regardless of the pathway of repair. This argues against current dogma that states that ZMM proteins, of which MSH4 and MSH5 are family members, do not operate outside of the Class I machinery. While our current data do not currently provide a mechanism by which MutSγ can orchestrate both CO pathways in mammals, studies from other organisms provide interesting insight into potential mechanisms. In *Tetrahymena*

thermophila, for example, which has no SC, COs are exclusively of the Class II variety, requiring Mus81-Mms4, but not the canonical ZMM family. Despite the absence of Class I CO events, MSH4 and MSH5 are essential for appropriate CO levels in this species, leading to the conclusion that these proteins function outside (or upstream) of the canonical Class I CO pathway (Figure 14) (Shodhan, Lukaszewicz, Novatchkova, & Loidl, 2014). In SC-bearing organisms, where Class I and Class II CO events occur in tandem to differing degrees, ZMM proteins appear to function exclusively in the metabolism of the former class of COs. In *S. cerevisiae*, CO assignment occurs prior to SC assembly, and the number of MSH5 foci observed in this species corresponds well with the final tally of Class I COs (Figure 14) (Agarwal & Roeder, 2000). However, this does not appear to be the case for organisms such as *C. elegans*, in which only Class I COs occur. Yokoo et al. have proposed that the installation of MSH-5 in worms represents a "CO licensing" stage during which the protein initially accumulates at a supernumerary frequency along the chromosome cores (Yokoo et al., 2012). These foci then diminish in number as the cell progresses through pachynema in *C. elegans*, accumulating the pro-crossover factor COSA-1 only once the final number of class I events is achieved. Thus, the final appearance of COSA-1 and MSH-5 bound foci at six sites across the worm genome represents the final "designation" of presumptive class I CO sites (Figure 14) (Yokoo et al., 2012). In the mouse, the same excessive number of MutSγ foci appear somewhat earlier in prophase I, at or soon after the completion of the axial elements in early zygonema, and these too get pared down through zygonema and pachynema coincident with the progression of CO designation. Loss of the entire MSH5 protein results in a failure to accumulate MutSγ or to complete synapsis in zygonema, resulting in cell death prior to pachynema or, at the very most, aberrant progression through pachynema (Edelmann et al., 1999; Kneitz et al., 2000). Thus in the mouse, CO licensing is tightly

Figure 14

Milano et al 2019
Figure 5

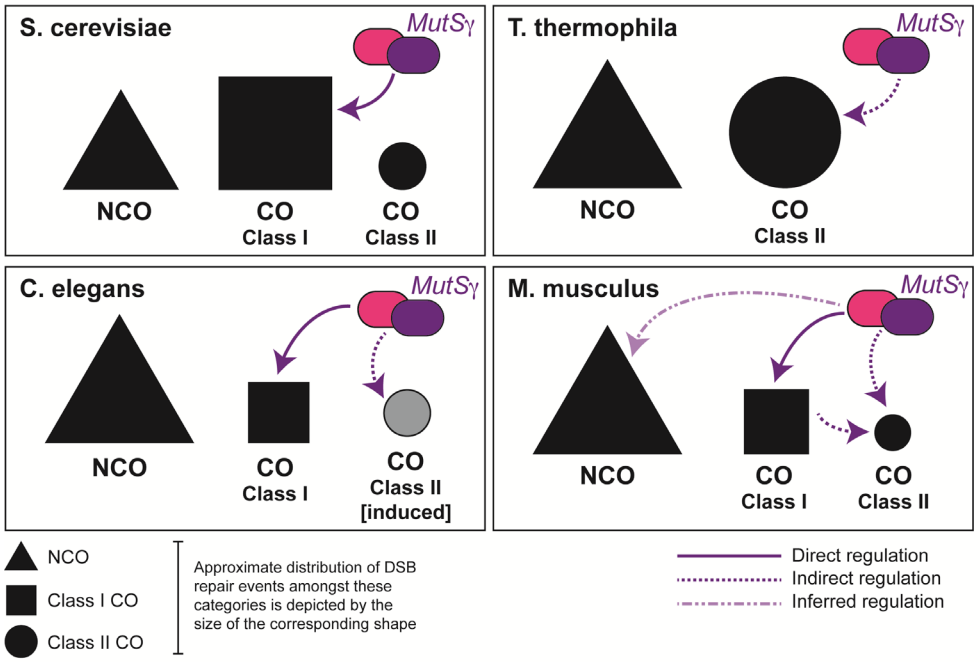

Model for MutSγ function during meiosis in different eukaryotes. Model of MutSγ role in CO establishment across eukaryotes. In *S. cerevisiae*, MutSγ functions specifically in promoting Class I COs. In *T. thermophila*, where Class I COs are absent, MutSγ functions to promote Class II COs. In *C. elegans*, MutSγ functions to drive COs, all of which are Class I COs under normal conditions. In conditions of induced DNA damage, MutSγ may also promote the extraneous Class II COs that arise. In *M. Musculus*, as shown by this study, MutSγ functions is essential to all CO repair, and is likely associated with a subset of non CO DNA repair events. See text for further details.

linked to appropriate synapsis and may reflect the requirement for distinct rearrangements in SC architecture by the MutSγ complex, similar to that proposed for *C. elegans* (Pattabiraman, Roelens, Woglar, & Villeneuve, 2017). However, in the current study, we find that loss of a functional ATPase domain in one component of MutSγ, MSH5, allows for partial synapsis implying that any structural changes to the SC can be orchestrated in the absence of full ATPase activity of the MutSγ complex. Under such circumstances, all COs are lost, regardless of their final pathway of biogenesis. Thus, CO processing through both the Class I and Class II pathways is

dependent on a fully functional MutSγ heterodimer, but may not be dependent on any SC changes induced by MutSγ in zygonema. Our data suggest either that functional activity of Class II machinery depends on the presence and processing of Class I COs (an indirect requirement perhaps involving more discrete localized changes in the SC state at the DSB site), or that loading of Class II pathway mediators requires the presence of MutSγ at these sites (a direct requirement for loading of MutSγ prior to recruitment of Class II repair factors). In either case, this would infer that MutSγ is required for CO licensing for both pathways and/or lies upstream of the licensing decision. This is not surprising given that, in the mouse, no fewer than 60% of the DSB sites become loaded with MutSγ (or 150 out of 250), and only a minor fraction of these licensed sites (approximately 20%) will become COs of the Class I or Class II variety (Cole et al., 2012; Kneitz et al., 2000). Thus, there is an over-abundance of available sites for crossing over and, suggesting that MutSγ loads as efficiently onto NCO-destined DSB repair intermediates as it does onto CO-destined DSB repair intermediates. Though the implication of this promiscuous MutSγ binding is not yet understood, it suggests that, while CO licensing in worms is achieved by MSH-5 association, this may not be the case in the mouse since MutSγ association with DSB repair intermediates appears to be more promiscuous than in worm and yeast. Taken together, our analysis of a point mutant mouse for Msh5 has allowed us for the first time to explore late prophase I roles for MSH5 in DSB repair and homologous recombination. Our observations demonstrate that the large number of MutSγ sites found in early prophase I may serve as intermediates for both Class I and Class II CO events, and indeed for NCO events. Moreover, unlike the situation in yeast, the early loading of MutSγ in mouse spermatocytes suggests progressive NCO formation through prophase I. Given that MutLγ is restricted to Class I CO events, these data suggest a functional distinction between the roles of MutSγ and MutLγ in DSB repair

during mammalian meiosis, and open the door for additional roles for MutSγ in orchestrating/overseeing DSB repair in the mammalian germline. In light of the role of other heterodimeric MutS complexes in recruiting a diverse array of repair pathways, we envisage that MutSγ serves a similar purpose in the context of DSB repair during mammalian meiosis, serving as a point of dialog between multiple repair pathways to achieve genome stability.

References

Agarwal, S., & Roeder, G. S. (2000). Zip3 provides a link between recombination enzymes and synaptonemal complex proteins. *Cell*, *102*(2), 245–255. doi:10.1016/S0092-8674(00)00029-5

Allers, T., & Lichten, M. (2001). Differential timing and control of noncrossover and crossover recombination during meiosis. *Cell*, *106*(1), 47–57. doi:10.1016/S0092-8674(01)00416-0

Baudat, F., & de Massy, B. (2007). Regulating double-stranded DNA break repair towards crossover or non-crossover during mammalian meiosis. *Chromosome Research*, *15*(5), 565–577. doi:10.1007/s10577-007-1140-3

Bocker, T., Barusevicius, A., Snowden, T., Rasio, D., Guerrette, S., Robbins, D., … Fishel, R. (1999). hMSH5: a human MutS homologue that forms a novel heterodimer with hMSH4 and is expressed during spermatogenesis. *Cancer Research*, *59*(4), 816–822.

Carlosama, C., Elzaiat, M., Patiño, L. C., Mateus, H. E., Veitia, R. A., & Laissue, P. (2017). A homozygous donor splice-site mutation in the meiotic gene MSH4 causes primary ovarian insufficiency. *Human Molecular Genetics*, *26*(16), 3161–3166. doi:10.1093/hmg/ddx199

Cole, F., Baudat, F., Grey, C., Keeney, S., de Massy, B., & Jasin, M. (2014). Mouse tetrad analysis provides insights into recombination mechanisms and hotspot evolutionary dynamics. *Nature Genetics*, *46*(10), 1072–1080. doi:10.1038/ng.3068

Cole, F., Kauppi, L., Lange, J., Roig, I., Wang, R., Keeney, S., & Jasin, M. (2012). Homeostatic control of recombination is implemented progressively in mouse meiosis. *Nature Cell Biology*, *14*(4), 424–430. doi:10.1038/ncb2451

De Vries, S. S., Baart, E. B., Dekker, M., Siezen, A., de Rooij, D. G., de Boer, P., & te Riele, H. (1999). Mouse MutS-like protein Msh5 is required for proper chromosome synapsis in male and female meiosis. *Genes & Development*, *13*(5), 523–531.

Edelmann, W., Cohen, P. E., Kane, M., Lau, K., Morrow, B., Bennett, S., … Kucherlapati, R. (1996). Meiotic pachytene arrest in MLH1-deficient mice. *Cell*, *85*(7), 1125–1134. doi:10.1016/S0092-8674(00)81312-4

Edelmann, W., Cohen, P. E., Kneitz, B., Winand, N., Lia, M., Heyer, J., … Kucherlapati, R. (1999). Mammalian MutS homologue 5 is required for chromosome pairing in meiosis. *Nature Genetics*, *21*(1), 123–127. doi:10.1038/5075

Gray, S., & Cohen, P. E. (2016). Control of meiotic crossovers: from double-strand break formation to designation. *Annual Review of Genetics*, *50*, 175–210. doi:10.1146/annurev-genet-120215-035111

Higgins, J. D., Vignard, J., Mercier, R., Pugh, A. G., Franklin, F. C. H., & Jones, G. H. (2008). AtMSH5 partners AtMSH4 in the class I meiotic crossover pathway in Arabidopsis thaliana, but is not required for synapsis. *The Plant Journal: For Cell and Molecular Biology*, *55*(1), 28–39. doi:10.1111/j.1365-313X.2008.03470.x

Holloway, J. K., Booth, J., Edelmann, W., McGowan, C. H., & Cohen, P. E. (2008). MUS81 generates a subset of MLH1-MLH3-independent crossovers in mammalian meiosis. *PLoS Genetics*, *4*(9), e1000186. doi:10.1371/journal.pgen.1000186

Holloway, J. K., Morelli, M. A., Borst, P. L., & Cohen, P. E. (2010). Mammalian BLM helicase is critical for integrating multiple pathways of meiotic recombination. *The Journal of Cell Biology*, *188*(6), 779–789. doi:10.1083/jcb.200909048

Holloway, J. K., Sun, X., Yokoo, R., Villeneuve, A. M., & Cohen, P. E. (2014). Mammalian CNTD1 is critical for meiotic crossover maturation and deselection of excess precrossover sites. *The Journal of Cell Biology*, *205*(5), 633–641. doi:10.1083/jcb.201401122

Hunter, N, & Borts, R. H. (1997). Mlh1 is unique among mismatch repair proteins in its ability to promote crossing-over during meiosis. *Genes & Development*, *11*(12), 1573–1582. doi:10.1101/gad.11.12.1573

Hunter, Neil. (2015). Meiotic recombination: the essence of heredity. *Cold Spring Harbor Perspectives in Biology*, *7*(12). doi:10.1101/cshperspect.a016618

Jessop, L., & Lichten, M. (2008). Mus81/Mms4 endonuclease and Sgs1 helicase collaborate to ensure proper recombination intermediate metabolism during meiosis. *Molecular Cell*, *31*(3), 313–323. doi:10.1016/j.molcel.2008.05.021

Kaur, H., De Muyt, A., & Lichten, M. (2015). Top3-Rmi1 DNA single-strand decatenase is integral to the formation and resolution of meiotic recombination intermediates. *Molecular Cell*, *57*(4), 583–594. doi:10.1016/j.molcel.2015.01.020

Keeney, S. (2008). Spo11 and the Formation of DNA Double-Strand Breaks in Meiosis. *Genome Dynamics and Stability*, *2*, 81–123. doi:10.1007/7050_2007_026

Kim, S., Peterson, S. E., Jasin, M., & Keeney, S. (2016). Mechanisms of germ line genome instability. *Seminars in Cell & Developmental Biology*, *54*, 177–187. doi:10.1016/j.semcdb.2016.02.019

Kneitz, B., Cohen, P. E., Avdievich, E., Zhu, L., Kane, M. F., Hou, H., … Edelmann, W. (2000). MutS homolog 4 localization to meiotic chromosomes is required for chromosome pairing during meiosis in male and female mice. *Genes & Development*, *14*(9), 1085–1097.

Kolas, N. K., Svetlanov, A., Lenzi, M. L., Macaluso, F. P., Lipkin, S. M., Liskay, R. M., … Cohen, P. E. (2005). Localization of MMR proteins on meiotic chromosomes in mice indicates distinct functions during prophase I. *The Journal of Cell Biology*, *171*(3), 447–458. doi:10.1083/jcb.200506170

Lahiri, S., Li, Y., Hingorani, M. M., & Mukerji, I. (2018). MutSγ-Induced DNA Conformational Changes Provide Insights into Its Role in Meiotic Recombination. *Biophysical Journal*, *115*(11), 2087–2101. doi:10.1016/j.bpj.2018.10.029

Lipkin, S. M., Moens, P. B., Wang, V., Lenzi, M., Shanmugarajah, D., Gilgeous, A., … Cohen, P. E. (2002). Meiotic arrest and aneuploidy in MLH3-deficient mice. *Nature Genetics*, *31*(4), 385–390. doi:10.1038/ng931

Lynn, A., Soucek, R., & Börner, G. V. (2007). ZMM proteins during meiosis: crossover artists at work. *Chromosome Research*, *15*(5), 591–605. doi:10.1007/s10577-007-1150-1

Modrich, P., & Lahue, R. (1996). Mismatch repair in replication fidelity, genetic recombination, and cancer biology. *Annual Review of Biochemistry*, *65*, 101–133. doi:10.1146/annurev.bi.65.070196.000533

Nishant, K. T., Chen, C., Shinohara, M., Shinohara, A., & Alani, E. (2010). Genetic analysis of baker's yeast Msh4-Msh5 reveals a threshold crossover level for meiotic viability. *PLoS Genetics*, *6*(8). doi:10.1371/journal.pgen.1001083

Nishant, K. T., Plys, A. J., & Alani, E. (2008). A mutation in the putative MLH3 endonuclease domain confers a defect in both mismatch repair and meiosis in Saccharomyces cerevisiae. *Genetics*, *179*(2), 747–755. doi:10.1534/genetics.108.086645

Novak, J. E., Ross-Macdonald, P. B., & Roeder, G. S. (2001). The budding yeast Msh4 protein functions in chromosome synapsis and the regulation of crossover distribution. *Genetics*, *158*(3), 1013–1025.

Oh, S. D., Lao, J. P., Taylor, A. F., Smith, G. R., & Hunter, N. (2008). RecQ helicase, Sgs1, and XPF family endonuclease, Mus81-Mms4, resolve aberrant joint molecules during meiotic recombination. *Molecular Cell*, *31*(3), 324–336. doi:10.1016/j.molcel.2008.07.006

Pattabiraman, D., Roelens, B., Woglar, A., & Villeneuve, A. M. (2017). Meiotic recombination modulates the structure and dynamics of the synaptonemal complex during C. elegans meiosis. *PLoS Genetics*, *13*(3), e1006670. doi:10.1371/journal.pgen.1006670

Pochart, P., Woltering, D., & Hollingsworth, N. M. (1997). Conserved properties between functionally distinct MutS homologs in yeast. *The Journal of Biological Chemistry*, *272*(48), 30345–30349. doi:10.1074/jbc.272.48.30345

Robert, T., Nore, A., Brun, C., Maffre, C., Crimi, B., Bourbon, H. M., & de Massy, B. (2016). The TopoVIB-Like protein family is required for meiotic DNA double-strand break formation. *Science*, *351*(6276), 943–949. doi:10.1126/science.aad5309

Romanienko, P. J., & Camerini-Otero, R. D. (2000). The mouse *Spo11* gene is required for meiotic chromosome synapsis. *Molecular Cell*, *6*(5), 975–987. doi:10.1016/S1097-2765(00)00097-6

Santucci-Darmanin, S., & Paquis-Flucklinger, V. (2003). [Homologs of MutS and MutL during mammalian meiosis]. *Medecine Sciences*, *19*(1), 85–91. doi:10.1051/medsci/200319185

Schwartz, E. K., & Heyer, W.-D. (2011). Processing of joint molecule intermediates by structure-selective endonucleases during homologous recombination in eukaryotes. *Chromosoma*, *120*(2), 109–127. doi:10.1007/s00412-010-0304-7

Shodhan, A., Lukaszewicz, A., Novatchkova, M., & Loidl, J. (2014). Msh4 and Msh5 function in SC-independent chiasma formation during the streamlined meiosis of Tetrahymena. *Genetics*, *198*(3), 983–993. doi:10.1534/genetics.114.169698

Snowden, T., Acharya, S., Butz, C., Berardini, M., & Fishel, R. (2004). hMSH4-hMSH5 recognizes Holliday Junctions and forms a meiosis-specific sliding

clamp that embraces homologous chromosomes. *Molecular Cell*, *15*(3), 437–451. doi:10.1016/j.molcel.2004.06.040

Snowden, T., Shim, K.-S., Schmutte, C., Acharya, S., & Fishel, R. (2008). hMSH4-hMSH5 adenosine nucleotide processing and interactions with homologous recombination machinery. *The Journal of Biological Chemistry*, *283*(1), 145–154. doi:10.1074/jbc.M704060200

Svetlanov, A., Baudat, F., Cohen, P. E., & de Massy, B. (2008). Distinct functions of MLH3 at recombination hot spots in the mouse. *Genetics*, *178*(4), 1937–1945. doi:10.1534/genetics.107.084798

Turner, J. M. A., Aprelikova, O., Xu, X., Wang, R., Kim, S., Chandramouli, G. V. R., … Deng, C.-X. (2004). BRCA1, histone H2AX phosphorylation, and male meiotic sex chromosome inactivation. *Current Biology*, *14*(23), 2135–2142. doi:10.1016/j.cub.2004.11.032

Wang, T. F., Kleckner, N., & Hunter, N. (1999). Functional specificity of MutL homologs in yeast: evidence for three Mlh1-based heterocomplexes with distinct roles during meiosis in recombination and mismatch correction. *Proceedings of the National Academy of Sciences of the United States of America*, *96*(24), 13914–13919.

Wiltshire, T., Park, C., Caldwell, K. A., & Handel, M. A. (1995). Induced premature G2/M-phase transition in pachytene spermatocytes includes events unique to meiosis. *Developmental Biology*, *169*(2), 557–567. doi:10.1006/dbio.1995.1169

Yokoo, R., Zawadzki, K. A., Nabeshima, K., Drake, M., Arur, S., & Villeneuve, A. M. (2012). COSA-1 reveals robust homeostasis and separable licensing and reinforcement steps governing meiotic crossovers. *Cell*, *149*(1), 75–87. doi:10.1016/j.cell.2012.01.052

Zalevsky, J., MacQueen, A. J., Duffy, J. B., Kemphues, K. J., & Villeneuve, A. M. (1999). Crossing over during Caenorhabditis elegans meiosis requires a conserved MutS-based pathway that is partially dispensable in budding yeast. *Genetics*, *153*(3), 1271–1283.

CHAPTER 3

THE C-TERMINAL 38 AMINO ACIDS OF MOUSE MSH5 ARE ESSENTIAL FOR NORMAL CROSSOVER REPAIR IN MOUSE MEIOSIS

Abstract

COs are important for normal segregation of homologous chromosomes in mouse, humans and budding yeast. There are at least two pathways for CO repair that are conserved between mouse and budding yeast. In mammals, the majority of CO repair is dependent on MutLγ to yield COs. MutLγ dependent COs are subject to interference, such that the repair of one CO will prevent proximal DSBs from also repairing as COs. The minor CO repair pathway utilizes structure-specific endonucleases. Among many eukaryotes, MutSγ, a heterodimer of MSH4 and MSH5, also serves a role in CO repair. The importance of MutSγ activity to CO repair, however, varies by organism. In budding yeast, loss of MutSγ activity reduces COs by about half, while in mouse all CO repair is dependent on MutSγ activity. The C-terminal 38 amino acids of MSH5 are highly conserved in mammals including mouse and human, but only partially conserved in budding yeast. To understand the importance of the MSH5 C-terminal domain during spermatogenesis, this work analyzed the *Msh5*$^{\Delta C}$ mouse allele, which encodes a truncated MSH5, missing the last 38 amino acids of the MSH5 C-terminus. The results of this Chapter identify the last the MSH5 C-terminus to be necessary for normal DSB repair and normal localization of both MutSγ and MutLγ to the SC. These results suggest the C-terminus is necessary for normal CO repair, but additional experiments are needed to test this hypothesis.

Credits

Dr. Winfried Edelman, Yimeng Fang, Talia Ostrow, and LeeAnne Marcello all contributed to the data presented within this Chapter. Specifically, Dr. Winfried Edelmann and his lab generated the mouse line utilized in this study (*Msh5*$^{\Delta C}$). Talia Ostrow and Yimeng Fang helped to maintain the *Msh5*$^{\Delta C}$ allele and mouse colony. Yimeng Fang, Talia Ostrow and LeeAnne Marcello helped to collect and record weights of mice and testes. The epididymal spermatozoa counts were recoded with assistance from Yimeng Fang. Yimeng Fang aided in H&E staining and imaging. Yimeng Fang and Talia Ostrow helped prepare chromosome spreads for localization studies. Immunofluorescence was done in collaboration with Talia Ostrow, Yimeng Fang, and LeeAnne Marcello. Talia Ostrow and LeeAnne Marcello imaged the RAD51 data. Yimeng Fang aided in imaging the MSH4 localization. MLH3 imaging was done in collaboration with Talia Ostrow. Dr. Vera Rinaldi, Yimeng Fang and LeeAnne Marcello provided valuable input and guidance in the data analysis obtained from ImageJ.

Introduction

During meiosis I, homologous chromosomes align at the metaphase plate prior to their segregation (Ohkura, 2015). Equal chromosome segregation depends on stable associations between the homolog pairs as the spindle pole assembles (Petronczki, Siomos, & Nasmyth, 2003). Failure to establish or maintain homolog associations during this time can result in the random segregation of chromosomes, creating aneuploid cells (Lamb, Sherman, & Hassold, 2005). The mechanisms that mediate the association between homolog pairs varies by species (Loidl, 2016). Budding yeast (*S. cerevisiae*), mice, and humans are among the many eukaryotic species to utilize crossovers (CO), the exchange of DNA between homologous chromosomes, to maintain a physical junction between homologous pairs (Gray & Cohen, 2016).

COs are created by the repair of endogenous double strand breaks (DSB) (Gray & Cohen, 2016; Keeney, 2008). The precise number and distribution of COs are maintained by the extensive regulation of the pathways driving CO repair (Gray & Cohen, 2016). This regulation ensures that at least one CO occurs between every homolog pair, often referred to as the obligate CO (Broman, Rowe, Churchill, & Paigen, 2002; Jones & Franklin, 2006). Additional regulation exists to maintain CO interference, such that CO repair at one location will inhibit proximal DSBs from completing CO repair, driving these sites to NCO repair (Broman, Rowe, Churchill, & Paigen, 2002; de Boer, Lhuissier, & Heyting, 2009). In the human population, instances of either too few or too many COs during meiosis are associated with a higher rate of aneuploid gametes (Lamb, Sherman, & Hassold, 2005; Saiyed, Bakshi, Muthuswamy, & Agarwal, 2018; Wang et al., 2017). The mechanisms that drive CO repair remain obscure.

The regulation driving human CO repair is well conserved and more amenable to investigation in mouse (Baudat & de Massy, 2007). In mouse, about 250 DSBs are induced by the topoisomerase-like protein SPO11 at the onset of prophase I (Keeney, 2008; Lange et al., 2016). Only 20-30 DSBs repair as COs per meiosis in spermatocytes (Holloway, Booth, Edelmann, McGowan, & Cohen, 2008; Kolas et al., 2005; Lipkin et al., 2002). COs are repaired by at least two pathways in mouse, dubbed the Class I and Class II COs. The Class I CO pathway, dependent on MutLγ (MLH1-MLH3), is responsible for approximately 90% of all CO repair in mouse (Lipkin et al., 2002). Only the Class I COs exhibit interference (Broman, Rowe, Churchill, & Paigen, 2002; de Boer, Lhuissier, & Heyting, 2009). The Class II COs are driven in-part by the structure specific endonuclease MUS81-EME1 and are not subject to interference (Broman, Rowe, Churchill, & Paigen, 2002; de Boer, Lhuissier, & Heyting, 2009; Holloway, Booth, Edelmann, McGowan, & Cohen, 2008; Lipkin et al., 2002). Both CO interference and the obligate CO promote the even distribution of COs across the 20 homologous chromosomes contained within the mouse genome (Gray & Cohen, 2016; Keeney, 2008).

As DSB repair progresses, a tripartite protein scaffold called the synaptonemal complex (SC) forms between homologous pairs (Moses, Dresser, & Poorman, 1984). The SC consists of two lateral elements (LE) between homologous chromosomes and a central element (CE) structure that polymerizes between homolog pairs in a process called synapsis (de Vries et al., 2005; Moses, Dresser, & Poorman, 1984; Plug et al., 1998). The five substages of prophase I are described in terms of the SC: leptonema, zygonema, pachynema, diplonema, and diakinesis. (Moses, Dresser, & Poorman, 1984). In leptonema, the LE begins to form an axis along the lengths of the chromosomes. Zygonema is characterized by fully formed LE structures and the initiation of synapsis between homolog pairs. The SC is fully formed by pachynema

and, in mouse, 20 discrete homolog pairs are observed for each of the chromosomes. In diplonema, the SC initiates disassembly at the CE. In diakinesis, the SC is fully disassembled, and it is at this time that chiasmata (the manifestation of crossover structures) can be observed. DSB repair occurs near the SC and proteins involved in these processes can be colocalized to fixed cells from the testes, allowing for a temporal measure to stage prophase I cells from a heterogenous cell population (Moses, Dresser, & Poorman, 1984; Page, Suja, Santos, & Rufas, n.d.). At the final stage of prophase I, regions of CO repair can be visualized as chiasmata (links between the dense chromatin of homologous chromosomes) (Jones, 1984).

Similar to mouse, budding yeast has both interfering and non-interfering COs, analogous to the Class I and Class II pathways in mouse (Argueso, Wanat, Gemici, & Alani, 2004; Hollingsworth, Ponte, & Halsey, 1995; Hunter & Borts, 1997; Novak, Ross-Macdonald, & Roeder, 2001; Ross-Macdonald & Roeder, 1994). The Class I-like COs in budding yeast are also dependent on MutLγ, while the Class II-like COs are repaired, in part, by structure specific endonucleases (de los Santos et al., 2003; Hunter & Borts, 1997). The regulation of those pathways in budding yeast, however, is different compared to that of mouse and humans (Baudat & de Massy, 2007). Only 10% of all DSBs repair as COs in mouse, while about 50% of all DSBs in budding yeast repair as COs (Lange et al., 2016; Mancera, Bourgon, Brozzi, Huber, & Steinmetz, 2008). Furthermore, in budding yeast, the Class I-like and Class II-like pathways contribute about equally to the total CO repair events while, in mouse, CO repair is predominately driven by the Class I CO pathway (Lipkin et al., 2002).

MutSγ, a heterodimer of MSH4 and MSH5, promotes COs in both budding yeast and mouse, but the activity of MutSγ is divergent between these species (de Vries et al., 1999; Edelmann et al., 1999; Hollingsworth, Ponte, & Halsey, 1995; Kneitz et al., 2000). In mouse, MutSγ localization on the SC presents dynamics that

are not observed in yeast. In zygotene spermatocytes, about 150 MutSγ localize to the SC. As prophase I progresses, the localization of MutSγ on the SC declines (Kolas et al., 2005; Moens et al., 2002). At pachynema, approximately 50 MutSγ foci localize to the SC. This is roughly half the number of MutLγ foci at final CO locations (Santucci-Darmanin et al., 2000). These localization dynamics are also observed in humans, suggesting the dynamic between MutSγ and MutLγ is conserved in mouse (Kolas et al., 2005; Plug et al., 1998; Santucci-Darmanin et al., 2000). The abundance of MutSγ in zygonema is thought to stabilize pre-CO locations and inhibit NCO repair (Lahiri, Li, Hingorani, & Mukerji, 2018). As prophase I progresses, MutSγ is subject to a paring down process, likely regulating the final number of COs that form (Plug et al., 1998; Santucci-Darmanin et al., 2000).

Budding yeast MutSγ, a heterodimer of MSH4 and MSH5, functions upstream of MutLγ to promote the Class I-like COs (Argueso, Wanat, Gemici, & Alani, 2004). In mouse and humans, loss of MutSγ is associated with infertility (Carlosama et al., 2017; Clark, Wu, & Her, 2013; de Vries et al., 1999; Edelmann et al., 1999; Guo et al., 2017; Ji et al., 2012; Kneitz et al., 2000; Mandon-Pépin et al., 2008; Ni et al., 2015). Mutation of the ATP binding domain in mouse *Msh5* results in a loss of all CO repair, identifying MutSγ activity as necessary for all CO repair in mouse (Chapter 2)(Milano et al., 2019). This is in stark contrast to the analogous mutation in *S. cerevisiae Msh5*, where CO repair is merely reduced (Nishant, Chen, Shinohara, Shinohara, & Alani, 2010).

This study utilizes a novel *Msh5* mutant mouse, the Msh5$^{\Delta C}$ mouse line, to further investigate MutSγ function during CO establishment**.** *Msh5$^{\Delta C}$* allele encodes a truncated MSH5 protein that is disrupted in the C-terminal 38 amino acids. The results presented establish the C-terminal of MutSγ as essential to mouse fertility, normal

DSB repair, and normal MutLγ recruitment, suggesting this domain also important for CO repair.

Methods

Mouse generation and genotyping

The mouse *Msh5* genomic locus was cloned from a P1 mouse ES cell genomic library (Genome Systems) (Edelmann et al., 1999). A 3.6 kb genomic HindIII fragment of mouse *Msh5* spanning exons 17-25 was inserted into a pBluescript SK vector. Positive clones were selected and identified by PCR. The $Msh5^{\Delta 38C}$ ($Msh5^{\Delta C}$) allele contained a termination substitution, modifying residue 795, and an analytic BclI restriction site, generated by site-directed mutagenesis in exon 23. A loxP flanked PGK hygromycin/neomycin cassette was inserted into the MscI site in intron 23. The targeting vector was linearized at the single NotI site and electroporated into WW6 ES cells. After selection in hygromycin, resistant colonies were isolated and screened by PCR. The positive clones were identified and injected into C57BL/6J blastocysts to produce chimeric animals. The PGK hygromycin/neomycin cassette was deleted by Cre-loxP-mediated recombination after mating of chimeric mice to Zp3Cre recombinase transgenic females (C57BL/6J). F1 offspring were genotyped and heterozygous animals were intercrossed to generate F2 homozygous mutant $Msh5^{\Delta C/\Delta C}$ mice and appropriate controls. All $Msh5^{+/+}$ and $Msh5^{\Delta C/\Delta C}$ mice used in these studies were backcrossed more than 10 times onto a C57BL/6J genetic background.

Mouse handling and $Msh5^{\Delta C}$allele maintenance

Mice were maintained under controlled conditions of light and temperature and with *ad libitum* access to food and water. All experiments were conducted with prior

approval from the Cornell Institutional Animal Care and Use Committee. The *Msh5*$^{\Delta C}$ allele that is maintained on the C57Bl/6J mouse line is from Jackson Laboratories (Bar Harbor, ME). For maintenance of this allele, ear tissue was collected, and DNA was extracted. The *Msh5* locus was amplified through PCR by utilizing the following genotyping primers: Forward 5' AAGCTCATTCGTGGCCTTCA 3' (M5Ex23d), Reverse: 5' CATGGAGACTTGTGAGGATG 3' (M5Ex24u). The WT allele resulted in a 600 base pair fragment and the *Msh5*$^{\Delta C}$ allele resulted in a 700 base pair fragment (Figure 16A).

Testis weights & sperm counts

For each mouse, each testis was removed and the weight recorded as a percentage of the whole body weight. Caudal epididymides were extracted and minced in sperm count media at room temperature (4% BSA in PBS). The sperm count media containing minced tissue was incubated at 30°C for 15 minutes. 30 µL of cell suspension was removed and fixed in 470 µL of 10% formalin at room temperature. Immediately following this, 10 µL of fixed Sperm was loaded onto a hemocytometer and counted twice.

Histology

Testes were extracted from 12-week-old mice and fixed in Bouin's fixative for 6 hours at room temperature or in 10% formalin for 6 hours at room temperature. Fixed tissue was washed in in 70% ethanol at room temperature at least 3 times for 15 minutes each. These samples were then sent to Cornell's Histology Core to paraffin-embed the tissue and then were sectioned at 5 µM. Hematoxylin and eosin (H&E) staining, as

well as TUNEL staining, was performed using previously established methods (Negoescu et al., 1996). All imaging was done utilizing the Aperio Scanscope Unit.

Meiotic chromosome spreads

To prepare chromosome spreads, a testis was removed at room temperature and decapsulated. Testis tubules were then incubated in hypotonic extraction buffer (HEB; 30 mM Tris, pH 8.2, 50 mM sucrose, 17 mM trisodium citrate dihydrate, 5 mM EDTA, 0.5 mM DTT, and 0.5 mM PMSF) for 1 hour on ice. A three to five-millimeter length piece of the seminiferous tubule was removed using forceps and transferred into a 20 µL drop of hypotonic sucrose at room temperature (100 mM, pH 8.2). After adding another drop of 20 µL sucrose, the tubule was macerated and the cell suspended, with another drop of 20 µL sucrose added and the mixture pipetted up and down 3-4 times. Any visible tubule fragments remaining in the mixture were removed, leaving only cell suspension. Glass slides were dipped in 1% paraformaldehyde, containing 0.15% Triton X at room temperature and the back and sides of the glass slide were wiped dry. The glass slide was then held at an angle so the remaining liquid on of the top of the slide pooled into a corner by gravity. At this point 20 µL of cell suspension was removed and added to the liquid on the glass slide. The liquid on the slide was gently rocked back and forth until the top was covered. Slides were transferred to a humid chamber for 1-2 hours at room temperature and then air dried at room temperature. The slides were washed three times for 3 minutes (0.4% Kodak Photo-Flo 200 in water) and air dried again. Dry samples were then stored at -80°C until later use, for no longer than 2 weeks.

Immunofluorescence

Glass slides containing the meiotic chromosome spreads were equilibrated to room temperature. Slides were washed at room temperature in 0.4% Kodak Photo-Flo 200 in PBS and 0.1% Triton X-100 in PBS for 5 minutes each and then blocked for 10 minutes in 10% antibody dilution buffer (ADB) in PBS (ADB: 3% bovine serum albumin, 0.05% Triton in 1 x PBS). This was followed by an overnight incubation in primary antibodies (at varying concentrations in ADB; Table 1) at room temperature in a humid chamber. After incubation in primary antibodies, slides were washed again at room temperature in 0.4% Kodak Photo-Flo 200 in PBS and 0.1% Triton X-100 in PBS for 5 minutes each and blocked for 10 minutes in 10% antibody dilution buffer (ADB) in PBS. Secondary antibody was then added to the slides and incubated in the dark for 1 hour at 37°C in secondary fluorochrome conjugated antibodies. Primary and secondary antibodies used: Sycp1 1:2000 (Abcam-AB150871), Sycp3 1:5000 (Custom & Abcam AB15093), 1:5000 yH2AX (EMD Millipore 07-164), 1:10000 H1t (custom), 1:1000 MSH4 (Abcam AB58666), 1:1000 MLH3, 1:1000 MLH1 (BD Biosciences 550838), 1:1000 RAD51 (EMD Millipore PC130). All secondary antibodies were raised specifically against Fc fraction, were Fab-fraction purified, and conjugated to Alexafluor 594, 488, or 647. After incubation with secondary antibody, slides were washed at room temperature in 0.4% Kodak Photo-Flo 200 in PBS and 0.1% Triton X-100 in PBS for 10 minutes each and then air dried in the dark at room temperature. Slides were treated with DAPI plus antifade and mounted with a glass cover slip. Slides were stored at 4°C until imaging.

All imaging was performed utilizing the AXIO vision and ZEN software. All photos were taken with a less than 1 second exposure. To ensure comparable results, all exposure times were the same for each experiment.

FIJI Image J Macro for SYCP1 & SYCP3 track measurements

Each image was opened as an RBG tiff, maintaining independence between the three fluorescent channels. For each cell to by analyzed, the cell boundaries were selected manually by the "freehand" command. The area outside the cell boundary was cleared by running "Clear Outside" to remove signal not associated with the cell being analyzed. The fluorescent signal was separated by running "Split Channels". An automatic threshold was set for the SYCP3 channel using "reniEntropy dark", converting the SYCP3 channel to a binary image. The SYCP3 image was then converted to vector lines, tracing the "skeleton" of this signal by running the "Skeletonize" command. The length of every SYCP3 branch was measured by running "Analyze Skeleton (2D/3D)", producing the lengths of all branches that make up the skeleton image. The summation of all branches in this image represents the total length of SYPC3 for this cell. The lengths of SYCP1 were obtained by following the same procedure done for the SYCP3 channel. The total length of SYCP1 was compared to the total length of SYCP3 for each cell, producing a value for synapsis.

Foci Count Macro for ImageJ Open Software

All focus counts, apart from anti-MLH1 experiments, were done automatically in ImageJ. Due to the variation in MLH1 foci size in the anti-MLH1 experiments, MLH1 foci were verified by hand counts. For ImageJ foci counting, each image was opened as RBG tiff, as previously described for SYCP1 and SYCP3 measurements. The cell was isolated utilizing the same "freehand" command, followed by "Clear Outside". RBG channels were split and an automatic threshold was set using "reniEntropy dark". To get the total foci count within the cell boundary, which represents the total foci in the nucleus, foci were counted by running "Analyze Particles". To quantify the total

foci associated specifically associated with the SC, the "Min" function of the image calculator was utilized to produce an image that only includes foci that over lap with SYCP3 signal. These foci were calculated by running "Analyze Particles".

Results

The difference in MutSγ activity between mouse and yeast could be attributed to differences in the peptide sequence of either the MSH4 or MSH5 subunit. For comparison, the mouse MSH5 peptide sequence was aligned to analogous peptide sequences of other eukaryotes to identify conserved and divergent amino acids (Figure 15). The alignment of these sequences allowed for the identification of 38 highly conserved residues in the C-terminus of mammalian MSH5 peptide, which has an uncharacterized function. Many of these residues are shared among other eukaryotes (Figure 15). Additionally, there are multiple predicted post translational modification **s**ites within the highly conserved C-terminal region, suggesting these amino acids could be subject to regulation (Figure 15**).** These include S/T residues that may act as phosphorylation sites and one predicted SUMOylation site, indicating this region could serve a signaling role (Figure 15). The position of the C-terminal is outside of the ring near domain V, exposing these residues to interact with other molecules in the cell (Rakshambikai et al., 2013).

This study utilized a mouse line bearing an early termination codon in *Msh5* (*Msh5*$^{\Delta C}$) that disrupts the last 38 amino acids of the MSH5 peptide in order to investigate the role of this C-terminal domain in mouse meiosis (Figure 16A). Specifically, the premature stop codon replaces the codon for amino acid residue 795 in exon 23 (Figure 16A). Animals carrying the *Msh5*$^{\Delta C}$ allele were identified by PCR

Figure 15

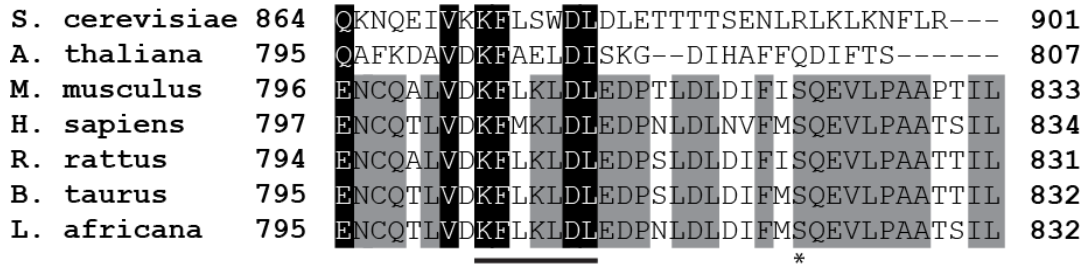

Clustal Omega alignment of MSH5 C-terminal region of MSH5 protein transcripts.

Peptide alignment of budding yeast (*S. cerevisiae*), plant (*A. thaliana*), mouse (*M. musculus*), human (*H. sapiens*), rat (*R. rattus*), cattle (*B. Taurus*), and elephant (*L. Africana*). Regions highlighted in black identify residues shared among all these species. Gray regions show regions of conservation in mammals, that is absent in the yeast and plant species. Underlined in black is a predicted SUMOlyation site conserved in mammals. The asterisk identifies a predicted phosphorylation site.

(Figure 16B). *Msh5*$^{+/+}$, *Msh5*$^{+/\Delta C}$, and *Msh5*$^{\Delta C/\Delta C}$ adult animals (10-12 weeks old) were all viable and healthy. *Msh5*$^{+/\Delta C}$ animals were fertile and utilized to maintain this allele. Mating among *Msh5*$^{\Delta C/\Delta C}$ male and female animals with wild-type animals resulted in no pups and the infertility phenotype was inferred. Loss of this domain is not expected to result in differences in MSH4 binding or disrupt the ATPase domain, due to its position away from these residues.

Figure 16

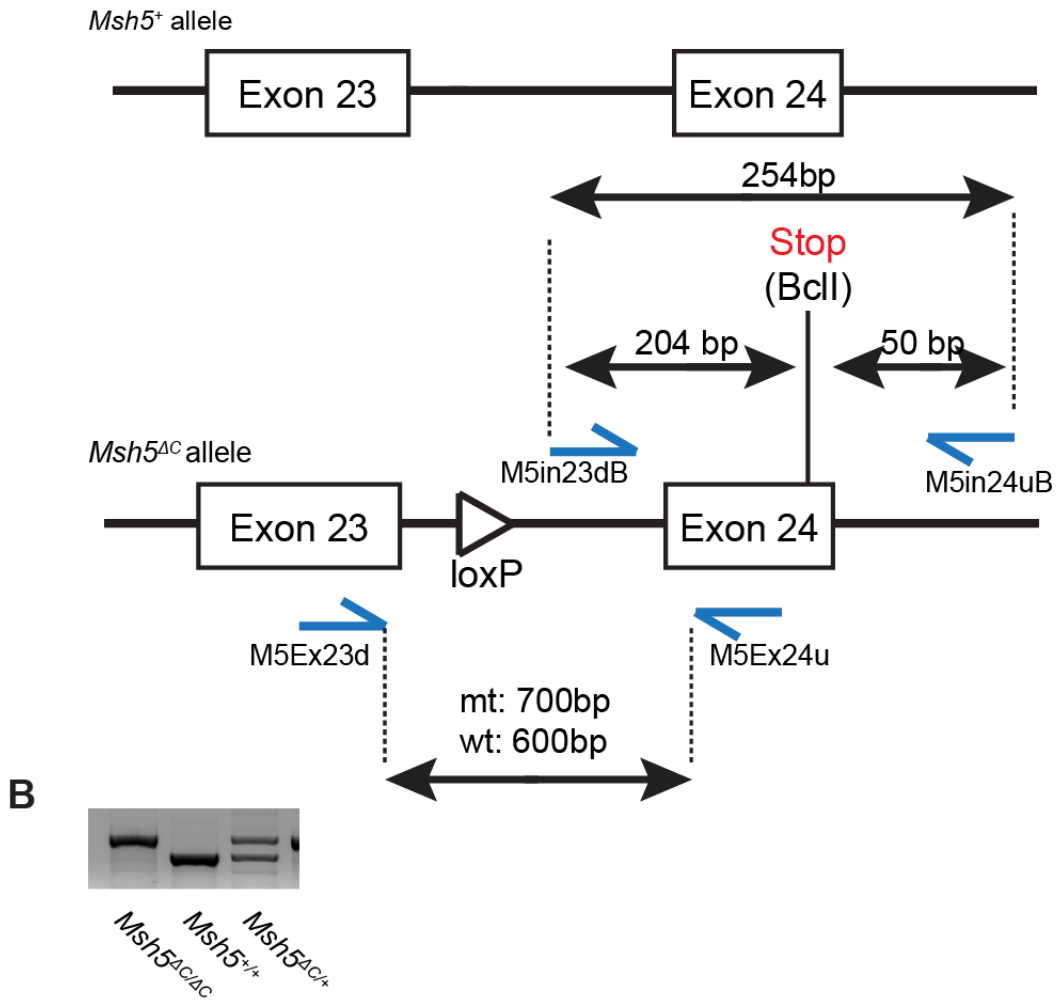

Generation of *Msh5*$^{\Delta C}$ allele truncates the MSH5 protein, removing the highly conserved 38 residues of mouse MSH5 C-terminus.

(A) Cartoon of genomic region targeted for mutation and genotyping strategy. Primers used to track this allele are in blue (B) Genotyping result using E5Ex23d and M5Ex24u primers.

The C-terminal 38 amino acids of MSH5 are essential for mouse fertility and spermatozoa production

Adult testis weights were compared among littermates across genotypes (Figure 17A). In order to compare between individuals, testis weights were calculated

as a percentage of total animal body weight. The testis weight of *Msh5*$^{+/+}$ mice was 0.42% ± 0.05% of total body weight (n=7). *Msh5*$^{+/\Delta C}$ testis weight was comparable to that of wild-type (WT) testis (0.44% ± 0.06%; n=5; p=0.63, unpaired t-test with Welch's correction). *Msh5*$^{\Delta C/\Delta C}$ animals had significantly lower testis weights compared to WT littermates (0.14% + 0.02%; n=12; p<0.0001, unpaired t-test with Welch's correction).

To evaluate spermatogenesis, epididymal spermatozoa were collected from each animal and quantified (Figure 17B). WT animals had an average of 15.88 ± 7.9 million sperm per animal (n=5). Sperm numbers in epididymides from *Msh5*$^{\Delta C/+}$ males were comparable with an average of 17.7 ± 4.4 million sperm per animal (n=5; p=0.0872, unpaired t-test with Welch's correction). By contrast, *Msh5*$^{\Delta C/\Delta C}$ males had no epididymal spermatozoa, making them significantly different from their WT littermates (n=7; p=0.0018, unpaired t-test with Welch's correction). These results support that the C-terminal 38 amino acids of MSH5 is essential for mouse fertility.

The testes of adult (age 10-12 weeks) *Msh5*$^{+/+}$, *Msh5*$^{+/\Delta C}$, and *Msh5*$^{\Delta C/\Delta C}$ animals were assessed for cellular structure and morphology by analyzing H&E stained cross sections of the testis (Figure 17C). *Msh5*$^{+/+}$ and *Msh5*$^{+/\Delta C}$ mice had normal populations of germ cells, including spermatocytes, round spermatids, and spermatozoa populations. Sertoli cells and spermatogonia were positioned around the basement membrane of the seminiferous tubule. Spermatocytes were positioned towards the lumen, adjacent to the spermatogonia and Sertoli cells (Figure 17C**)**. Near the lumen were round spermatids and elongating spermatozoa (Figure 17C). *Msh5*$^{\Delta C/\Delta C}$ testis sections lacked elongating spermatids as well as mature spermatozoa (Figure 17C). Metaphase cells were characterized as having highly condensed homologous chromosomes aligned at the center of the cell, while anaphase I cells were identified by the appearance of highly condensed homologs, segregating in the

Figure 17

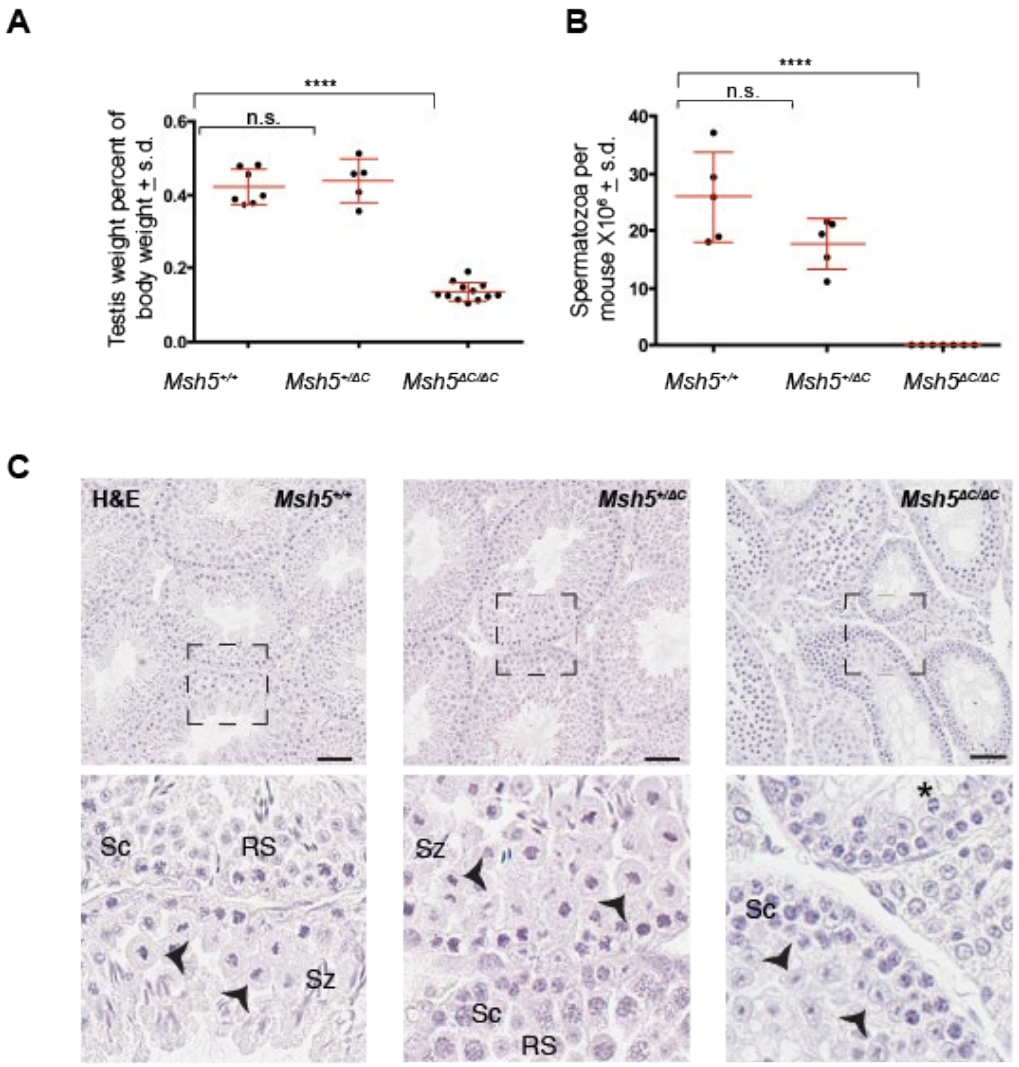

Msh5$^{\Delta C/\Delta C}$ animals have no spermatozoa.

(A)Testis weights measured as percentage of body weight are shown for each mouse across all genotypes. Error bars in red show mean + SD. Mouse N# WT-7; *Msh5*$^{\Delta C/\Delta C}$ -12, *Msh5*$^{+/\Delta C}$ -5 numbers. (B) Epididymal sperm counts for each mouse across all genotypes. Error bars in red again show mean + SD. Mouse N# WT-5; *Msh5*$^{\Delta C/\Delta C}$ - 7; *Msh5*$^{+/\Delta C}$ -5. (C) H&E of testis sections across genotypes at 90 days. Arrow heads depict cells exiting prophase I Asterisk identities rare anaphase population. Scale bars are 50 uM, boxes are magnified below image. Sz=spermatozoa Sc=spermatocytes RS=round spermatids. P<0.0001 **** P<0.001 *** P<0.01 ** P<0.05 *

center of the cell (Oakberg, 1956). Unexpectedly, *Msh5*$^{\Delta C/\Delta C}$ testis sections did contain metaphase I and anaphase I cells (a cell population that is absent in *Msh5*$^{-/-}$ males) (Figure 17C, asterisk**)** (de Vries et al., 1999; Edelmann et al., 1999). These

observations suggest that the *Msh5*$^{\Delta C/\Delta C}$ spermatocytes progress beyond prophase I but are unable to complete spermatogenesis.

Spermatocytes progress though prophase I with minimal synapsis defects in Msh5$^{\Delta C/\Delta C}$ *animals*

To explore the progression of prophase I in the absence of the MSH5 C-terminus, meiotic chromosome spreads from male mice were prepared form all genotypes. SC assembly in chromosome spreads was visualized using immunofluorescent antibodies targeting components of the SC. LE structures were observed using anti-SYCP3 (Page & Hawley, 2004). An anti-SYCP1 was used to observe the transverse filaments that synapse LE of homolog pairs together, forming the CE (Page & Hawley, 2004). The SC was fully assembled in pachynema, when all 20 homologs formed discrete SC formations (Moses, Dresser, & Poorman, 1984). WT and *Msh5*$^{\Delta C/+}$ animals showed distinct prophase I stages from leptonema through diplonema as expected (Figure 18A). Similarly, based solely on the original definition of prophase I progression, each prophase I substage was clearly visible in *Msh5*$^{\Delta C/\Delta C}$ spermatocytes (Moses et al., 1984). Notably, not every pachytene cell from *Msh5*$^{\Delta C/\Delta C}$ males escaped synapsis defects (Figure 18B). A subset of *Msh5*$^{\Delta C/\Delta C}$ spermatocytes had apparent asynapsis on either the autosomes or the XY pair, while other spermatocytes had asynapsis on both autosomes and the XY pair (in an otherwise pachytene-like spermatocyte). The *Msh5*$^{\Delta C/\Delta C}$ pachytene-like spermatocytes, which had asynapsis on only X and Y chromosomes, can indicate normal desynapsis, as spermatocytes transition from pachytene to diplotene, or could be a malfunction of synapsis among the sex chromosomes (Figure 18A). Some *Msh5*$^{\Delta C/\Delta C}$ spermatocytes contained 20 discrete homolog pairs, but no obvious XY pair (Figure 18B, bottom left).

Figure 18

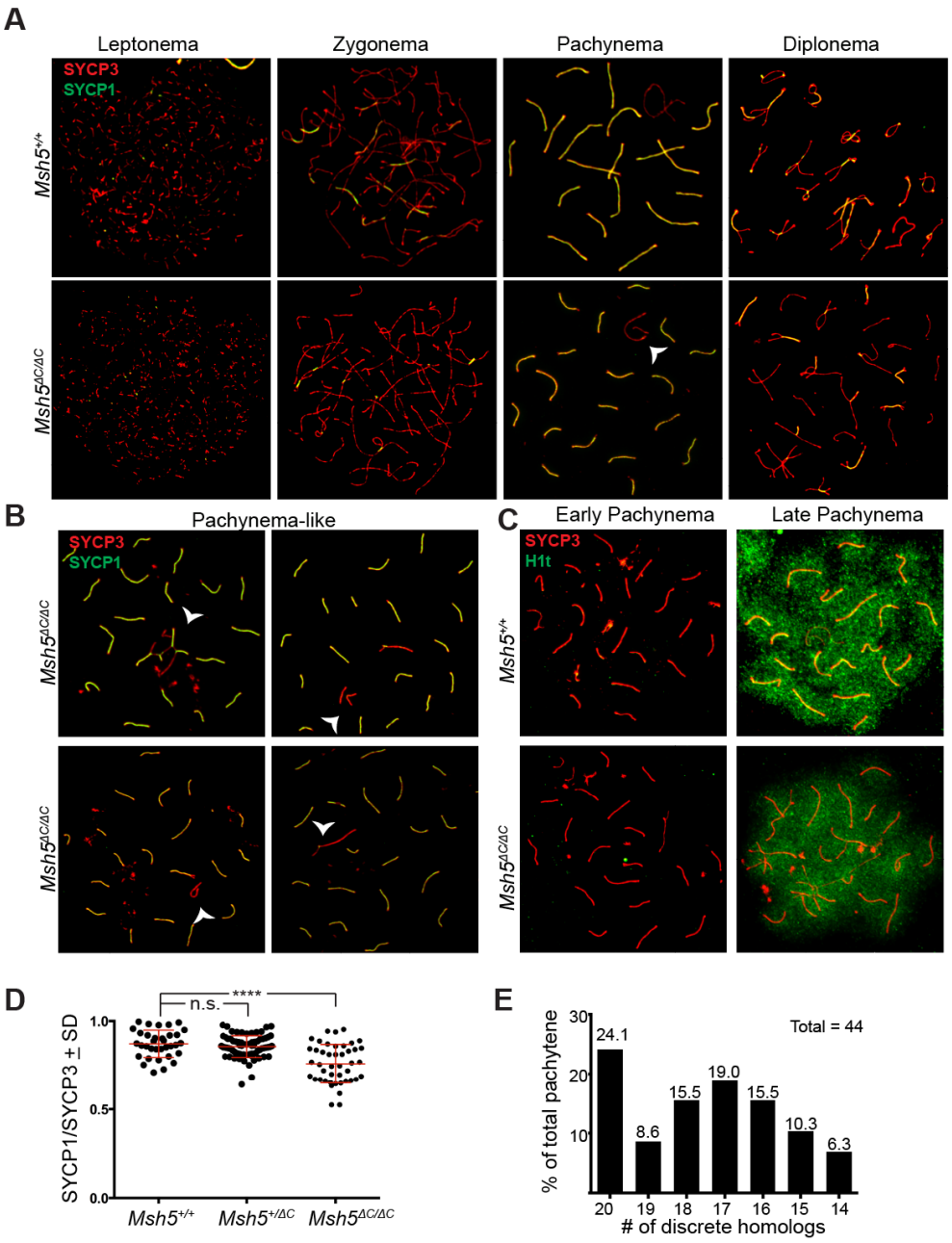

Msh5ΔC/ΔC animals progress through prophase I.(A) Immunofluorescence of adult spermatocytes across genotypes. Representative images of each substage of prophase I are shown, except for diakinesis, where SC is fully disassembled. SYCP3 depicts LE in red, TF shown by SYCP1 green. Arrow head acknowledges synapsis defects observed in pachynema Msh5$^{\Delta C/\Delta C}$ chromosome spreads. (B) Additional images depicting common synapsis defects observed in homozygous chromosomes spreads. Variations in synapsis defects are shown by arrow heads (described from top left, moving clockwise) ranging from multichromatid synapsis events, single autosome asynapsis, elongated XY pair, and single asynapsis chromatids. (C) Representative images of H1t signal before and after mid-pachytene in WT and *Msh5*$^{\Delta C/\Delta C}$. (D) Synapsis quantitation derived from pachytene cells across genotypes measured using imageJ. For each pachynema spermatocyte, the fraction of SYCP1/SYCP3 is plotted. Error bars in red show mean Mouse and cell # utilized: WT- 1 mouse, 34 cells; *Msh5*$^{\Delta C/\Delta C}$ - 3 mice, 44 cells; *Msh5*$^{+/\Delta C}$ 3 mice, 74 cells (E) The number of independent homologs were recorded for all *Msh5*$^{\Delta C/\Delta C}$ pachynema cells (44 cells total). On the X axis is the number of discrete SC observed, and on the Y axis is the percentage of cells that bin accounts for within the total pachytene population. Above each bar is the actual percentage that bin makes in the population. The largest population of all pachynema cells counted contained 20 independently synapsed homologs as expected in WT pachynema. P<0.0001 **** P<0.001 *** P<0.01 ** P<0.05 *

Other *Msh5*$^{\Delta C/\Delta C}$ spermatocytes contained synapsis junctions between more than two chromosomes (Figure 18B, top left).

The presence of the mid-pachynema marker, Histone H1t, provided additional confidence for prophase I progression in *Msh5*$^{\Delta C/\Delta C}$ animals (Figure 18C). In WT populations, H1t localized to the nucleus of prophase I cells, beginning at mid-pachynema and remaining present for the remainder of prophase I (Drabent, Bode, Bramlage, & Doenecke, 1996). H1t localization was apparent in the nucleus mid-pachynema through diplonema across all genotypes (Figure 18C). These results suggest that *Msh5*$^{\Delta C/\Delta C}$ animals are proficient in achieving at least a mid-pachynema like stage.

To quantify synapsis in pachytene-like cells, the definition for what is considered pachytene-like must be redefined from the canonical definition of 20 discrete SC observed in WT. Synapsis defects have been previously analyzed in *Msh5*$^{GA/GA}$ spermatocytes, which have severe SC defects in that pachytene-like spermatocytes rarely achieved discrete synapsis on more than 10 homolog pairs (Chapter 2) (Milano et al., 2019). In this previous study, a spermatocyte is considered pachytene-like if at least 4 discrete homolog pairs synapse (Milano et al., 2019). The SC defects in *Msh5*$^{\Delta C/\Delta C}$ are less severe and, so for this analysis, a spermatocyte was arbitrarily considered to be pachytene-like when at least 14 discrete fully synapsed homolog pairs were achieved, about ¾ of the genome. Following these criteria, 24% of all pachynema cells in *Msh5*$^{\Delta C/\Delta C}$ animals achieved 20 discrete homolog pairs (n=58) (Figure 18E). Cells containing 19, 18, 17, 16, 15, and 14 discrete homolog pairs represented 8.6%, 15.5%, 19.0%, 15.5%, 10.3%, 6.9% of the total *Msh5*$^{\Delta C/\Delta C}$ pachynema cell population, respectively (Figure 18E).

In a complete SC, the LEs and CEs will be equal in length, while a SC that is not fully synapsed will have a shorter CE compared to LE. By measuring the total

length of CE in a cell and dividing it by the total length of the LE in that cell, the degree of synapsis for that cell can be expressed as a value between 0 and 1, with 0 being no synapsis and 1 being compete synapsis. Using ImageJ open software, LE and CE measurements were taken from each cell and synapsis was quantified. In WT spermatocytes, because the X & Y only synapse at the pseudo-autosomal region, they exhibited slightly longer LE compared to CE (Hamer et al., 2003; Royo et al., 2010). The ratio of CE/LE in WT pachytene spermatocytes was 0.87 $\pm$ 0.08 (n=34) (Figure 18D). *Msh5*$^{\Delta C/+}$ pachytene-like spermatocytes were similar to WT and had a CE/LE ratio of 0.856 $\pm$ 0.06 (n=74; p=0.3029, unpaired t-test with Welch's correction) (Figure 18D). Pachytene-like *Msh5*$^{\Delta C/\Delta C}$ spermatocytes had significantly less synapsis than WT spermatocytes, a ratio of 0.76 $\pm$ 0.11 (n=44; p<0.0001, unpaired t-test with Welch's correction) (Figure 18D). These results identify the C-terminus of MSH5 as important for complete synapsis.

Repair of DSBs is abnormal in Msh5$^{\Delta C/\Delta C}$ males through prophase I

To assess the progression of meiotic DSB repair in in *Msh5*$^{\Delta C/\Delta C}$ mutants, anti-γH2AX, a marker of DSBs, was localized on chromosome spreads (Figure 19A) (Hamer et al., 2003). In WT, γH2AX signal appears throughout the nuclease of leptonema spermatocytes and progressively declines until pachynema, at which time most DSB repair is complete (Hamer et al., 2003). In pachynema, γH2AX signal persists only at the XY bivalent, promoting chromatin silencing independent of DSB repair (Fernandez-Capetillo et al., 2003). The dynamics of γH2AX signal in leptonema and zygonema spermatocytes in *Msh5*$^{\Delta C/\Delta C}$ mice were like that observed in WT animals, indicating that the induction of DSBs occurs normally (Figure 19A). Unlike WT and *Msh5*$^{+/\Delta C}$ spermatocytes, pachynema as well as diplonema *Msh5*$^{\Delta C/\Delta C}$

spermatocytes had γH2AX signal along their autosomes, suggesting the presence of DSBs in these stages (Figure 19A). The occurrence of DSBs in diplonema of

Figure 19

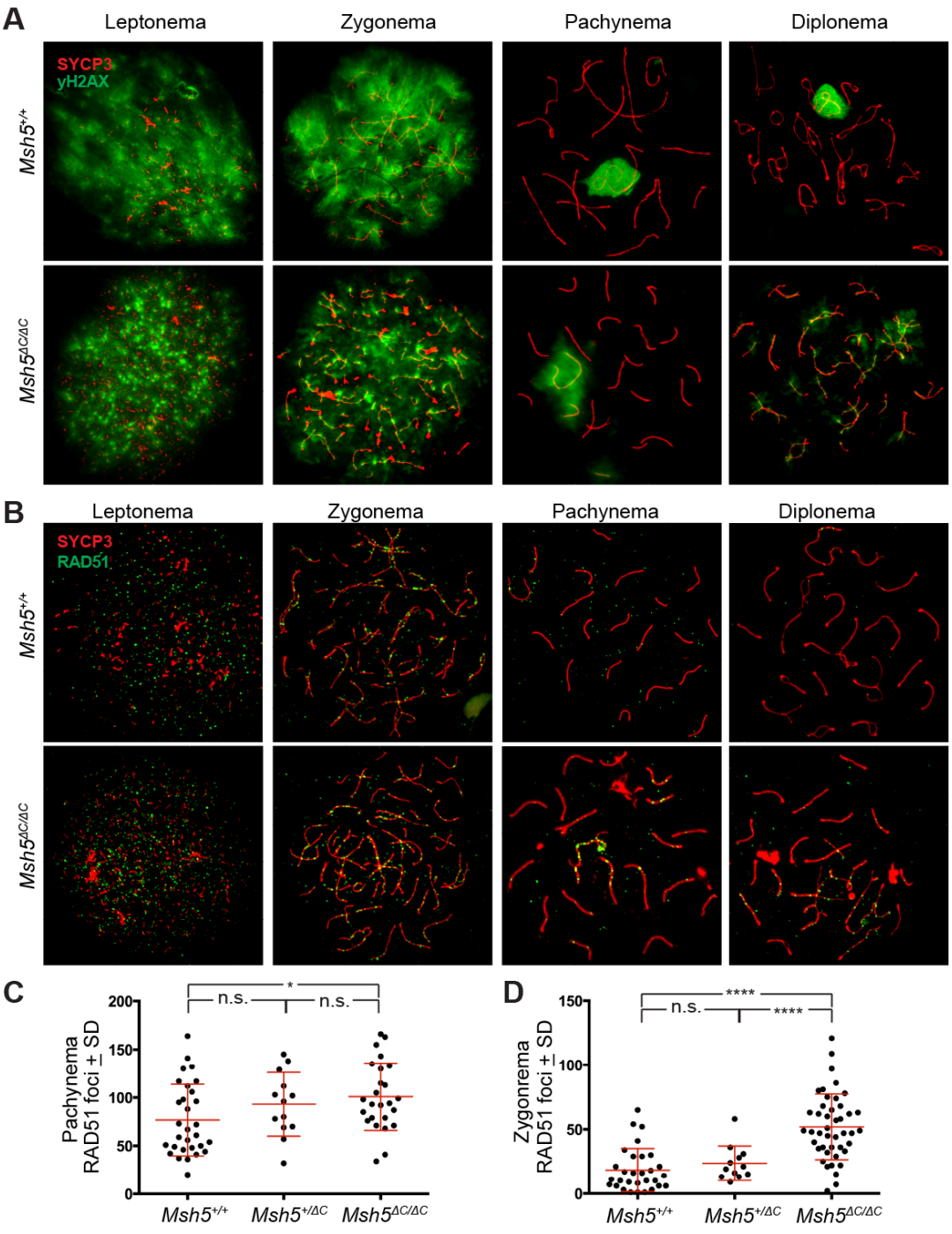

Repair of DSBs is abnormal in *Msh5*$^{\Delta C/\Delta C}$ spermatocytes. (A) immunofluorescence of adult spermatocytes across genotypes show LE (SYPC3 in red) and DSBs (γH2AX in green) for WT and *Msh5*$^{\Delta C/\Delta C}$ spermatocytes. γH2AX shows persistent signal suggesting remaining DSBs in mutants. (B) Representative images of RAD51 (green) localization to the SC (red) in different stages of prophase I in WT and *Msh5*$^{\Delta C/\Delta C}$ spermatocytes. Heterozygous spermatocytes across these stages are indistinguishable from WT (see panel C & D). (C) RAD51 foci associated with the SC during zygonema across all genotypes. Quantitation for each cell obtained using Image J. Mouse and cell # utilized: WT- 1 mouse, 30 cells; *Msh5*$^{\Delta C/+}$ - 1 mouse, 13 cells; *Msh5*$^{\Delta C/\Delta C}$ - 2 mice, 25 cells. (D) RAD51 foci associated with the SC during pachynema. Mouse and cell # utilized: WT 1 mouse, 30 cells; Het 1 mouse, 12 cells; Mut 2 mice, 44 cells. *P<0.0001* **** *P<0.001* *** *P<0.01* ** *P<0.05* *

Msh5$^{\Delta C/\Delta C}$ animals could reflect new DSBs induced by the presence of asynaptic regions, as described in previous studies (Kauppi et al., 2013). Alternatively, γH2AX in diplonema could reflect persistent unrepaired DSBs that remain from initial SPO11 DSB induction. Without additional experiments to track DSB formation in specific substages of the prophase I spermatocytes, these possibilities cannot be demonstrated.

One of the first DSB repair steps common to NCO and CO repair is strand invasion mediated in-part by the RecA homologs, DMC1 and RAD51 (Hunter & Kleckner, 2001; Lange et al., 2016). To observe the early dynamics of DSB repair, anti-RAD51 antibodies were used to localize RAD51 to meiotic chromosome spreads for all genotypes (Figure 19B) (Bannister & Schimenti, 2004; Barlow, Benson, West, & Hultén, 1997; Moens et al., 1997). In WT zygonema, 76.7$\pm$ 37.1 RAD51 foci associated with the SC (n=30) (Figure 19D). The majority of DSBs were repaired during pachynema and only 18.3 $\pm$ 16.8 RAD51 foci associated to the SC in WT (n=30) (Figure 19C) (Barlow, Benson, West, & Hultén, 1997; Keeney, 2008; Moens et al., 1997). Like WT, the *Msh5*$^{+/\Delta C}$ spermatocytes had 93.2 $\pm$ 33.0 RAD51 foci associated to the SC in zygonema (n=13; p=0.1278, Mann-Whitney). *Msh5*$^{+/\Delta C}$ pachytene spermatocytes were also similar to WT and had 23.6 $\pm$ 13.5 foci on the SC (n=12; p=0.1051, Mann-Whitney).

Msh5$^{\Delta C/\Delta C}$ cells, however, had 101.0 $\pm$ 35.0 foci per nucleus in zygonema, a significantly higher amount of RAD51 foci on SC (n=25; p=0.0195, Mann-Whitney) (Figure 19D). This trend continued in pachytene spermatocytes where 51.9 $\pm$ 25.5 RAD51 foci were found to have associated to the SC in *Msh5*$^{\Delta C/\Delta C}$ cells, significantly more than WT pachynema cells (n=44; p<0.0001, Mann-Whitney) (Figure 19C). The similar RAD51 dynamics of WT and *Msh5*$^{+/\Delta C}$ spermatocytes suggest that strand invasion occurs and resolves similarly in WT and *Msh5*$^{+/\Delta C}$ spermatocytes. The elevated number of RAD51 foci in zygonema and pachynema suggests that the C-

terminus of MSH5 is important for the disappearance, or repair, of RAD51-associated DSBs in meiosis.

Together, the results of γH2AX and RAD51 staining in *Msh5*$^{\Delta C/\Delta C}$ spermatocytes substantiates the idea that the last 38 amino acids of the MSH5 C-terminal are necessary for normal DSB repair dynamics during prophase I.

Normal MutSγ dynamics through prophase I in Msh5$^{\Delta C/\Delta C}$ *spermatocytes*

MutSγ localizes on the SC in pachynema to induce the final number of Class I COs. MLH1 and MLH3 localize on the SC in the form of foci (Kolas et al., 2005). To assess how loss of the MSH5 C-terminus affects the dynamics of MutSγ during prophase I, anti-MSH4 antibody was used to localize MSH4 to chromosome spreads across genotypes (Figure 20). In WT spermatocytes, MSH4 foci were present in the nucleus on, and away from, the SC (Figure 20). The total number of MSH4 foci were counted in each spermatocyte, as well as the number of MSH4 foci specifically associated with the SC.

In WT zygotene spermatocytes, the MSH4 foci were abundant both in the nucleus and on the SC. Specifically, WT zygotene cells had 104.1 $\pm$ 26.0 MSH4 foci in the nucleus and 60.7 $\pm$ 25.7 MSH4 foci associated with the SC (n=16) (Figure 20C,D). As expected, the number of MSH4 foci in pachynema were reduced from that of zygonema, both on and away from the SC. During WT pachynema, there were 87.3 $\pm$ 15.3 MSH4 foci in the nucleus and 46.7 $\pm$ 17.8 MSH4 foci associated to the SC (n=27) (Figure 20E,F).

Msh5$^{+/\Delta C}$ zygotene cells, like those in WT animals, had 112.3 $\pm$ 54.1 MSH4 foci in the nucleus (n=10; p=0.8557, Mann-Whitney) (Figure 20). 76.2 $\pm$ 24.4 MSH4 associated with the SC in *Msh5*$^{+/\Delta C}$ zygotene cells, similar to WT

Figure 20

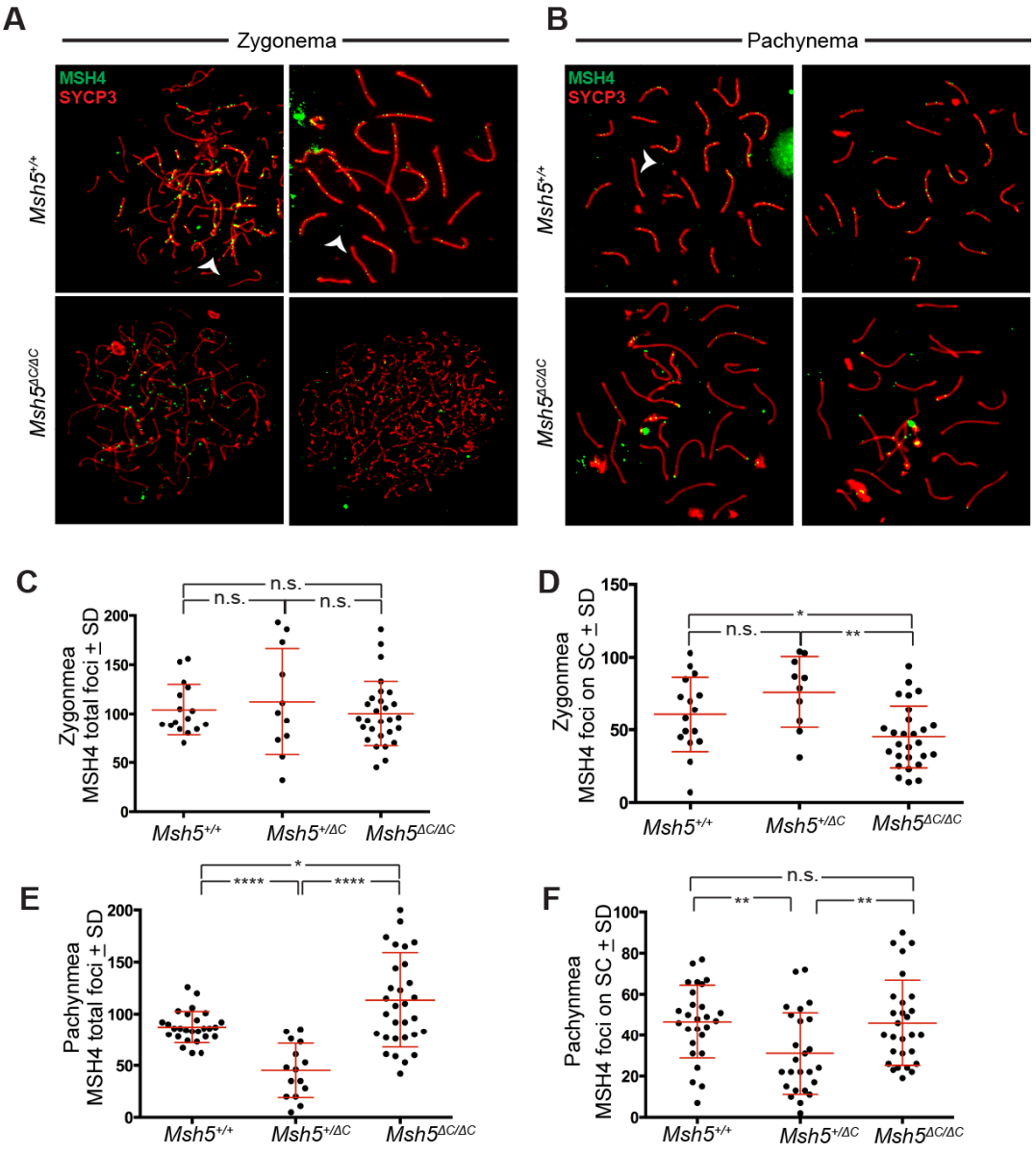

MSH4 localization in *Msh5*$^{\Delta C/\Delta C}$ spermatocytes is reduced on the SC early in zygonema, but in pachynema MSH4 localizes to the SC in normal numbers.
(A) Immunofluorescence of adult spermatocytes show LE (SYCP3 in red) and MSH4 in green *Msh5*$^{+/\Delta C}$ and *Msh5*$^{\Delta C/\Delta C}$ spermatocytes for zygonema chromosome spreads. Two representative images are shown for both *Msh5*$^{+/\Delta C}$ and *Msh5*$^{\Delta C/\Delta C}$ spermatocytes. (B) Same as panel A but for pachynema spermatocytes. (C) Quantitation of total MSH4 in the nucleus during zygonema. Mouse and cell # utilized: 2 WT mice, 16 cells; 4 Het mice, 10 cells; 4 mutant mice, 27 cells. Quant of MSH4 on the SC during zygonema (D) Quantitation of MSH4 associated to the SC in zygonema. (Same N# as C) (E) Quantitation of total MSH4 in the nucleus during pachynema. Mouse and cell # utilized: 2 WT mice, cells 27; 2 Het mice, 25 cells; 4 Mut mice; 28 cells (F) Quantitation of MSH4 associated to the SC in pachynema (Same N# as E) *P<0.0001* **** *P<0.001* *** *P<0.01* ** *P<0.05* *

(n=10; p=0.1311, Mann-Whitney) (Figure 20). In *Msh5*$^{+/\Delta C}$ pachynema, however, MSH4 foci were significantly less than what was observed in WT. *Msh5*$^{+/\Delta C}$ cells only had 45.3 $\pm$ 26.2 MSH4 foci in the nucleus during pachynema (n=15; p<0.0001, Mann-Whitney) (Figure 20). 31.1 $\pm$ 31.1 MSH4 foci associated to the SC in *Msh5*$^{+/\Delta C}$ pachynema, another significant reduction from what was observed in WT (n=25; p=0.0074, Mann-Whitney) (Figure 20). These results identify the C-terminus of MSH5 as important for MutSγ activity in pachynema. The simplest explanation for these results is that the MSH5 C-terminus is important for protein stability. Interestingly, differences in MSH4 localization were observed in the *Msh5*$^{+/\Delta C}$ phenotype, demonstrating that a single WT *Msh5* allele is insufficient to achieve MSH4 foci localization in pachynema.

Msh5$^{\Delta C/\Delta C}$ zygotene spermatocytes had 100.2 $\pm$ 33.1 MSH4 foci in the nucleus, similar to what was observed in both WT and *Msh5*$^{+/\Delta C}$ littermates (n=28; p=0.6948, p=0.6279 respectively, Mann-Whitney). Only 45.3 $\pm$ 21.5 MSH4 foci associated with the SC, significantly fewer MSH4 foci than what was observed in WT or *Msh5*$^{+/\Delta C}$ (n=27; p=0.0442, p<0.0016 respectively, Mann-Whitney). These results confirm the C-terminus of MSH5 as important for MSH4 foci accumulation in zygonema. Yet, by pachynema, *Msh5*$^{\Delta C/\Delta C}$ spermatocytes had 113.5 $\pm$ 45.6 MSH4 foci in the nucleus, more than what was observed in the nucleus of either WT or *Msh5*$^{+/\Delta C}$ spermatocytes (n=28; p=0.0484, p<0.0001 respectively, Mann-Whitney). Of these MSH4 foci, 46.1 $\pm$ 20.9 associated to the SC, comparable to what was observed in WT (n=28; p=0.6072, Mann-Whitney; p=0.6072).

A probable explanation for the differences in MSH4 localization is that the C-terminus of MSH5 is necessary for either protein stability or for the stable association of MutSγ to the SC. Nevertheless, protein levels for MSH4 in these animals have yet to be tested, so neither possibility can be ruled out. Consistent with the C-terminal of

MSH5 serving a function related to MutSγ stability, *Msh5*$^{\Delta C/\Delta C}$ spermatocytes have reduced MSH4 associated to the SC in zygotene, earlier than what was observed in pachytene *Msh5*$^{+/\Delta C}$ spermatocytes. Despite this, MSH4 in *Msh5*$^{\Delta C/\Delta C}$ spermatocytes achieve a normal number of MSH4 foci associated on the SC in pachynema. This suggests that the *Msh5*$^{\Delta C/\Delta C}$ spermatocytes are able to compensate for the complete loss of the MSH5 C-terminal domain. Collectively, these results identify the last 38 amino acids of the MSH5 C-terminus as essential for normal MutSγ association to the SC in spermatocytes.

Loss of MSH5 C-terminal region disrupts MutLγ localization

To understand how loss of the MSH5 C-terminus affects localization of MutLγ, anti-MLH3 and anti-MLH1 antibodies were used to localize MutLγ to spermatocytes of all genotypes (Figure 21). MLH1 and MLH3 normally form discrete foci on the SC of synapsed homologs in numbers that tightly correlate with the final number of COs in pachynema spermatocytes (Lipkin et al., 2002; Moens et al., 2002). This pattern was detected for MLH3 foci in pachytene spermatocytes of all genotypes, including *Msh5*$^{\Delta C/\Delta C}$ (Figure 21A). To compare the number of MLH3 foci that appear in pachynema, MLH3 foci were counted in cells across genotypes (Figure 21C). WT cells had 24.5 $\pm$ 3.2 MLH3 foci associated to the SC (n=17). MLH3 foci associated to the SC in *Msh5*$^{+/\Delta C}$ spermatocytes were not much different from WT (23.7 $\pm$ 4.3 foci; n=37; p=0.6732, Mann-Whitney). In *Msh5*$^{\Delta C/\Delta C}$, only 11.7 $\pm$ 7.7 MLH3 foci associated to the SC, significantly less than WT MLH3 foci (n=37; p<0.0001, Mann-Whitney) (Figure 21C).

Dissimilar to what is observed in WT, many of the MLH1 foci appeared away from the SC in *Msh5*$^{\Delta C/\Delta C}$ spermatocytes (Figure 21B). MLH1 foci were also observed

Figure 21

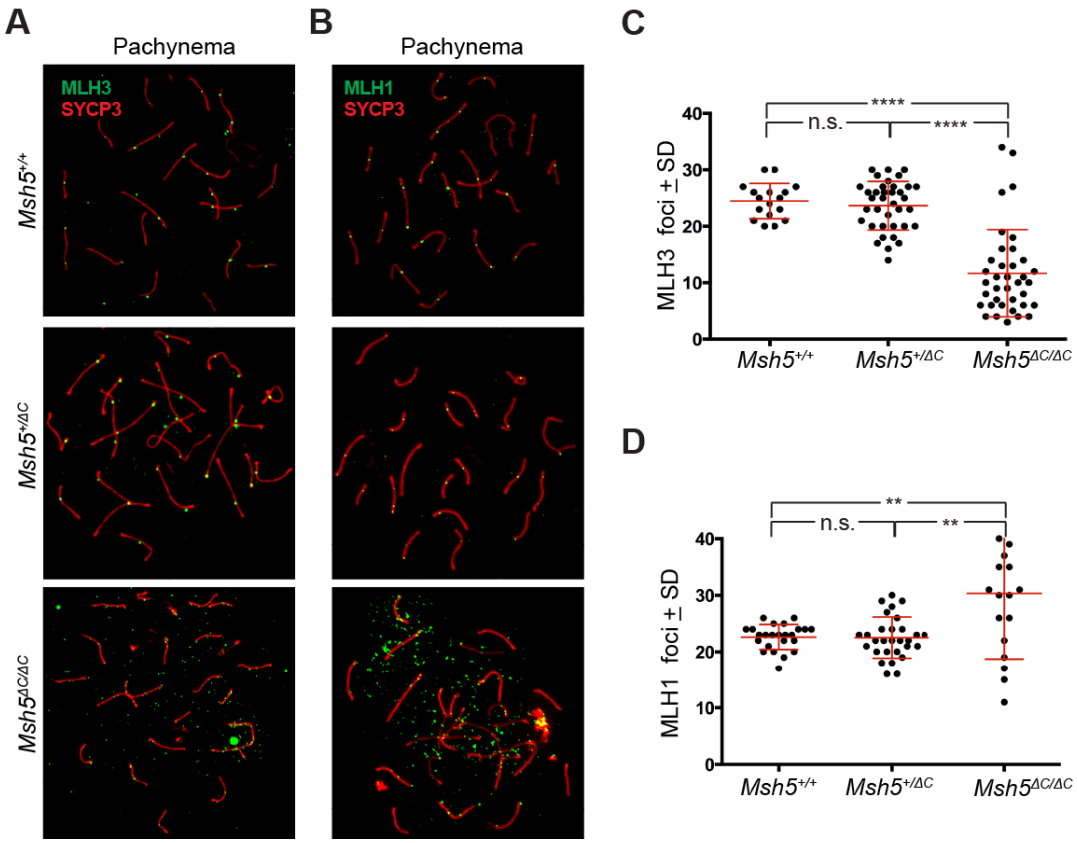

MutLγ localization in *Msh5*$^{\Delta C/\Delta C}$ spermatocytes is abnormal.
(A) Immunofluorescence of adult chromosome spreads show LE (SYCP3 in red) and MLH3 (in green) in *Msh5*$^{+/\Delta C}$ and *Msh5*$^{\Delta C/\Delta C}$ pachytene spermatocytes. (B) Same as A for MLH1 (in green). (D) MLH3 foci counts in Pachynema spermatocytes across genotypes. Error bars in red show mean ± SD MLH1 in heterozygous and homozygous animals. Mouse and cell # utilized: WT- 1 mouse, 17 cells; *Msh5*$^{\Delta C/+}$ - 2 mouse, 37 cells; *Msh5*$^{\Delta C/\Delta C}$ - 2 mice, 37 cells. (E) Same as C for MLH1. Mouse and cell # utilized: WT- 1 mouse, 24 cells; *Msh5*$^{\Delta C/+}$ - 2 mouse, 29 cells; *Msh5*$^{\Delta C/\Delta C}$ - 2 mice, 24 cells. *P<0.0001* **** *P<0.001* *** *P<0.01* ** *P<0.05* *

in *Msh5*$^{\Delta C/\Delta C}$ cells, however the foci were small and often closely spaced (Figure 21B). MLH1 foci associated to the SC were counted and compared across genotypes. In WT cells, 22.6 ± 2.2 MLH1 foci associated to the SC (n=24). *Msh5*$^{+/\Delta C}$ cells had approximately the same amount of foci as WT (22.5 ± 3.7; n=29; p=0.5171, Mann-Whitney). *Msh5*$^{\Delta C/\Delta C}$ cells, however, had 30.3 ± 11.6 MLH1 foci on the SC, more than in WT cells (n=18; p=0.0074, Mann-Whitney) or *Msh5*$^{+/\Delta C}$ spermatocytes (p<0.0058, Mann-Whitney) (Figure 21D). These results identify the C-terminal of MSH5 as necessary for normal MutLγ localization to the SC.

Discussion

The results of this Chapter have determined that the last 38 amino acids of the MSH5 C-terminus are essential for normal spermatogenesis in mice. Specific to the experiments discussed in this Chapter, abnormal SC and DSB repair was observed in *Msh5*$^{\Delta C/\Delta C}$ prophase I spermatocytes. All substages of prophase I were represented in cell preparations from *Msh5*$^{\Delta C/\Delta C}$ testes, however it remains to be determined if the timing of this progress is normal. The SC assembled similar to WT in a subset of *Msh5*$^{\Delta C/\Delta C}$ pachytene spermatocytes, while the remaining pachynema population displayed a variety of synapsis defects (Figure 18). DSBs appeared normally in zygotene *Msh5*$^{\Delta C/\Delta C}$ spermatocytes but in pachynema, abundant DSBs remained (Figure 19). This indicates the MSH5 C-terminus is necessary for the timely repair of DSBs. Finally, MutSγ and MutLγ localized to the SC abnormally in *Msh5*$^{\Delta C/\Delta C}$ spermatocytes, identifying the C-terminus of MSH5 as essential for normal localization of both MutSγ and MutLγ complexes (Figure 20&21). This discussion will relate the conclusions of this Chapter to the current understanding of MutSγ in mouse meiosis and highlight the most pressing questions that remain to be answered. Experiments are proposed in the next Chapter to address these questions.

Previous studies have shown that mouse MutSγ activity is needed for spermatocyte progression through prophase I, normal SC assembly, and all CO repair (Chapter 2) (de Vries et al., 1999; Edelmann et al., 1999; Kneitz et al., 2000; Milano et al., 2019). This study utilized immunofluorescent anti-MSH4 antibodies to document the localization dynamics of the MSH4 MutSγ subunit in the absence of the MSH5 C-terminus. Similar to what was previously reported, high numbers of MSH4 localized to the SC in WT zygonema and, in pachynema, a low number of MSH4 foci remained on the SC (Figure 20) (Santucci-Darmanin et al., 2000). Compared to WT, the pachytene MSH4 foci on the SC was reduced in *Msh5*$^{+/\Delta C}$ spermatocytes, identifying

one copy of *Msh5*$^{+}$ as insufficient to achieve normal MSH4 foci accumulation during pachynema (Figure 20). A similar reduction of MSH4 foci was observed in *Msh5*$^{\Delta C/\Delta C}$ spermatocytes, but this reduction was apparent in zygonema, even earlier than *Msh5*$^{+/\Delta C}$ spermatocytes (Figure 20). The most likely explanation for the observed localization dynamics is that the C-terminal 38 amino acids of MSH5 is necessary for MutSγ complex stability and, therefore, to the overall activity of the MutSγ complex.

Msh5$^{\Delta C/\Delta C}$ pachytene spermatocytes achieve WT numbers of MSH4 foci (Figure 20). This result cannot be explained by an unstable MutSγ complex. Additionally, unlike WT, abundant MSH4 foci were present away from the SC in the nucleus of *Msh5*$^{\Delta C/\Delta C}$ pachytene spermatocytes (Figure 20). The affect the C-terminus of MSH5 has on the overall stability of the MutSγ complex remains to be tested. It is also possible that *Msh4* and *Msh5* are upregulated to compensate for reduced MutSγ activity. Nevertheless, without further experiments to compare the abundance of *Msh4* and *Msh5* transcription between all genotypes, this remains speculation. Despite this uncertainty, the pattern of MSH4 localization in *Msh5*$^{+/\Delta C}$ and *Msh5*$^{\Delta C/\Delta C}$ spermatocytes, when compared to WT, suggests that the C-terminus of MSH5 is important to normal dynamics of the MutSγ complex.

MutSγ activity is necessary for all CO repair in mouse (Chapter 2). MutSγ is thought to bind heteroduplex DNA that arises after D-loop formation and is protects DSBs from NCO repair, enabling them to be acted on later by MutLγ (Baudat & de Massy, 2007; Hanne et al., 2018; Novak, Ross-Macdonald, & Roeder, 2001; Shinohara, Oh, Hunter, & Shinohara, 2008; Snowden, Acharya, Butz, Berardini, & Fishel, 2004). In *Msh5*$^{\Delta C/\Delta C}$ spermatocytes, markers for DSB repair were abundant during pachynema and diplonema, identifying the abnormal timing of DSB repair in these cells (Figure 19). If the C-terminus of MSH5 is needed for MutSγ complex stability, then absence of these residues will likely result in a reduction of normal

MutSγ activity reducing (the amount of?) normal CO repair. Without monitoring DSB formation in *Msh5*$^{\Delta C/\Delta C}$ spermatocytes, it remains unclear if DSBs in pachytene are new or persistent. Alternatively, the abundant RAD51 foci observed in pachytene *Msh5*$^{\Delta C/\Delta C}$ spermatocytes could represent locations in which DSB repair cannot complete.

As the number of MutSγ foci reduce from zygonema to pachynema, the MutSγ foci that remain on the SC colocalize with additional proteins necessary for CO formation to proceed (Gray & Cohen, 2016; Moens et al., 2002; Plug et al., 1998; Santucci-Darmanin et al., 2000). Previous genetic studies have shown these proteins act to increase or decrease the number of MutSγ associated to the SC and, later, CO repair (Cole et al., 2012; Gray & Cohen, 2016; Reynolds et al., 2013). To fully understand how loss of the C-terminus of MSH5 affects CO repair, it will be important to also analyze the localization dynamics of these proteins and their colocalization with MutSγ in these genotypes. MutLγ does associate with the SC across all genotypes, albeit to a lower degree in *Msh5*$^{\Delta C/\Delta C}$ spermatocytes (Figure 21). This is unlike what is observed in *Msh5*$^{GA/GA}$ animals, where MLH3 localization is lost on the SC (Chapter 2). Additionally, while MutLγ is associated with the SC in *Msh5*$^{\Delta C/\Delta C}$ mutants, MLH1 and MLH3 foci are abnormal (Figure 21). This identifies the C-terminal 38 amino acids of MSH5 as essential for normal MutSγ activity, and later recruitment of MutLγ foci.

It remains unclear if the MutLγ sites that appear in *Msh5*$^{\Delta C/\Delta C}$ represent CO locations. The results of this Chapter suggest that the C-terminus of MSH5 is likely needed for normal CO formation, but chiasmata have yet to be properly visualized and counted. Further investigation of CO repair in *Msh5*$^{\Delta C/\Delta C}$ spermatocytes needs to be conducted to fully address the importance of the MSH5 C-terminus during CO repair. Notably, MutLγ is thought to also localize to meiotic chromosomes in pachytene for

reasons independent of CO repair, specifically MLH3 has also been shown to colocalize with MSH2-MSH3 in order to repair repetitive DNA sequences (Kolas et al., 2005). It is therefore possible that the MutLγ localization observed in these studies are not associated with CO repair. In addition to assessing the number of COs repaired in these genotypes, MSH4 and MLH3 colocalization should be assessed.

Altogether, these results indicates that the MSH4-MSH5$^{\Delta C}$ complex retains some MutSγ activity when the C-terminus of MSH5 is lost. However, the abnormal DSB repair and MutSγ and MutLγ localization suggests that the C-terminus of MSH5 is likely necessary for normal CO formation in mouse. The remaining questions related to MutSγ in CO formation are addressed with proposed experiments in Chapter 4

.

References

Acharya, S., Foster, P. L., Brooks, P., & Fishel, R. (2003). The coordinated functions of the E. coli MutS and MutL proteins in mismatch repair. *Molecular Cell*, *12*(1), 233–246.

Bannister, L. A., & Schimenti, J. C. (2004). Homologous recombinational repair proteins in mouse meiosis. *Cytogenetic and Genome Research*, *107*(3-4), 191–200. doi:10.1159/000080597

Bishop, D. K., & Zickler, D. (2004). Early decision; meiotic crossover interference prior to stable strand exchange and synapsis. *Cell*, *117*(1), 9–15.

Bocker, T., Barusevicius, A., Snowden, T., Rasio, D., Guerrette, S., Robbins, D., … Fishel, R. (1999). hMSH5: a human MutS homologue that forms a novel heterodimer with hMSH4 and is expressed during spermatogenesis. *Cancer Research*, *59*(4), 816–822.

Börner, G. V., Kleckner, N., & Hunter, N. (2004). Crossover/noncrossover differentiation, synaptonemal complex formation, and regulatory surveillance at the leptotene/zygotene transition of meiosis. *Cell*, *117*(1), 29–45. doi:10.1016/S0092-8674(04)00292-2

Broman, K. W., Rowe, L. B., Churchill, G. A., & Paigen, K. (2002). Crossover interference in the mouse. *Genetics*, *160*(3), 1123–1131.

Carlosama, C., Elzaiat, M., Patiño, L. C., Mateus, H. E., Veitia, R. A., & Laissue, P. (2017). A homozygous donor splice-site mutation in the meiotic gene MSH4 causes primary ovarian insufficiency. *Human Molecular Genetics*, *26*(16), 3161–3166. doi:10.1093/hmg/ddx199

Clark, N., Wu, X., & Her, C. (2013). MutS Homologues hMSH4 and hMSH5: Genetic Variations, Functions, and Implications in Human Diseases. *Current Genomics*, *14*(2), 81–90. doi:10.2174/1389202911314020002

De Boer, E., Lhuissier, F. G. P., & Heyting, C. (2009). Cytological analysis of interference in mouse meiosis. *Methods in Molecular Biology*, *558*, 355–382. doi:10.1007/978-1-60761-103-5_21

De los Santos, T., Hunter, N., Lee, C., Larkin, B., Loidl, J., & Hollingsworth, N. M. (2003). The Mus81/Mms4 endonuclease acts independently of double-Holliday junction resolution to promote a distinct subset of crossovers during meiosis in budding yeast. *Genetics*, *164*(1), 81–94.

De Vries, S. S., Baart, E. B., Dekker, M., Siezen, A., de Rooij, D. G., de Boer, P., & te Riele, H. (1999). Mouse MutS-like protein Msh5 is required for proper chromosome synapsis in male and female meiosis. *Genes & Development*, *13*(5), 523–531.

Edelmann, W., Cohen, P. E., Kneitz, B., Winand, N., Lia, M., Heyer, J., … Kucherlapati, R. (1999). Mammalian MutS homologue 5 is required for chromosome pairing in meiosis. *Nature Genetics*, *21*(1), 123–127. doi:10.1038/5075

Fernandez-Capetillo, O., Mahadevaiah, S. K., Celeste, A., Romanienko, P. J., Camerini-Otero, R. D., Bonner, W. M., … Nussenzweig, A. (2003). H2AX is required for chromatin remodeling and inactivation of sex chromosomes in male mouse meiosis. *Developmental Cell*, *4*(4), 497–508. doi:10.1016/S1534-5807(03)00093-5

Gray, S., & Cohen, P. E. (2016). Control of meiotic crossovers: from double-strand break formation to designation. *Annual Review of Genetics*, *50*, 175–210. doi:10.1146/annurev-genet-120215-035111

Groothuizen, F. S., Winkler, I., Cristóvão, M., Fish, A., Winterwerp, H. H. K., Reumer, A., … Sixma, T. K. (2015). MutS/MutL crystal structure reveals that the MutS sliding clamp loads MutL onto DNA. *eLife*, *4*, e06744. doi:10.7554/eLife.06744

Guiraldelli, M. F., Eyster, C., Wilkerson, J. L., Dresser, M. E., & Pezza, R. J. (2013). Mouse HFM1/Mer3 is required for crossover formation and complete synapsis of homologous chromosomes during meiosis. *PLoS Genetics*, *9*(3), e1003383. doi:10.1371/journal.pgen.1003383

Guo, T., Zhao, S., Zhao, S., Chen, M., Li, G., Jiao, X., … Chen, Z.-J. (2017). Mutations in MSH5 in primary ovarian insufficiency. *Human Molecular Genetics*, *26*(8), 1452–1457. doi:10.1093/hmg/ddx044

Hamer, G., Roepers-Gajadien, H. L., van Duyn-Goedhart, A., Gademan, I. S., Kal, H. B., van Buul, P. P. W., & de Rooij, D. G. (2003). DNA double-strand breaks and gamma-H2AX signaling in the testis. *Biology of Reproduction*, *68*(2), 628–634.

Henderson, K. A., & Keeney, S. (2004). Tying synaptonemal complex initiation to the formation and programmed repair of DNA double-strand breaks. *Proceedings of the National Academy of Sciences of the United States of America*, *101*(13), 4519–4524. doi:10.1073/pnas.0400843101

Hollingsworth, N. M., Ponte, L., & Halsey, C. (1995). MSH5, a novel MutS homolog, facilitates meiotic reciprocal recombination between homologs in

Saccharomyces cerevisiae but not mismatch repair. *Genes & Development*, *9*(14), 1728–1739. doi:10.1101/gad.9.14.1728

Holloway, J. K., Booth, J., Edelmann, W., McGowan, C. H., & Cohen, P. E. (2008). MUS81 generates a subset of MLH1-MLH3-independent crossovers in mammalian meiosis. *PLoS Genetics*, *4*(9), e1000186. doi:10.1371/journal.pgen.1000186

Hong, S., Joo, J. H., Yun, H., & Kim, K. (2019). The nature of meiotic chromosome dynamics and recombination in budding yeast. *Journal of Microbiology*. doi:10.1007/s12275-019-8541-9

Ji, G., Long, Y., Zhou, Y., Huang, C., Gu, A., & Wang, X. (2012). Common variants in mismatch repair genes associated with increased risk of sperm DNA damage and male infertility. *BMC Medicine*, *10*, 49. doi:10.1186/1741-7015-10-49

Jiricny, J. (2000). Mismatch repair: the praying hands of fidelity. *Current Biology*, *10*(21), R788–90. doi:10.1016/S0960-9822(00)00772-7

Jones, G. H. (1984). The control of chiasma distribution. *Symposia of the Society for Experimental Biology*, *38*, 293–320.

Kauppi, L., Barchi, M., Lange, J., Baudat, F., Jasin, M., & Keeney, S. (2013). Numerical constraints and feedback control of double-strand breaks in mouse meiosis. *Genes & Development*, *27*(8), 873–886. doi:10.1101/gad.213652.113

Keeney, S. (2008). Spo11 and the Formation of DNA Double-Strand Breaks in Meiosis. *Genome Dynamics and Stability*, *2*, 81–123. doi:10.1007/7050_2007_026

Kneitz, B., Cohen, P. E., Avdievich, E., Zhu, L., Kane, M. F., Hou, H., … Edelmann, W. (2000). MutS homolog 4 localization to meiotic chromosomes is required

for chromosome pairing during meiosis in male and female mice. *Genes & Development*, *14*(9), 1085–1097.

Kolas, N. K., Svetlanov, A., Lenzi, M. L., Macaluso, F. P., Lipkin, S. M., Liskay, R. M., … Cohen, P. E. (2005). Localization of MMR proteins on meiotic chromosomes in mice indicates distinct functions during prophase I. *The Journal of Cell Biology*, *171*(3), 447–458. doi:10.1083/jcb.200506170

Kunkel, T. A., & Erie, D. A. (2005). DNA mismatch repair. *Annual Review of Biochemistry*, *74*, 681–710. doi:10.1146/annurev.biochem.74.082803.133243

Lange, J., Yamada, S., Tischfield, S. E., Pan, J., Kim, S., Zhu, X., … Keeney, S. (2016). The Landscape of Mouse Meiotic Double-Strand Break Formation, Processing, and Repair. *Cell*, *167*(3), 695–708.e16. doi:10.1016/j.cell.2016.09.035

Lipkin, S. M., Moens, P. B., Wang, V., Lenzi, M., Shanmugarajah, D., Gilgeous, A., … Cohen, P. E. (2002). Meiotic arrest and aneuploidy in MLH3-deficient mice. *Nature Genetics*, *31*(4), 385–390. doi:10.1038/ng931

Lu, X., Liu, X., An, L., Zhang, W., Sun, J., Pei, H., … Zhang, C. (2008). The Arabidopsis MutS homolog AtMSH5 is required for normal meiosis. *Cell Research*, *18*(5), 589–599. doi:10.1038/cr.2008.44

Lynn, A., Schrump, S., Cherry, J., Hassold, T., & Hunt, P. (2005). Sex, not genotype, determines recombination levels in mice. *American Journal of Human Genetics*, *77*(4), 670–675. doi:10.1086/491718

Lynn, A., Soucek, R., & Börner, G. V. (2007). ZMM proteins during meiosis: crossover artists at work. *Chromosome Research*, *15*(5), 591–605. doi:10.1007/s10577-007-1150-1

Mandon-Pépin, B., Touraine, P., Kuttenn, F., Derbois, C., Rouxel, A., Matsuda, F., … Fellous, M. (2008). Genetic investigation of four meiotic genes in women with premature ovarian failure. *European Journal of Endocrinology*, *158*(1), 107–115. doi:10.1530/EJE-07-0400

Moens, P. B., Kolas, N. K., Tarsounas, M., Marcon, E., Cohen, P. E., & Spyropoulos, B. (2002). The time course and chromosomal localization of recombination-related proteins at meiosis in the mouse are compatible with models that can resolve the early DNA-DNA interactions without reciprocal recombination. *Journal of Cell Science*, *115*(Pt 8), 1611–1622.

Moses, M. J., Dresser, M. E., & Poorman, P. A. (1984). Composition and role of the synaptonemal complex. *Symposia of the Society for Experimental Biology*, *38*, 245–270.

Negoescu, A., Lorimier, P., Labat-Moleur, F., Drouet, C., Robert, C., Guillermet, C., … Brambilla, E. (1996). In situ apoptotic cell labeling by the TUNEL method: improvement and evaluation on cell preparations. *The Journal of Histochemistry and Cytochemistry*, *44*(9), 959–968. doi:10.1177/44.9.8773561

Ni, B., Lin, Y., Sun, L., Zhu, M., Li, Z., Wang, H., … Sha, J. (2015). Low-frequency germline variants across 6p22.2-6p21.33 are associated with non-obstructive azoospermia in Han Chinese men. *Human Molecular Genetics*, *24*(19), 5628–5636. doi:10.1093/hmg/ddv257

Novak, J. E., Ross-Macdonald, P. B., & Roeder, G. S. (2001). The budding yeast Msh4 protein functions in chromosome synapsis and the regulation of crossover distribution. *Genetics*, *158*(3), 1013–1025.

Oakberg, E. F. (1956). Duration of spermatogenesis in the mouse and timing of stages of the cycle of the seminiferous epithelium. *The American Journal of Anatomy*, *99*(3), 507–516. doi:10.1002/aja.1000990307

Obmolova, G., Ban, C., Hsieh, P., & Yang, W. (2000). Crystal structures of mismatch repair protein MutS and its complex with a substrate DNA. *Nature*, *407*(6805), 703–710. doi:10.1038/35037509

Rakshambikai, R., Srinivasan, N., & Nishant, K. T. (2013). Structural insights into Saccharomyces cerevisiae Msh4-Msh5 complex function using homology modeling. *Plos One*, *8*(11), e78753. doi:10.1371/journal.pone.0078753

Ross-Macdonald, P., & Roeder, G. S. (1994). Mutation of a meiosis-specific MutS homolog decreases crossing over but not mismatch correction. *Cell*, *79*(6), 1069–1080. doi:10.1016/0092-8674(94)90037-X

Royo, H., Polikiewicz, G., Mahadevaiah, S. K., Prosser, H., Mitchell, M., Bradley, A., … Turner, J. M. A. (2010). Evidence that meiotic sex chromosome inactivation is essential for male fertility. *Current Biology*, *20*(23), 2117–2123. doi:10.1016/j.cub.2010.11.010

Santucci-Darmanin, S., Walpita, D., Lespinasse, F., Desnuelle, C., Ashley, T., & Paquis-Flucklinger, V. (2000). MSH4 acts in conjunction with MLH1 during mammalian meiosis. *The FASEB Journal*, *14*(11), 1539–1547.

Snowden, T., Acharya, S., Butz, C., Berardini, M., & Fishel, R. (2004). hMSH4-hMSH5 recognizes Holliday Junctions and forms a meiosis-specific sliding clamp that embraces homologous chromosomes. *Molecular Cell*, *15*(3), 437–451. doi:10.1016/j.molcel.2004.06.040

Valerie, K., & Povirk, L. F. (2003). Regulation and mechanisms of mammalian double-strand break repair. *Oncogene*, *22*(37), 5792–5812. doi:10.1038/sj.onc.1206679

Winand, N. J., Panzer, J. A., & Kolodner, R. D. (1998). Cloning and characterization of the human and Caenorhabditis elegans homologs of the Saccharomyces cerevisiae MSH5 gene. *Genomics*, *53*(1), 69–80. doi:10.1006/geno.1998.5447

Zalevsky, J., MacQueen, A. J., Duffy, J. B., Kemphues, K. J., & Villeneuve, A. M. (1999). Crossing over during Caenorhabditis elegans meiosis requires a conserved MutS-based pathway that is partially dispensable in budding yeast. *Genetics*, *153*(3), 1271–1283.

CHAPTER 4

THE ATP BINDING DOMAIN, AS WELL AS THE C-TERMINAL 38 AMINO ACIDS OF MSH5 ARE NECESSARY FOR THE FULL SPECTRUM OF MutSγ ACTIVITY IN MOUSE SPERMATOGENESIS

Introduction

In mouse meiosis, MutSγ activity is necessary for normal DSB repair progression, SC assembly, and spermatocyte progression through prophase I (de Vries et al., 1999; Edelmann et al., 1999; Kneitz et al., 2000). MutSγ also functions to promote COs in a wide range of eukaryotes, including the budding yeast *S. cerevisea*, the plant *A. thaliana*, and the nematode *C. elegans* (Lu et al., 2008; Novak, Ross-Macdonald, & Roeder, 2001; Zalevsky, MacQueen, Duffy, Kemphues, & Villeneuve, 1999). Until now, the cell death induced during *Msh4*$^{-/-}$ or *Msh5*$^{-/-}$ mouse spermatogenesis has precluded the analysis of MutSγ activity during CO formation. Utilizing novel mouse lines harboring targeted mutations in the *Msh5* locus, the findings presented in this thesis have further defined MutSγ activity during spermatogenesis. By placing the findings of this thesis in the context of previous MutSγ literature, this chapter will present the current model of MutSγ activity during mouse spermatogenesis.

The results outlined in Chapter 2 demonstrate that disruption of the MSH5 ATP binding domain (*Msh5*^{GA}) results in abnormal SC assembly (Milano et al., 2019). A subset of *Msh5*$^{GA/GA}$ spermatocytes progress through prophase I, allowing for the first investigation of MutSγ function in mouse CO repair (Chapter 2). In *Msh5*$^{GA/GA}$ spermatocytes that do achieve diakinesis, all chiasmata are lost, identifying MutSγ activity to be necessary for any CO formation in mouse (Chapter 2) (Milano et al., 2019). The results presented in Chapter 3 identified the C-terminal 38 amino acids of

MSH5 (*Msh5*$^{\Delta C}$) to be important for MutSγ activity, and therefore normal DSB repair in mouse. However, in what step of CO repair is the MutSγ activity necessary, remains to be determined. To further investigate MutSγ activity in CO repair, experimental procedures aimed to complete the analysis of the *Msh5*$^{\Delta C}$ mouse line, ultimately identifying the importance of the C-terminal of CO repair, are proposed.

Mouse MutSγ activity is necessary to coordinate homolog interactions with SC assembly in spermatocytes

Initial homolog pairing in mouse meiosis is mediated in-part by telomere attachments prior to DSB induction (Boateng, Bellani, Gregoretti, Pratto, & Camerini-Otero, 2013). Prior to leptonmea, about 250 DSBs are induced and the resulting DNA ends are rapidly processed to promote HR repair between homologous chromosomes (Lake & Hawley, 2016; Lange et al., 2016; Neale, Pan, & Keeney, 2005). It is this simultaneous repair of DSBs that maintain homolog pairing and alignment during prophase I (Lange et al., 2016; Morozumi et al., 2012; Romanienko & Camerini-Otero, 2000). The SC initiates at DSB sites and repair proceeds in close proximity to the SC (Keeney, 2008; Lange et al., 2016; Moens et al., 2002).

Similar to the localization of DSB repair proteins on the SC, around 150 MutSγ foci associate to the SC in zygonema (Kneitz et al., 2000). This is about half of the total number of DSBs induced by SPO11 (Keeney, 2008). Absence of MutSγ in mouse spermatocytes results in inappropriate pairing and synapsis among homologs, suggesting MutSγ activity is important for these events (de Vries et al., 1999; Edelmann et al., 1999; Kneitz et al., 2000). However, it is unlikely that mouse MutSγ plays a direct role in homolog pairing and/or synapsis during meiosis since initial SC protein deposition occurs in the absence of either component of the heterodimer, and

since the canonical function of the MutS homologs is one of DNA structure recognition and binding.

MutSγ activity is important during HR repair, as demonstrated all reports of *Msh5* mutations (Edelmann et al., 1999; Milano et al., 2019). Direct protein-protein interactions have been reported between human MutSγ and RAD51 (the protein involved in SEI events) from both *in vivo* and *in vitro* studies, although these results remain to be rigorously tested (Moens et al., 2002; Neyton et al., 2004). Furthermore, *in vitro* binding assays have identified a strong affinity for the human MutSγ complex to heteroduplex DNA, similar to the SEI event induced by RAD51, as well as to Holliday junctions (Hanne et al., 2018; Lahiri, Li, Hingorani, & Mukerji, 2018; Snowden, Acharya, Butz, Berardini, & Fishel, 2004). Together, these studies suggest MutSγ acts during SEI of DSB repair. The substrate for MutSγ activity *in vivo* remains to be elucidated.

The dynamics of the human MutSγ complex on DNA *in vitro* are driven by ATPase domains (Snowden et al., 2004). Human MutSγ binds to Holliday junctions independent of ATP

Figure 22

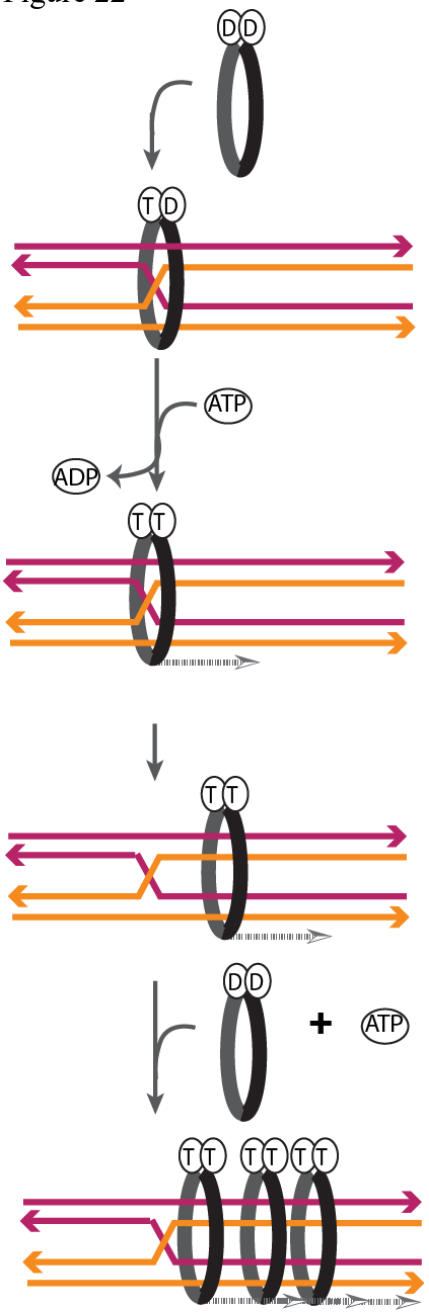

Predicted MSH4-MSH5 ATP binding dynamics *in vivo.* ADP binding is shown as a "D" and ATP is shown as a "T". MSH4-MSH5 bind HJ structures in the ATP-ADP bound state. ADP is rapidly exchanged for ATP, converting MSH4-MSH5 into a sliding clamp that moves away from initial binding substrate in an ATP-hydrolysis independent manor. Movement away from the initial binding junction allows for additional loading of MSH4-MSH5 complexes

and, upon ADP-ATP exchange, MutSγ forms an ATP hydrolysis-independent sliding clamp, that moves away from its substrate (Figure 22) (Snowden et al., 2004; Snowden, Shim, Schmutte, Acharya, & Fishel, 2008). The results of Chapter 2 identify the ATP binding domain of MSH5 as necessary for normal homolog pairing/synapsis during mouse spermatogenesis. These observations, in addition to previously established data, fit a model in which MutSγ stabilizes heteroduplex DNA by binding to D-loop structures (Figure 22).

The majority of extended D-loop repair intermediates undergo disassembly, likely driven in-part by the helicase BLM, to complete NCO repair (De Muyt et al., 2012; West et al., 2015). Extrapolating from previously reported *in vitro* data, and what is known of MutSγ function in *S. cerevisiae*, Figure 22 describes a role for MutSγ in stabilizing D-loop junctions (Börner, Kleckner, & Hunter, 2004). The binding of MutSγ at this heteroduplex junction acts to inhibit D-loop disassembly and repair via SDSA. Upon DNA binding, the MutSγ complex binds ATP, forming an ATP hydrolysis-independent sliding clamp, that moves away from original binding junction Figure 23. Figure 23 depicts MutSγ moving towards the extending D-loop, however it remains unclear if MutSγ moves in any specific direction once bound to heteroduplex DNA. The sliding of MutSγ opens the D-loop junction up for subsequent loading of additional MutSγ complexes, or other repair proteins such as structure specific endonucleases (Figure 23).

From the known dynamics of MutSγ complex *in vitro* and our observations of *Msh5*$^{GA/GA}$ *in vivo*, the MSH4-MSH5^{GA} complex is predicted to bind to D-loop structures and, without MSH5-ATP binding, form a clamp that does not move (or is slow to move away from the initial DNA junction). Notably, the ATP binding domain of MSH4 is retained in this complex. Previous work describes unequal ATP binding among other MutS complexes and the two subunits of the heterodimer act together to

achieve ATP dynamics (Hingorani, 2016). This, in addition to the severity of synapsis/pairing defects in the *Msh5*$^{GA/GA}$ spermatocytes, suggest MSH4 ATP binding is insufficient to compensate for loss of MSH5 ATP binding. During HR repair, the search for a homologous template is rapid and acts in coordination with the SC formation (Zickler & Kleckner, 2015) The defective ATP dynamics of the MSH4-MSH5^{GA} complex is predicted to slow the progression of HR events, stabilizing D-loop structures between non-homologous, as well as homologous partners. The reduced localization of MSH4 to the SC in *Msh5*$^{GA/GA}$ spermatocytes suggests that the MSH4-MSH5^{GA} complex does not load or is not stable. The inappropriate pairing established in *Msh5*$^{GA/GA}$ spermatocytes suggest the MSH4-MSH5^{GA} complex is still able to promote stabilization between non homolog pairs, likely by stabilizing DNA interactions, indirectly resulting in extensive synapsis between inappropriate homologs (Chapter 2). In this model, the MSH4-MSH5^{GA} is released more slowly from the DNA substrate than normal MutSγ, promoting extensive synapsis between homologous and non-homologous chromosomes.

MutSγ activity during the zygotene-pachytene cell progression

Previous work has established the mouse MutSγ complex to be essential for spermatocyte progression through prophase I (de Vries et al., 1999; Edelmann et al., 1999; Kneitz et al., 2000). The results of this thesis have provided the first examples of MutSγ mutations (*Msh5*^{GA}, *Msh5*$^{\Delta C}$) able to bypasses cell death, or at least in which cell death is very much reduced relative to that seen in *Msh5*$^{-/-}$ spermatocytes (Edelmann et al., 1999; Kneitz et al., 2000). This work has identified the ATP binding domain, and the C-terminal domain of MSH5 as at least partially dispensable for the MutSγ activity needed for spermatocyte cell progression. The reason MutSγ activity is needed for spermatocyte progression through prophase I remains to be determined.

It is known that other mouse MutS complexes in mouse directly influence the cell cycle during MMR (Seifert & Reichrath, 2006; van Oers et al., 2014)**.** Previous reports have identified interaction between human MutSγ and the proteins involved in cell signaling including c-ABL1, a critical non-receptor tyrosine kinase critical for many cell functions including DNA damage response, VBP1, a tumor suppressor-binding protein, and GPS2, an inhibitor of some types of ubiquitination (Her, Wu, Griswold, & Zhou, 2003; Xu, Wu, & Her, 2015; Yi et al., 2006). Protein interactions have been identified between human MutSγ and FANCJ and, together, these signal to Chk1 and Chk2 to regulate the cell cycle (Lee, Yi, Griswold, Zhu, & Her, 2006). These interactions remain to be demonstrated during mouse spermatogenesis *in vivo* in mouse. Nevertheless, a direct role for mouse MutSγ complex in cell signaling cannot be ruled out.

Alternatively, the spermatocyte cell death in mutants could be caused be an indirect result of abnormal MutSγ activity. Persistent asynapsis in mouse spermatocytes results in the misexpression of normally silenced genes, causing cell lethality (Royo et al., 2010). MutSγ function is necessary for complete SC formation and in the absence of MutSγ as in *Msh5*$^{-/-}$, cell death is triggered indirectly of the MutSγ complex, by asynapsis. Persistent DSBs can also lead to cell death, and normal repair of DSBs is necessary for spermatocyte progression through prophase I (Cole et al., 2012; Kauppi et al., 2013). An alternative explanation is that MutSγ activity is necessary for DSB repair, and the unrepaired DSBs results in cell death observed in Msh4 or Msh5 spermatocytes. In either of these situations, the spermatocytes which progress in *Msh5*$^{GA/GA}$ or *Msh5*$^{\Delta C/\Delta C}$ spermatocytes had enough MutSγ activity during SC formation and DSB repair to fulfil the threshold required for cell progression. In the future it will be important to investigate the cause of cell death in *Msh5*$^{-/-}$ mutant spermatocytes.

The MutSγ complex is necessary to establish all CO repair locations in mouse spermatocytes

The last DNA repair step common to both NCO and CO repair fate is SEI, driven by RAD51 and DMC1 in mouse (Bannister & Schimenti, 2004). The resulting D-loop extends on the 3' end by the action of DNA polymerase β, utilizing the invaded chromatid as a template (Figure 22) (Plug, Clairmont, Sapi, Ashley, & Sweasy, 1997). The majority of extended D-loops disassemble and the 3' end reanneals to the original DSB site for subsequent NCO repair (Figure 22) (Karran, 2000; Lange et al., 2016; Szostak, Orr-Weaver, Rothstein, & Stahl, 1983; Valerie & Povirk, 2003). Only a subset of D-loops are stabilized for later CO repair (Figure 22) (Lange et al., 2016; Szostak et al., 1983).

The data obtained from the *Msh5*$^{GA/GA}$ spermatocytes identify MutSγ activity as necessary for all CO repair in mouse (Chapter 2). This suggests that MutSγ is necessary to stabilize all joint molecules, including those acted on by the Class I and Class II CO proteins. In this model, during zygotene, MutSγ functions to stabilize a subset of DSBs with the potential to repair as COs (also referred to as nascent CO locations) (Figure 22). It remains unclear if MutSγ functions to directly recruit either the Class I or Class II CO machinery to CO locations.

In Class I CO repair, the 3' end of the extended D-loop undergoes second end capture with the other end of the DSB, forming a dHJ between the homologs (Lange et al., 2016) Figure 23. The asymmetric cleavage of a dHJ results in Class I CO repair (Figure 23) (Szostak et al., 1983). The Class I COs in mouse are driven by MutLγ and only the remaining DSBs associated with MutLγ in pachytene will repair into COs (Lipkin et al., 2002). Class I COs maintain the obligate CO and interference properties (de Boer, Lhuissier, & Heyting, 2009). dHJs that do not meet this criteria are

Figure 23

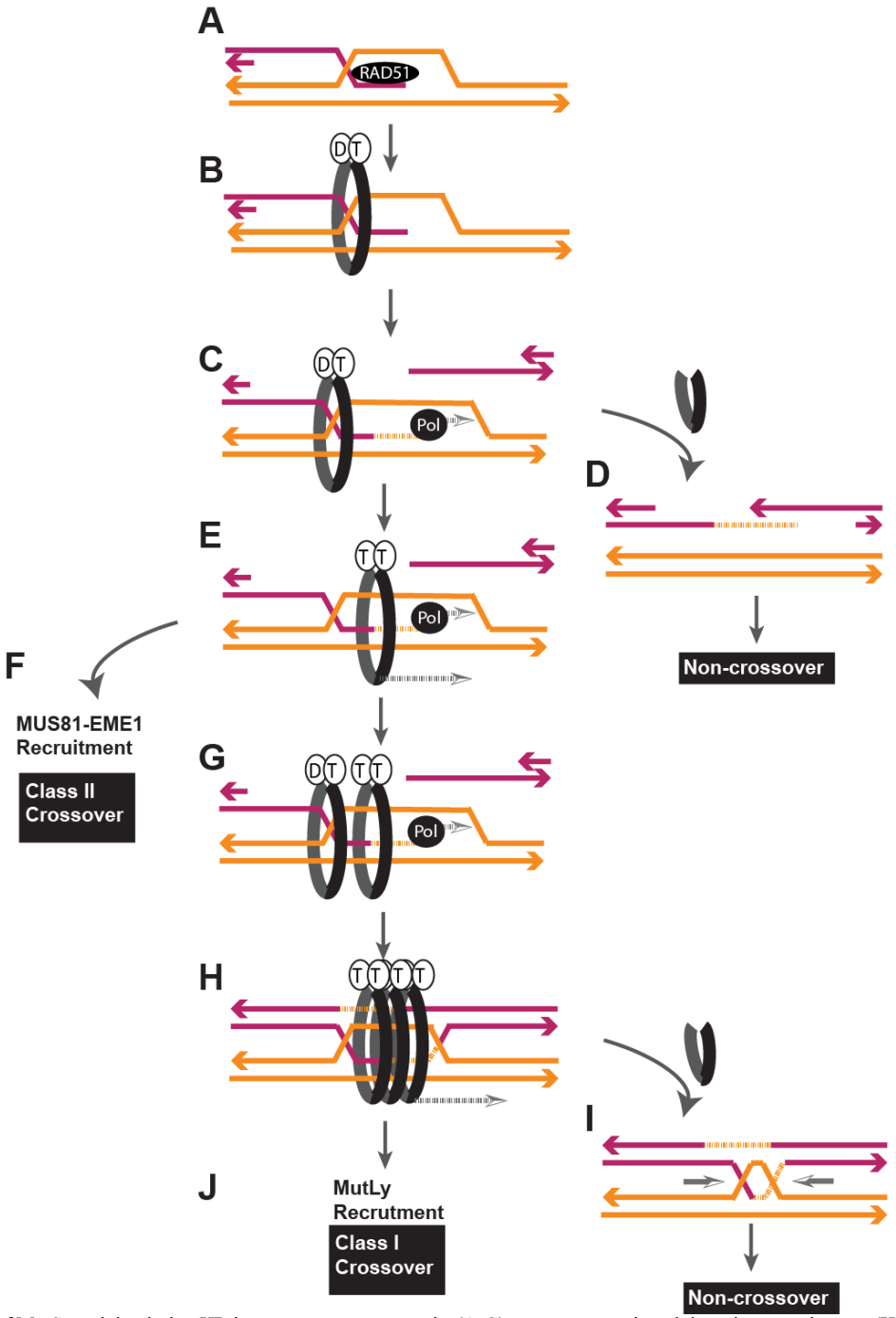

Model of MutSγ activity during HR in mouse spermatogenesis. (A-G) represents repair activity prior to pachytene. (H-J) repair activity after entry into pachytene. A) SEI is mediated in part by RAD51, forming the D-loop. B) MutSγ can bind to the HJ formed in the D-loop structure, independent of ATP binding. C) 3' end is extended by the action of polymerase. D) Upon MutSγ removal, the D-loop can be disassembled, and NCO repair can proceed. E) Upon ATP binding, MutSγ forms an ATP hydrolysis independent, clamp moving away from the original substrate. F) Stabilized extended D-loops can undergo further repair as a Class II CO, mediated in part by structure specific endonuclease MUS81-EME1. G) Extended D-loops can undergo further stabilization by recruiting additional MutSγ complexes, promoting Class I CO repair. H) The extended D-loop can undergo further processing into a dHJ structure. These will be acted on by class I CO regulators including RNF212, HEI10, and CNTD1 for later processing by either I or J. I) MutSγ is no longer stable and disassociates. Dissolution of the D-loop results in NCO repair. J) MutSγ is stabilized and these locations recruit MutLγ for Class I CO repair.

presumable repaired by dHJ dissolution or by the asymmetric cleavage followed by subsequent NCO repair (Lange et al., 2016; Szostak et al., 1983). The findings of this thesis have demonstrated that both the ATP binding domain of MSH5, as well as the C-terminal domain of MSH5, is necessary for normal MutLγ recruitment. Mutation of the MSH5 ATP binding domain results in reduced MutSγ and failure to recruit MutLγ to the SC (Chapter 2). Loss of the MSH5 C-terminal domain results in abnormal MutSγ localization, as well as abnormal MutLγ localization (Chapter 3).

Many more MutSγ foci localize to the SC in zygotene than the final number of MutLγ observed (Kolas et al., 2005). This observation suggests that MutSγ functions to designate excess nascent CO locations in zygotene, for CO repair in pachytene. As spermatocytes progress from zygotene to pachytene the number of MutSγ foci decline until about double the number of MutSγ foci remain compared to the final of MutLγ sites (Kolas et al., 2005). The nascent CO locations are subject to a paring down process (also called CO maturation) resulting in only a subset of MutSγ locations being competent to recruit MutLγ and subsequent Class I CO repair. This implies tight regulation of MutSγ to maintain the 20-30 CO repair events per meiosis.

Previous reports indicate the strict regulation of the MutSγ complex *in vivo*. Hunter *et al.* demonstrate that yeast MutSγ is an intrinsically unstable complex (He et al., 2018). Specifically, the N-terminus of *Msh4* contains sequences that drive degradation and, without phosphorylation of this region, MutSγ is rapidly degrading (He et al., 2018). Additionally, several proteins function to regulate the localization of MutSγ in pachytene, including RNF212, HEI10, and CNTD1 (Holloway, Sun, Yokoo, Villeneuve, & Cohen, 2014; Qiao et al., 2014; Reynolds et al., 2013). The first of these proteins to influence MutSγ activity is RNF212, a SUMO ligase (Reynolds et al., 2013). In zygotene RNF212 localizes to the SC independent of MutSγ (Reynolds et al., 2013). A sub population MutSγ foci colocalize with RNF212 foci on the SC and it

is at these sites of colocalization that MutSγ remains associated to the SC (Qiao et al., 2014; Reynolds et al., 2013).

The cyclin-related protein CNTD1 protein, and the ubiquitin ligase HEI10 are necessary to further progress MutSγ-RNF212 locations for further CO processing (Holloway et al., 2014; Qiao et al., 2014; Reynolds et al., 2013). In spermatocytes that lack either CNTD1 or HEI10, abundant MutSγ and RNF212 foci remain associated to the SC and fail to pare down (Holloway et al., 2014). CNTD1 likely acts prior to HEI10 because loss of CNTD1 results in the failure to recite HEI10 to the SC (Holloway et al., 2014; Qiao et al., 2014). HEI10, also colocalizes with RNF212-MutSγ locations, and is necessary to remove remaining RNF212 and MutSγ sites that are not colocalized (Qiao et al., 2014).

In association with SC, MutSγ establishes nascent COs by stabilizing excess joint molecules in late zygonema, protecting them from NCO repair (Figure 22). CO regulators RNF212, HEI10, and CNTD1 act to mature the subset of MutSγ locations into final MutLγ CO locations. The data generated from the *Msh5*$^{\Delta C/\Delta C}$ animals suggest an importance for the MSH5 C-terminal domain in regulating MutSγ activity. In the future it will be important to identify how the C-terminus of MSH5 affects the dynamics of these CO regulators.

Future Directions

The results presented in Chapter 3 suggest that the C-terminus of MSH5 is dispensable for normal pairing and synapsis events but is necessary for normal MutLγ localization. During zygonema in *Msh5*$^{\Delta C/\Delta C}$ spermatocytes, MSH4 localization to the SC is reduced, while MutLγ foci fail to localize during pachynema. These findings identify the C-terminal of MSH5 as important for CO repair; however, the number chiasmata that form in *Msh5*$^{\Delta C/\Delta C}$ spermatocytes is still unknown, and is currently

under investigation. Furthermore, CO maturation is a multi-step process that ultimately leads to MutLγ localization. The importance of the C-terminus of MSH5 to this process remains unknown.

The following section outlines experiments that aim to clarify the importance of the MSH5 C-terminus in CO formation. All experiments should be conducted with age-matched *Msh5*$^{+/+}$, *Msh5*$^{+/\Delta C}$, and *Msh5*$^{\Delta C/\Delta C}$ littermates. As a negative control, *Msh5*$^{-/-}$ animals should be included in these experiments and, if this is unavailable, these experiments should utilize *Msh4*$^{-/-}$. Outlined below are experiments proposed to address these questions:

How does the C-terminal of MSH5 affect the abundance of MSH5 protein? To complete the characterization of the *Msh5* allele, it is important to consider the affect this mutation has on protein abundance. The C-terminus of MSH5 is not a part of the residues that with MSH4. Loss of the C-terminus is not expected to affect MutSγ complex formation and. The *Msh5*$^{\Delta C/\Delta C}$ allele is also not expected to change the protein abundance. To validate this, the abundance of MSH4 and MSH5 protein during spermatogenesis should be determined by quantitative western blot analysis for each genotype and compared. The testis contains a heterogenous population of both somatic and meiotic cell populations. Spermatocyte populations can be isolated from the testis by utilizing previously established STA-put cell isolation techniques (Bellvé et al., 1977). Protein can be extracted from the isolated spermatocytes populations, followed by a quantitative WB analysis utilizing antibodies against MSH4 and MSH5, if this antibody becomes available.

How does the C-terminus of MSH5 affect CO formation in mouse spermatocytes? The abnormal localization of MLH1 and MLH3 in *Msh5*$^{\Delta C/\Delta C}$ spermatocytes suggests that CO formation is abnormal. To validate this, chiasmata can be counted in *Msh5*$^{\Delta C/\Delta C}$ diakinesis cells to identify the number of COs that form.

Diakinesis cells can be collected from an adult testis using previously establish methods (Holloway, Booth, Edelmann, McGowan, & Cohen, 2008; Jones, 1984). Chiasmata structures are visualized by treating cell preparations with Giemsa stain to visualize DNA. The number of chiasmata per cell, as well as the number of univalent chromosomes per cell, should be counted and compared across genotypes.

It will also be of interest to observe how CO repair in *Msh5*$^{\Delta C/\Delta C}$ spermatocytes affects subsequent homolog segregation in anaphase I. To investigate this, anaphase cells are collected from an adult testis and prepared by previously established methods (Bellvé et al., 1977). Homolog segregation is visualized by immunofluorescent antibodies against α-tubulin, a major component of the spindle, and DAPI stained to visualize DNA (O'Donnell & O'Bryan, 2014). If CO formation is abnormal in *Msh5*$^{\Delta C/\Delta C}$ spermatocytes, the homolog segregation is expected to be unequal.

How does the C-terminus of MSH5 affect MutLγ recruitment? The localization of MutLγ subunits, MLH1 and MLH3, appear abnormal in *Msh5*$^{\Delta C/\Delta C}$ spermatocytes. Utilizing the images generated in Chapter 3, the localization of MLH1 and MLH3 can be analyzed for the appearance of the obligate CO. For each pachytene cell, the number of MLH1 or MLH3 foci associated with every homologous chromosome should be recorded. If the C-terminal of MSH5 does not affect obligate CO designation, every homolog pair in *Msh5*$^{\Delta C/\Delta C}$ pachytene spermatocytes is expected to have at least one MLH1 and an MLH3 focus.

Normally, MLH1 and MLH3 foci display interference. Utilizing the previously mentioned images of MLH1 and MLH3 localization, interference can be calculated for MLH1 and MLH3 foci in pachytene. Interference is calculated using previously established methods (Broman, Rowe, Churchill, & Paigen, 2002; McPeek & Speed, 1995). If the C-terminal of MSH5 is important for establishing MutLγ interference,

MLH1 and MLH3 foci in *Msh5*$^{\Delta C/\Delta C}$ spermatocytes will have reduced or no interference.

How does the C-terminal of MSH5 affect Class I CO maturation? In *Msh5*$^{\Delta C/\Delta C}$ spermatocytes, MSH4 localization on the SC is reduced. It remains to be seen if the remaining foci are capable of progressing through CO maturation. To monitor CO repair in *Msh5*$^{\Delta C/\Delta C}$ spermatocytes, chromosome spreads are prepared from an adult testis and stained with immunofluorescent antibodies specific to proteins important for CO repair. Assuming an antibody is available, this analysis should include a record of foci counts for RNF212, HEI10, and CNTD1 (individually) in pachytene *Msh5*$^{\Delta C/\Delta C}$ spermatocytes. These values should be compared across genotypes. If the C-terminal of MSH5 is not important for the localization of these CO regulators, the foci in *Msh5*$^{\Delta C/\Delta C}$ spermatocytes will be similar to WT.

CO regulators function to maintain the number of COs by altering the amount of MutSγ foci associated to the SC. Previous studies have identified colocalization between MSH4 and CO regulators (Holloway et al., 2014; Qiao et al., 2014; Reynolds et al., 2013). If the C-terminal of MSH5 is not important for MSH4 association with CO regulators, these proteins are expected to colocalize with MSH4. To see how colocalization of MSH4 and CO regulators differs among genotypes, chromosome spreads should be co-stained with antibodies against MSH4 and RNF212 (as well as HEI10 and CNTD1). The number of colocalization events recorded for each dataset, with each specific CO regulator should be recorded and compared between genotypes.

Class I COs are associated with establishing the obligate CO and maintaining interference properties. In addition to the interference observed in MutLγ foci, interference properties have been reported for earlier CO proteins such as RNF212 and MutSγ (de Boer et al., 2009). Previous studies have identified that RNF212 colocalize to the SC, independent of MutSγ. Given this, the C-terminal domain of MSH5 is not

likely to affect interference of RNF212 (Reynolds et al., 2013). To understand how the C-terminal of MSH5 affects interference of RNF212, interference should be calculated for both MSH4 and RNF212 and compared across genotypes.

Finally, if possible what proteins are good candidate MSH5-C-terminal interactors? It is possible that the C-terminal functions in coordination with other proteins to affect the dynamics of the MutSγ complex. The sequence of the C-terminal domain suggests that it is a target of post translational modification sites. To test if we can identify potential candidates for modifications, we have synthesized a peptide representing the last 38 amino acids of MSH5. Using the peptide bait, we will identify candidate MSH5 C-terminal interacting proteins by IP of adult testis lysate across genotypes. The resultant isolated complexes are then be run on SDS-PAGE gel followed by a western blot using antibodies against candidate proteins. Antibodies are available for predicted MutSγ interacting proteins, including RAD51, BLM, MLH1, and MLH3. Positive interactions found by this screening are then be verified by a yeast two hybrid.

The last 38 amino acids of the MSH5 C-terminus are highly conserved across mammals and is largely absent from other eukaryotes. While the function of this domain is unknown, this may be the result of a potentially divergent characteristic of the protein in mammals. In mouse loss of the MSH5 C-terminus results in reduced MSH4 foci in zygotene, normal SC assembly, and normal recruitment of MutLγ (Chapter 3). The experiments proposed here will facilitate the role of the MSH5 C-terminus in mouse CO repair, however later experiments will be needed to identify if this domain functions specifically in mouse, or has some shared function with other eukaryotic systems such as in budding yeast.

References

Qiao, H., Prasada Rao, H. B. D., Yang, Y., Fong, J. H., Cloutier, J. M., Deacon, D. C., … Hunter, N. (2014). Antagonistic roles of ubiquitin ligase HEI10 and SUMO ligase RNF212 regulate meiotic recombination. Nature Genetics, 46(2), 194–199. doi:10.1038/ng.2858

Reynolds, A., Qiao, H., Yang, Y., Chen, J. K., Jackson, N., Biswas, K., … Hunter, N. (2013). RNF212 is a dosage-sensitive regulator of crossing-over during mammalian meiosis. Nature Genetics, 45(3), 269–278. doi:10.1038/ng.2541

Romanienko, P. J., & Camerini-Otero, R. D. (2000). The mouse Spo11 gene is required for meiotic chromosome synapsis. Molecular Cell, 6(5), 975–987. doi:10.1016/S1097-2765(00)00097-6

Royo, H., Polikiewicz, G., Mahadevaiah, S. K., Prosser, H., Mitchell, M., Bradley, A., … Turner, J. M. A. (2010). Evidence that meiotic sex chromosome inactivation is essential for male fertility. Current Biology, 20(23), 2117–2123. doi:10.1016/j.cub.2010.11.010

Snowden, T., Acharya, S., Butz, C., Berardini, M., & Fishel, R. (2004). hMSH4-hMSH5 recognizes Holliday Junctions and forms a meiosis-specific sliding clamp that embraces homologous chromosomes. Molecular Cell, 15(3), 437–451. doi:10.1016/j.molcel.2004.06.040

Snowden, T., Shim, K.-S., Schmutte, C., Acharya, S., & Fishel, R. (2008). hMSH4-hMSH5 adenosine nucleotide processing and interactions with homologous recombination machinery. The Journal of Biological Chemistry, 283(1), 145–154. doi:10.1074/jbc.M704060200

Xu, Y., Wu, X., & Her, C. (2015). hMSH5 Facilitates the Repair of Camptothecin-induced Double-strand Breaks through an Interaction with FANCJ. The Journal of Biological Chemistry, 290(30), 18545–18558. doi:10.1074/jbc.M115.642884

Yi, W., Lee, T.-H., Tompkins, J. D., Zhu, F., Wu, X., & Her, C. (2006). Physical and functional interaction between hMSH5 and c-Abl. Cancer Research, 66(1), 151–158. doi:10.1158/0008-5472.CAN-05-3019

Bannister, L. A., & Schimenti, J. C. (2004). Homologous recombinational repair proteins in mouse meiosis. Cytogenetic and Genome Research, 107(3-4), 191–200. doi:10.1159/000080597

Bellvé, A. R., Cavicchia, J. C., Millette, C. F., O'Brien, D. A., Bhatnagar, Y. M., & Dym, M. (1977). Spermatogenic cells of the prepuberal mouse. Isolation and morphological characterization. The Journal of Cell Biology, 74(1), 68–85. doi:10.1083/jcb.74.1.68

Boateng, K. A., Bellani, M. A., Gregoretti, I. V., Pratto, F., & Camerini-Otero, R. D. (2013). Homologous pairing preceding SPO11-mediated double-strand breaks in mice. Developmental Cell, 24(2), 196–205. doi:10.1016/j.devcel.2012.12.002

Börner, G. V., Kleckner, N., & Hunter, N. (2004). Crossover/noncrossover differentiation, synaptonemal complex formation, and regulatory surveillance at the leptotene/zygotene transition of meiosis. Cell, 117(1), 29–45. doi:10.1016/S0092-8674(04)00292-2

Broman, K. W., Rowe, L. B., Churchill, G. A., & Paigen, K. (2002). Crossover interference in the mouse. Genetics, 160(3), 1123–1131.

Cole, F., Kauppi, L., Lange, J., Roig, I., Wang, R., Keeney, S., & Jasin, M. (2012). Homeostatic control of recombination is implemented progressively in mouse meiosis. Nature Cell Biology, 14(4), 424–430. doi:10.1038/ncb2451

De Boer, E., Lhuissier, F. G. P., & Heyting, C. (2009). Cytological analysis of interference in mouse meiosis. Methods in Molecular Biology, 558, 355–382. doi:10.1007/978-1-60761-103-5_21

De Muyt, A., Jessop, L., Kolar, E., Sourirajan, A., Chen, J., Dayani, Y., & Lichten, M. (2012). BLM helicase ortholog Sgs1 is a central regulator of meiotic recombination intermediate metabolism. Molecular Cell, 46(1), 43–53. doi:10.1016/j.molcel.2012.02.020

De Vries, S. S., Baart, E. B., Dekker, M., Siezen, A., de Rooij, D. G., de Boer, P., & te Riele, H. (1999). Mouse MutS-like protein Msh5 is required for proper chromosome synapsis in male and female meiosis. Genes & Development, 13(5), 523–531.

Edelmann, W., Cohen, P. E., Kneitz, B., Winand, N., Lia, M., Heyer, J., … Kucherlapati, R. (1999). Mammalian MutS homologue 5 is required for chromosome pairing in meiosis. Nature Genetics, 21(1), 123–127. doi:10.1038/5075

Hanne, J., Britton, B. M., Park, J., Liu, J., Martín-López, J., Jones, N., … Fishel, R. (2018). MutS homolog sliding clamps shield the DNA from binding proteins. The Journal of Biological Chemistry, 293(37), 14285–14294. doi:10.1074/jbc.RA118.002264

He, W., Rao, H. B. D. P., Tang, S., Bhagwat, N., Kulkarni, D., Ma, Y., … Hunter, N. (2018). The crossover function of MutSγ is activated via Cdc7-dependent stabilization of Msh4. BioRxiv. doi:10.1101/386458

Her, C., Wu, X., Griswold, M. D., & Zhou, F. (2003). Human MutS homologue MSH4 physically interacts with von Hippel-Lindau tumor suppressor-binding protein 1. Cancer Research, 63(4), 865–872.

Hingorani, M. M. (2016). Mismatch binding, ADP-ATP exchange and intramolecular signaling during mismatch repair. DNA Repair, 38, 24–31. doi:10.1016/j.dnarep.2015.11.017

Holloway, J. K., Booth, J., Edelmann, W., McGowan, C. H., & Cohen, P. E. (2008). MUS81 generates a subset of MLH1-MLH3-independent crossovers in mammalian meiosis. PLoS Genetics, 4(9), e1000186. doi:10.1371/journal.pgen.1000186

Holloway, J. K., Sun, X., Yokoo, R., Villeneuve, A. M., & Cohen, P. E. (2014). Mammalian CNTD1 is critical for meiotic crossover maturation and deselection of excess precrossover sites. The Journal of Cell Biology, 205(5), 633–641. doi:10.1083/jcb.201401122

Jones, G. H. (1984). The control of chiasma distribution. Symposia of the Society for Experimental Biology, 38, 293–320.

Karran, P. (2000). DNA double strand break repair in mammalian cells. Current Opinion in Genetics & Development, 10(2), 144–150. doi:10.1016/S0959-437X(00)00069-1

Kauppi, L., Barchi, M., Lange, J., Baudat, F., Jasin, M., & Keeney, S. (2013). Numerical constraints and feedback control of double-strand breaks in mouse meiosis. Genes & Development, 27(8), 873–886. doi:10.1101/gad.213652.113

Keeney, S. (2008). Spo11 and the Formation of DNA Double-Strand Breaks in Meiosis. Genome Dynamics and Stability, 2, 81–123. doi:10.1007/7050_2007_026

Kneitz, B., Cohen, P. E., Avdievich, E., Zhu, L., Kane, M. F., Hou, H., … Edelmann, W. (2000). MutS homolog 4 localization to meiotic chromosomes is required for chromosome pairing during meiosis in male and female mice. Genes & Development, 14(9), 1085–1097.

Kolas, N. K., Svetlanov, A., Lenzi, M. L., Macaluso, F. P., Lipkin, S. M., Liskay, R. M., … Cohen, P. E. (2005). Localization of MMR proteins on meiotic chromosomes in mice indicates distinct functions during prophase I. The Journal of Cell Biology, 171(3), 447–458. doi:10.1083/jcb.200506170

Lahiri, S., Li, Y., Hingorani, M. M., & Mukerji, I. (2018). MutSγ-Induced DNA Conformational Changes Provide Insights into Its Role in Meiotic Recombination. Biophysical Journal, 115(11), 2087–2101. doi:10.1016/j.bpj.2018.10.029

Lake, C. M., & Hawley, R. S. (2016). Becoming a crossover-competent DSB. Seminars in Cell & Developmental Biology, 54, 117–125. doi:10.1016/j.semcdb.2016.01.008

Lange, J., Yamada, S., Tischfield, S. E., Pan, J., Kim, S., Zhu, X., … Keeney, S. (2016). The Landscape of Mouse Meiotic Double-Strand Break Formation, Processing, and Repair. Cell, 167(3), 695–708.e16. doi:10.1016/j.cell.2016.09.035

Lee, T.-H., Yi, W., Griswold, M. D., Zhu, F., & Her, C. (2006). Formation of hMSH4-hMSH5 heterocomplex is a prerequisite for subsequent GPS2 recruitment. DNA Repair, 5(1), 32–42. doi:10.1016/j.dnarep.2005.07.004

Lipkin, S. M., Moens, P. B., Wang, V., Lenzi, M., Shanmugarajah, D., Gilgeous, A., … Cohen, P. E. (2002). Meiotic arrest and aneuploidy in MLH3-deficient mice. Nature Genetics, 31(4), 385–390. doi:10.1038/ng931

Lu, X., Liu, X., An, L., Zhang, W., Sun, J., Pei, H., … Zhang, C. (2008). The Arabidopsis MutS homolog AtMSH5 is required for normal meiosis. Cell Research, 18(5), 589–599. doi:10.1038/cr.2008.44

McPeek, M. S., & Speed, T. P. (1995). Modeling interference in genetic recombination. Genetics, 139(2), 1031–1044.

Milano, C. R., Holloway, J. K., Zhang, Y., Jin, B., Smith, C., Bergman, A., … Cohen, P. E. (2019). Mutation of the ATPase Domain of MutS Homolog-5 (MSH5) Reveals a Requirement for a Functional MutSγ Complex for All Crossovers in Mammalian Meiosis. G3 (Bethesda, Md.). doi:10.1534/g3.119.400074

Moens, P. B., Kolas, N. K., Tarsounas, M., Marcon, E., Cohen, P. E., & Spyropoulos, B. (2002). The time course and chromosomal localization of recombination-

related proteins at meiosis in the mouse are compatible with models that can resolve the early DNA-DNA interactions without reciprocal recombination. Journal of Cell Science, 115(Pt 8), 1611–1622.
Morozumi, Y., Ino, R., Takaku, M., Hosokawa, M., Chuma, S., & Kurumizaka, H. (2012). Human PSF concentrates DNA and stimulates duplex capture in DMC1-mediated homologous pairing. Nucleic Acids Research, 40(7), 3031–3041. doi:10.1093/nar/gkr1229
Neale, M. J., Pan, J., & Keeney, S. (2005). Endonucleolytic processing of covalent protein-linked DNA double-strand breaks. Nature, 436(7053), 1053–1057. doi:10.1038/nature03872
Neyton, S., Lespinasse, F., Moens, P. B., Paul, R., Gaudray, P., Paquis-Flucklinger, V., & Santucci-Darmanin, S. (2004). Association between MSH4 (MutS homologue 4) and the DNA strand-exchange RAD51 and DMC1 proteins during mammalian meiosis. Molecular Human Reproduction, 10(12), 917–924. doi:10.1093/molehr/gah123
Novak, J. E., Ross-Macdonald, P. B., & Roeder, G. S. (2001). The budding yeast Msh4 protein functions in chromosome synapsis and the regulation of crossover distribution. Genetics, 158(3), 1013–1025.
O'Donnell, L., & O'Bryan, M. K. (2014). Microtubules and spermatogenesis. Seminars in Cell & Developmental Biology, 30, 45–54. doi:10.1016/j.semcdb.2014.01.003
Plug, A. W., Clairmont, C. A., Sapi, E., Ashley, T., & Sweasy, J. B. (1997). Evidence for a role for DNA polymerase beta in mammalian meiosis. Proceedings of the National Academy of Sciences of the United States of America, 94(4), 1327–1331.
Qiao, H., Prasada Rao, H. B. D., Yang, Y., Fong, J. H., Cloutier, J. M., Deacon, D. C., … Hunter, N. (2014). Antagonistic roles of ubiquitin ligase HEI10 and SUMO ligase RNF212 regulate meiotic recombination. Nature Genetics, 46(2), 194–199. doi:10.1038/ng.2858
Reynolds, A., Qiao, H., Yang, Y., Chen, J. K., Jackson, N., Biswas, K., … Hunter, N. (2013). RNF212 is a dosage-sensitive regulator of crossing-over during mammalian meiosis. Nature Genetics, 45(3), 269–278. doi:10.1038/ng.2541
Romanienko, P. J., & Camerini-Otero, R. D. (2000). The mouse Spo11 gene is required for meiotic chromosome synapsis. Molecular Cell, 6(5), 975–987. doi:10.1016/S1097-2765(00)00097-6
Royo, H., Polikiewicz, G., Mahadevaiah, S. K., Prosser, H., Mitchell, M., Bradley, A., … Turner, J. M. A. (2010). Evidence that meiotic sex chromosome inactivation is essential for male fertility. Current Biology, 20(23), 2117–2123. doi:10.1016/j.cub.2010.11.010
Seifert, M., & Reichrath, J. (2006). The role of the human DNA mismatch repair gene hMSH2 in DNA repair, cell cycle control and apoptosis: implications for pathogenesis, progression and therapy of cancer. Journal of Molecular Histology, 37(5-7), 301–307. doi:10.1007/s10735-006-9062-5
Snowden, T., Acharya, S., Butz, C., Berardini, M., & Fishel, R. (2004). hMSH4-hMSH5 recognizes Holliday Junctions and forms a meiosis-specific sliding

clamp that embraces homologous chromosomes. Molecular Cell, 15(3), 437–451. doi:10.1016/j.molcel.2004.06.040

Snowden, T., Shim, K.-S., Schmutte, C., Acharya, S., & Fishel, R. (2008). hMSH4-hMSH5 adenosine nucleotide processing and interactions with homologous recombination machinery. The Journal of Biological Chemistry, 283(1), 145–154. doi:10.1074/jbc.M704060200

Szostak, J. W., Orr-Weaver, T. L., Rothstein, R. J., & Stahl, F. W. (1983). The double-strand-break repair model for recombination. Cell, 33(1), 25–35. doi:10.1016/0092-8674(83)90331-8

Valerie, K., & Povirk, L. F. (2003). Regulation and mechanisms of mammalian double-strand break repair. Oncogene, 22(37), 5792–5812. doi:10.1038/sj.onc.1206679

Van Oers, J. M. M., Edwards, Y., Chahwan, R., Zhang, W., Smith, C., Pechuan, X., … Edelmann, W. (2014). The MutSβ complex is a modulator of p53-driven tumorigenesis through its functions in both DNA double-strand break repair and mismatch repair. Oncogene, 33(30), 3939–3946. doi:10.1038/onc.2013.365

West, S. C., Blanco, M. G., Chan, Y. W., Matos, J., Sarbajna, S., & Wyatt, H. D. M. (2015). Resolution of recombination intermediates: mechanisms and regulation. Cold Spring Harbor Symposia on Quantitative Biology, 80, 103–109. doi:10.1101/sqb.2015.80.027649

Xu, Y., Wu, X., & Her, C. (2015). hMSH5 Facilitates the Repair of Camptothecin-induced Double-strand Breaks through an Interaction with FANCJ. The Journal of Biological Chemistry, 290(30), 18545–18558. doi:10.1074/jbc.M115.642884

Yi, W., Lee, T.-H., Tompkins, J. D., Zhu, F., Wu, X., & Her, C. (2006). Physical and functional interaction between hMSH5 and c-Abl. Cancer Research, 66(1), 151–158. doi:10.1158/0008-5472.CAN-05-3019

Zalevsky, J., MacQueen, A. J., Duffy, J. B., Kemphues, K. J., & Villeneuve, A. M. (1999). Crossing over during Caenorhabditis elegans meiosis requires a conserved MutS-based pathway that is partially dispensable in budding yeast. Genetics, 153(3), 1271–1283.

Zickler, D., & Kleckner, N. (2015). Recombination, Pairing, and Synapsis of Homologs during Meiosis. Cold Spring Harbor Perspectives in Biology, 7(6). doi:10.1101/cshperspect.a016626